UNIVERSITY OF OKLAHOMA

GRADUATE COLLEGE

PREDICTIONS OF CRITICAL GAS RATES IN HORIZONTAL AND DEVIATED WELLS

A DISSERTATION

SUBMITTED TO THE GRADUATE FACULTY

in partial fulfillment of the requirements for the

Degree of

DOCTOR OF PHILOSOPHY

By

YOUNESS EL FADILI
Norman, Oklahoma
2014

PREDICTIONS OF CRITICAL GAS RATES IN HORIZONTAL AND DEVIATED WELLS

A DISSERTATION APPROVED FOR THE
MEWBOURNE SCHOOL OF PETROLEUM AND GEOLOGICAL ENGINEERING

BY

_____
Dr. Subhash Shah, Chair

_____
Dr. Randy Keller

_____
Dr. Maysam Pournik

_____
Dr. Rouzbeh Moghanloo

_____
Dr. Mashhad Fahes

DEDICATION

To my parents, children, and grandparents

ACKNOWLEDGEMENTS

Thank you God first and foremost.

I would like to thank Dr. Subhash Shah, my academic advisor, for his guidance, support, and motivation throughout the years even when I doubted myself. Dr. Shah, your leadership taught more than academics, so I am grateful for that.

I would like to thank my parents, Ahmed and Khadija, for their support and belief in me. My parents and family were the motivation I needed to endure the challenges faced to complete this work.

Many thanks to every instructor I had throughout the years. Special thanks to the committee members, Dr. Maysam Pournik, Dr. Randy Keller, Dr. Mashhad Fahes, and Dr. Rouzbeh Moghanloo for their valuable time and suggestions.

I am also grateful to the University of Oklahoma especially, the Petroleum Engineering department for the opportunity to accomplish this work.

Thanks to the organizations that hired me and trusted in my skills and leadership. The experience I have accumulated in the oil and gas industry during the years of work helped me improve and become the engineer that I am today.

Last but not least, I would like to thank my children, Yasmin and Ilias, and wife for standing by me and cheering me up.

TABLE OF CONTENTS

LIST OF TABLES

LIST OF FIGURES

ABSTRACT

The author's intent through this work is to shed light on the current methods of predicting the onsets of liquid loading and to clarify that there is a difference in critical gas rate predictions between horizontal and vertical wells.

A new model that predicts the critical gas rates for horizontal and deviated wells is presented. Literature data comprised of 69 horizontal and deviated wells reported in various studies in addition to experimental data from two horizontal wells are used to test the accuracy of the model and compare it to currently available models.

Results using literature data show that the new model is capable of predicting the critical gas flow rates in horizontal wells within 15.7% of the actual values, a 2–6% improvement over the currently available horizontal well models, and 8–20% improvement over the currently available vertical well models. Results from the experiment tend to support the finding from literature comparison with a deviation of 5% from actual observed rates, an 18-24% improvement over the current horizontal well models, and 23-35% improvement over the current vertical well models. The New model yield best results for rates less than 10,000 Mscf/d and BUR's between 4 and 30^{o}/100 ft. The Conventional models (such as the Turner and Coleman) are not suitable for usage in horizontal wells and should only be used for vertical wells. The new model accounts for the effect of geometry on flow especially particle impact with the flow conduit wall as a result of change in geometry present in horizontal wells. When this effect is accounted for, as in the new model, the estimation of the critical gas rate is more accurate and yields optimized production performance from horizontal wells.

CHAPTER I

Introduction

1.1 Problem statement

Multiple wells are drilled and put on production each year, with the majority flowing a multiphase gas and liquids mixture. Initially, a multiphase gas dominated well has sufficient energy to flow naturally. Wallis (1969) stated that at very high velocities, the liquid film thickness approaches zero and all liquids are entrained in the gas stream, and as the gas velocity decreases, fluids accumulate to form a thicker film surrounding a gas core with entrained droplets. However, as production continues for a certain flow period, the well starts to lack the necessary energy to move liquids out of the wellbore (Fig. 1.1). The latter creates conditions conducive for the entrained liquid droplets to fall and accumulate and therefore, the formation of a hydrostatic column in the wellbore causes the well to flow at lesser than capacity rate or to load up and eventually cease to flow.

Multiple drawbacks are associated with wells flowing below the critical rate. These drawbacks are not limited to the loss of production, but are also extended to affect reservoir deliverability through the possible change of relative permeability, which in turn damages the formation. Loading also causes the well to veer off its natural decline, hence undermining the economic model that approved and justified the viability of the well in terms of reserves and return on investment.

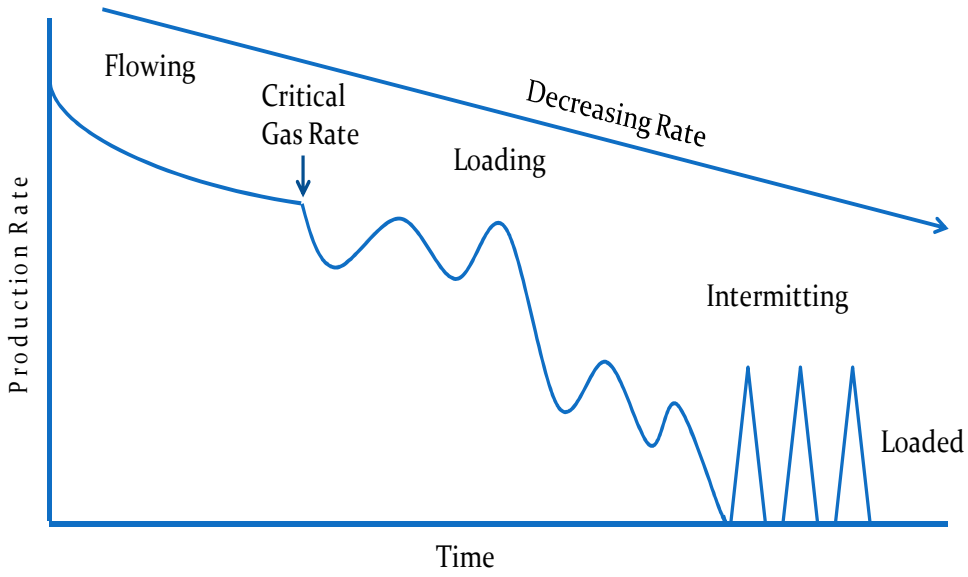

Figure 1.1: Liquid loading occurs when the gas rate is no longer sufficient to maintain an upward movement of entrained liquid droplets throughout the wellbore

In terms of the bigger picture, having multiple wells that exhibit loading problems and remain unattended to has significant effects on natural gas supply and demand. The latter can be a major driving mechanism behind gas price instability and the continuous need to drill for new prospects to maintain production profiles that can keep up with the continually rising demand. In the United States, for example, competitive market aggressiveness of companies drilling and marketing natural gas, along with a significant lack and availability of qualified manpower, are the main drivers behind continuous drilling programs. Each company has to achieve its production target goals within their budget capabilities. Therefore the drilling model, whether efficient or not, has been a model of necessity rather than a model of choice to achieve production targets because in most cases, it realizes acceptable returns on investments. The aggressive drilling model is not a permanent solution; however, it can be very efficient if used as a way to tend to existing wells. If given enough attention to either optimize production or restore

production, the majority of wells can contribute a fair amount of production to the bottom line. An increase of few Mscf/d and few BOPD from each well can have a significant impact on how the world manages its energy balance and evaluates supply and demand, which in turn affects market stability. Since the vertical models do not accurately predict the critical gas rate, usually under-predict it, it is suspected that the change in geometry in horizontal wells causes an effect that is not accounted for by the vertical models. The hypothesis is that the droplets entrained in the gas stream impact the wall of the flow conduit due to continuous change in the build rate throughout the curved section which causes the droplets to lose a fraction of their energy. If the hypothesis is true, then there should be an increase in the required velocity to keep the droplets from falling and accumulating in the wellbore. Accounting for this effect will yield better prediction of the critical gas rate. Chronologically, the transformation of flow regime goes from the initial annular mist flow to churn flow, to slug flow, to bubble flow, and finally, to a non-flowing well (see Fig. 1.2). For well production management purposes, it is important to benchmark each well with its critical rate to respond appropriately prior to the well reaching its critical rate and starting to load up.

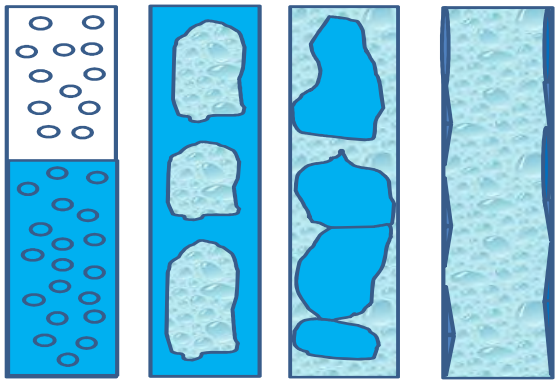

Bubble Flow Slug Flow Churn Flow Annular Mist Flow

Figure 1.2: Succession of flow type leading to a loaded condition, Brill (2005)

1.2 Dissertation outline

This research studies the critical gas rate needed to maintain well flow, with an emphasis on horizontal and deviated wells. Although extensive research and development have been performed in this general area, most of the focus has been on vertical wells. Recently, with the emergence of horizontal drilling, more efforts are oriented to tending to these types of wells.

This work includes the following aspects:

- Conduct a literature review and understand the status quo with its advantages and disadvantages.
- Examine and understand the underlying causes of liquid loading in horizontal and deviated wells.
- Provide a model that helps predict the critical gas rate for horizontal and deviated wells.
- Test the model against other available models using data from the literature.
- Set up a practical experiment to observe and identify the critical gas rate for horizontal and deviated wells.
- Test the model predictions of the critical gas rate against the observed rates.

This dissertation is outlined as follows:

- Chapter 2 defines the critical gas velocity concept and its importance. It also discusses common methods of artificial lift currently used to combat liquid loading.

- Chapter 3 presents an extensive literature review which starts with the original work by Turner et al. (1969), considered to be the foundation of the critical gas rate prediction theory.
- Chapter 4 introduces the effect of impact and rebound on flowing droplets and used this concept to derive the new model for predicting the critical gas rate in horizontal and deviated wells.
- Chapter 5 uses literature data from current horizontal models and tests the new model using their data. A total of 69 horizontal wells and 162 vertical wells data were used for comparison.
- Chapter 6 describes the experimental setup and how it works in addition to offering solutions to some of the issues encountered during its operation.
- Chapter 7 compares the observed critical gas rate from two horizontal wells with the predicted critical gas rate from the new model. A comparison with other models from the literature is also presented in this chapter.
- Chapter 8 discusses the effect of geometry on liquid holdup and offers a proposal for how to adjust the liquid holdup calculation for horizontal and deviated wells. It also discusses the effect of the adjusted holdup on tubing design and placement within the wellbore.
- Chapter 9 provides conclusions and recommendations for further investigation of the critical gas flow rate in horizontal and deviated wells.

CHAPTER II

Critical velocity

2.1 Critical velocity theory

Numerous papers have been published regarding critical gas velocity, and several of them addressed the issue of liquid loading in the wellbore. The main reason liquid loading occurs is because the gas velocity becomes no longer sufficient to keep liquid droplets present in the stream suspended and moving upward. It is important to predict when the latter condition occurs in order to take appropriate measures. The most common method of calculating that velocity is the Turner equation. The theoretical work lies mainly on the required velocity of the streaming gas to offset the terminal velocity of a spherical liquid droplet with a diameter d_p (see Fig 2.1). The velocity where the particle becomes stationary is called the critical velocity below which the particle would settle further and above which the particle will start moving upward. The critical velocity at which the forces are balanced is derived by equating the gravitational force, buoyancy, and the drag force.

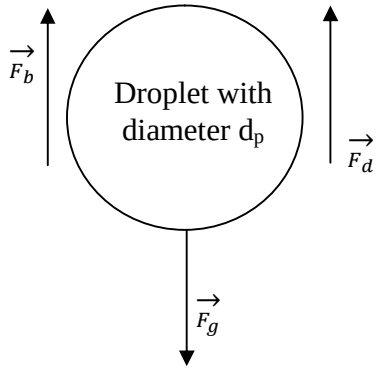

Figure 2.1: Force balance on a liquid droplet with diameter d_p flowing in a gas stream

In Fig. 2.1, F_d is the drag force exerted on the droplet by the flowing gas, F_b is the buoyancy force action on the droplet, and F_g is the force of gravity.

The droplet is subjected to different forces, when these forces are equal, the droplet becomes stationary and the force balance is expressed as follows:

$$F_g = F_b + F_d \qquad \text{----------} \qquad (2.1)$$

where, for a spherical liquid droplet with density ρ_l in a gas stream with density ρ_g:

$$F_d = \frac{1}{2g_c}\,\rho_g\,C_d\,A_d\,V_c^2 \qquad \text{----------} \qquad (2.2)$$

$$F_b = \rho_g\,\pi\,\frac{d_p^3}{6} \qquad \text{----------} \qquad (2.3)$$

and

$$F_g = \rho_l\,\pi\,\frac{d_p^3}{6} \qquad \text{----------} \qquad (2.4)$$

Replacing Eq. 2.2 through 2.4 into Eq. 2.1 and rearranging leads to

$$\left(\rho_l - \rho_g\right)\pi\,\frac{d_p^3}{6} = \frac{1}{2g_c}\,\rho_g\,C_d\,A_d\,V_c^2 \qquad \text{----------} \qquad (2.5)$$

Solving for V_c, Eq. 2.5 can be written as:

$$V_c = \sqrt{\frac{4}{3}\,g\,\frac{(\rho_l-\rho_g)}{\rho_g}\,\frac{d_p}{C_d}} \qquad \text{----------} \qquad (2.6)$$

where, ρ_l is liquid density, ρ_g is gas density, C_d is the drag coefficient, d_p the droplet diameter, and g is the acceleration of gravity.

Equation 2.6 represents the required gas velocity to offset the droplet terminal velocity.

Because the particle diameter is unknown, Turner used the Webber number (We) from Hinze (1949) to represent the change in diameter as function of velocity. The Webber number measures the ratio of inertia to surface tension; while inertia tries to break up the droplet, the surface tension keeps it together.

$$We = \frac{\rho_g \, d_p \, V_c^2}{\sigma \times g_c} \qquad \text{----------} \qquad (2.7)$$

where, σ is the surface tension, and g_c is gravitational factor 32.17 lbm-ft/lbf-sec. Re-arranging Eq. 2.7 to represent the droplet diameter leads to:

$$d_p = \frac{We \ \sigma \ g_c}{\rho_g \times V_c^2} \qquad \text{----------} \qquad (2.8)$$

Replacing d with its value allows Eq. 2.6 to be re-written as:

$$V_c = \sqrt{\frac{4}{3} \, g \, \frac{(\rho_l - \rho_g)}{\rho_g} \, \frac{1}{C_d} \, \frac{We \, \sigma g_c}{\rho_g \times V_c^2}} \qquad \text{----------} \qquad (2.9)$$

Turner elected the use the highest value of the Webber number, 30, to represent the biggest particle diameter. Later, he revised that number to 60 to better fit the observed data. Turner reported the flowing condition of the wells to be in the turbulent region where the drag coefficient C_d for a solid spherical particle is constant at 0.44 (see Fig. 2.2).

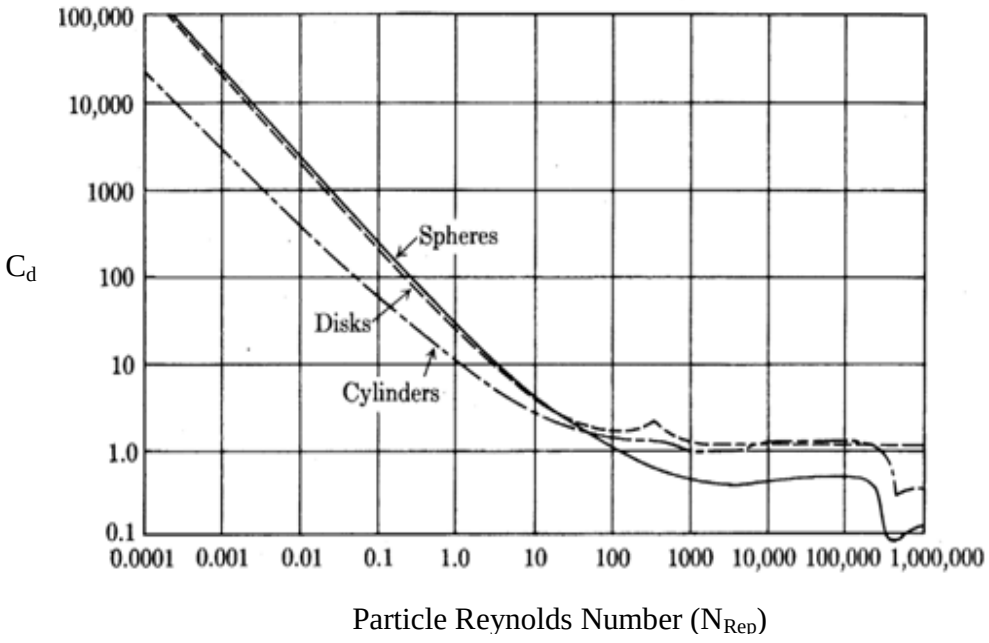

Figure 2.2: Drag coefficient of different particle shapes as function of N_{Rep}

Replacing We, C_d and converting σ from $lb_f/ft=6.852\ 10^{-5}$ dyne/cm, Eq. 2.9 can be expressed as follows:

$$V_c = 1.593\left(\frac{(\rho_l-\rho_g)}{{\rho_g}^2}\sigma\right)^{\frac{1}{4}} \quad \text{----------} \quad (2.10)$$

Equation 2.10 is the Turner equation expressed as function of liquid density ρ_l in lbm/ft^3, gas density ρ_g in lbm/ft^3, and σ surface tension in dynes/cm.

Because it is common to express production in terms of flow rates and not velocity, the critical velocity can be converted to the critical rate at standard conditions for a given pressure, P, and tubular dimensions using the following equation:

$$q_C = \frac{V_c\, A}{B_g} \quad \text{----------} \quad (2.11)$$

where B_g is the gas formation volume factor defined as follows:

$$B_g = \frac{Z\, T\, P_{std}}{P \times T_{std}} \quad \text{----------} \quad (2.12)$$

Substituting for standard conditions, pressure P_{std} = 14.65 psi and temperature T_{std} = 520 ^oR, Eq. 2.11 can be written as:

$$q_c = \frac{3.067\ P\ A\ V_c}{T \times Z} \quad \text{----------} \quad (2.13)$$

where V_c is critical gas velocity in ft/sec, A is the flow conduit cross sectional area in ft^2, P is the pressure at the evaluation point in psi, T is the temperature at the evaluation point in ^oR, and Z is the gas compressibility factor.

2.2 Overview of artificial lift methods

Artificial lift (AL) techniques are used to maintain well flow status, and they can be divided into two major categories. The first category manages to use the well's own energy to keep it flowing, i.e., by using plunger lifts, intermitters, or velocity strings.

The second category adds external energy to the system, mechanical or non-mechanical, i.e., in gas lift, ESP, or compression. Hybrid methods of AL are also available and typically include a mixture of both categories. The selection of the appropriate AL method is based on numerous factors ranging from well type to economics. Following is a brief description of different methods of AL that are commonly used in the oil and gas industry.

2.2.1 Managed energy AL methods

a. Velocity string

Velocity string is smaller internal diameter (ID) tubing, or coil tubing, used to reduce the required critical gas velocity to lift liquids. The main advantage of using this method is that there is no additional associated operating cost, and it is relatively maintenance free. Some of the drawbacks are the initial installation cost and the additional friction, a potential scaling associated with the decreased tubing ID. Velocity string can also be a hybrid form of lift.

b. Plunger lift

A plunger lift consists of a plunger, bottom hole assembly or bumper spring, lubricator, plunger catcher, arrival sensor, control valve, and the control logic. This method can only be applied to wells that satisfy certain conditions related to the well own ability to build pressure and the gathering system for available pressure. Plunger lift, once optimized, can be operated at low cost and minimum maintenance. While running, the plunger can also maintain the tubing clean of scale, paraffin, or other causes of restriction. On the other hand, the shut-in period associated with this operation means

deferred production unless a bypass plunger can also be run. Also, plunger lift is not preferable for high fluid volume wells, especially deep wells, wells with a low gas to liquid ratio (GLR), and wells with high deviations. Plunger lift can also be a hybrid form of lift.

c. Chemicals

Chemicals, especially foamers, are used to lighten the hydrostatic column in the well and reduce the water surface tension. The foaming agent is introduced to the system either in a solid form (soap sticks) or a liquid form by means of a chemical pump that discharges it downhole through a capillary string. Periodic batch treatment is also used if needed. This is a low cost method that is readily available and easy to use. However, care has to be taken to ensure that the chemicals will dissolve and will not form a residue downhole that could act as an obstruction to the flow. Also, in the case of capillary string application, access to the wellbore becomes limited.

Chemicals can also be a hybrid from of lift.

2.2.2 Added energy AL methods

a. Swabbing

This is a quick method to mechanically remove the liquid column that is causing back pressure on the formation. Swabbing is the easiest, quickest, and most convenient method to resume production from a completely loaded non-flowing well. On the other hand, this operation has an associated cost, requires a low pressure environment, and does constitute a permanent solution for liquid loading. Swabbing is not a hybrid form of lift.

b. Electric Submersible Pumps (ESP)

This is a downhole pump used to lift high liquid rate wells by means of a centrifugal force created by the rotation of impellers. A typical ESP consists of downhole motor, intake, pump with lift stages, electric cable, and power drive. Multiple other components can be added if necessary for the better handling of gas or solids. The ESP keeps fluid always moved out of the wellbore, ensuring low bottom hole flowing pressure (BHFP). Some of the drawbacks of an ESP are poor gas and solid handling capacity and high cost; they also require electricity and stringent design criteria.

c. Rod pumping

This is the most widely used form of lift. The energy from the electric or natural gas fired prime mover is transferred to the up-and-down-movement of the rod string and pump to mechanically move fluids from the wellbore. This operation is simple, effective, and well-understood. On the other hand, installing a rod pump requires a relatively higher initial cost, especially for electric units. Rod pump efficiency is reduced at higher depths and higher deviations; also, they do not operate well in the presence of both solids and gas. From a safety standpoint, having moving parts can constitute a danger while operating.

d. Gas lift (GL)

During gas lift operations, a desired amount of gas is added to the well through the mean of injection to lighten the hydrostatic head caused by liquid accumulation in the wellbore; this allows the formation to continue producing at a lower BHFP and the liquid to move outside the wellbore. The advantage of gas lift is its capacity for handling both gas and solids in addition to the absence of downhole moving parts that

can restrict the flow from the reservoir. Disadvantages include requiring a compressor at the surface, a reliable supply gas source, and installation cost.

Gas lift can be either conventional or unconventional. Conventional GL requires the installation of a packer set below a series of gas lift valves spaced along the tubing to act as ports for gas entry. Unconventional GL only requires open-ended tubing where the end of tubing is considered to be the injection point, and gas is allowed to enter and lift fluid from that depth. Unconventional GL is also referred to in the industry as continuous gas circulation (CGC).

In this study, CGC was used to add gas to the well to identify the effective gas rate for horizontal and deviated wells.

CHAPTER III

Literature review

3.1 Vertical well models

Turner et al. (1967; 1969) pioneered the effort to understand the causes of liquid loading. In their work, they pursued both a film model and a droplet model and concluded that the film model was not adequate because it did not fit their data. However, the droplet model, when compared to the 106 wells included in their data set, had a good fit after adjusting it by a certain factor. Turner suggested increasing the Webber number to 60 to better fit the observed data. This increase resulted in, as mentioned earlier, approximately 20% upward adjustment to the derived Eq. 2.10. Turner believed that the increase compensates for the assumptions made while deriving the equation, such as:

- The use of the drag coefficient for solid spheres.
- The effect of natural gas on the Webber number as opposed to air as developed by Heinz (1949).
- Assuming the particle becomes stationary when the critical condition is satisfied.

Therefore, the adjusted Turner equation is as follows:

$$V_c = 1.912 \left(\frac{(\rho_l - \rho_g)}{{\rho_g}^2} \sigma \right)^{\frac{1}{4}} \qquad \text{----------} \qquad (3.1)$$

where, V_c is critical gas velocity, ft/sec, ρ_l is the liquid density, lbm/ft^3, ρ_g is the gas density, lbm/ft^3, and σ is the surface tension, dynes/cm. Turner further simplified his equation by using standard values for gas specific gravity, temperature, and the Z factor

to calculate gas density, ρ_g, from the real gas law in addition to assuming a constant water density and surface tension.

The gas density is obtained from the real gas law as follows:

$$\rho_g = 2.715\,\gamma_g\,\frac{P}{(T+460)\,Z} \qquad \text{----------} \qquad (3.2)$$

where γ_g is the gas specific gravity, T is the evaluating point temperature in ^oF, P is the evaluating point pressure in psia, and Z is the Gas Deviation Factor.

Substituting $\gamma_g = 0.6$, T=60 ^oF, Z= 0.9 into Eq. 3.2 and simplifying, we get:

$$\rho_g = 0.0031P \qquad \text{----------} \qquad (3.3)$$

Equation 3.1 can then be re-written using Eq. 3.3 and the typical values of water density ρ_w= 67 lbm/ft^3, oil density ρ_o = 45 lbm/ft^3, water surface tension σ_w = 60 dynes/cm, and oil surface tension σ_o = 20 dynes/cm as follows:

Therefore, for condensate, the equation is:

$$V_c = \frac{4.043\,(45-0.0031P)^{\frac{1}{4}}}{(0.0031P)^{1/2}} \qquad \text{----------} \qquad (3.4)$$

and for water:

$$V_c = \frac{5.321\,(67-0.0031P)^{\frac{1}{4}}}{(0.0031P)^{1/2}} \qquad \text{----------} \qquad (3.5)$$

Equations 3.4 and 3.5 are the simplified version of the Turner equation for both condensate and water. They yield approximate values. However, for more accuracy, it is advised to use the appropriate correlations for PVT calculations or, if available, to use actual values as described in the original equations. If both phases, oil and water, are produced, it is recommended to use the water equation to account for the heavier phase. Turner used surface as the evaluation point and therefore, did not account for the effects of pressure and temperature changes with depth, or changes in tubular dimensions on

the critical velocity. Turner et al. calculated the critical gas rate for the 106 vertical wells included in their data set.

The results from the calculation were compared to the well status to check if the Turner model predicts the actual well flow condition. For example, if the calculated Turner value was higher than the actual flow rate while the well status shows it to be unloaded, then the model did not predict the well condition, and "F" for a false prediction was recorded in the column. On the other hand, if the calculated Turner value was higher than the actual flow rate while the well status shows it to be loaded, then the model was able to predict the well condition, and "T" for a true prediction was recorded in the column. However, if the calculated Turner value was lower than the actual flow rate while the well status show that the well was loaded, then the model was not able to predict the well condition, and "F" for a false prediction was recorded in the column. Finally, if the calculated Turner value was lower than the actual flow rate while the well status show that the well is unloaded, then the model was able to predict the well condition and "T" for a true prediction was recorded in the column. Table 3.1 summarizes the comparison method used by Turner et al.

Table 3.1: Turner et al. critical gas rate predictions compared to actual observed rates

Q_{Turner} vs. Q_{actual}	Well Status	Prediction
$Q_{Turner} > Q_{actual}$	Loaded	T
$Q_{Turner} > Q_{actual}$	Unloaded	F
$Q_{Turner} < Q_{actual}$	Loaded	F
$Q_{Turner} < Q_{actual}$	Unloaded	T

Coleman et al. (1991) presented a series of papers discussing liquid loading onset for low pressure wells, i.e., less than 500 psi. Their study included 56 data points. They

conducted 17 tests in wells that would normally have stable gas rates are above the critical rate. They continuously changed the wellhead flowing pressure (WHFP) of these wells until showing signs of liquid loading. Then they obtained the remaining 39 data points from other gas wells showing a similar trend to determine their critical gas rates. Coleman et al. (1991) then compared the Turner equation to all 56 wells and concluded that the 20% adjustment suggested by Turner is not necessary for wells flowing at less than 500 psi. They also proposed, like Turner, that the water equation should always be used, even if only condensate is produced. This is because water vapor is always present due to water condensation throughout the wellbore length as both pressure and temperature drop. Coleman et al. (1991) stated that liquid load up effects can be far more severe than a mere drop in daily production rate and may cause a reduction of reservoir deliverability. They also stated that, in some cases, water condensation can cause formation damage in formations that contain swelling clays.

Hence, the Turner Eq. 2.10 should stay unchanged (without the 20% upward adjustment). Therefore, for condensate, the equation is:

$$V_c = \frac{3.369\,(45-0.0031P)^{\frac{1}{4}}}{(0.0031P)^{1/2}} \qquad \text{----------} \qquad (3.6)$$

and for water,

$$V_c = \frac{4.434\,(67-0.0031P)^{\frac{1}{4}}}{(0.0031P)^{1/2}} \qquad \text{----------} \qquad (3.7)$$

Coleman et al. (1991) mentioned that temperature, gas and liquid specific gravities, and interfacial tension do not have as significant effect on critical velocity as tubular dimension and flowing pressure. They stated that the surface conditions can be used as a control point to determine the critical rate. However, if the end of the tubing is set at a

significant distance from the producing interval, the larger diameter should be used for the calculation.

Nosseir et al. (2000) noted that the turbulent flow regime assumed by Turner, $10^4 < N_{Rep} < 2x10^5$, is not necessarily true in all cases. In addition, in some low flow rate wells, the flow regime is rather transitional. In the latter case, the use of Allen's method, Eq. 3.8, for the purpose of calculating the critical gas velocity is more appropriate. The proposed equation is as follows:

$$V_c = 14.6\,\sigma^{0.35}\frac{(\rho_l-\rho_g)^{0.21}}{\mu^{0.134}\times\rho_g{}^{0.426}} \qquad \text{----------} \quad (3.8)$$

where, density ρ_l in lbm/ft^3, gas density ρ_g in lbm/ft^3, and σ surface tension in dynes/cm, and viscosity μ in lbm/ft/sec..

Nosseir et al. (2000) calculated the particle Reynolds number (N_{Rep}) for Turner's data and another set of data provided by Exxon. They found that the Reynolds number for the Turner data exceeded the 200,000 value and for those conditions, the drag coefficient is 0.2 (see Fig. 2.2). However, for Exxon's data, the calculated N_{Rep} fell within the Turner assumed region and, in that case, the drag coefficient was indeed 0.44. The results from incorporating the calculation of N_{Rep} causes the estimation of the critical gas velocity to increase by 5% compared to the method proposed by Turner et al. The new proposed equation is as follows:

$$V_c = 21.3\,\sigma^{0.25}\frac{(\rho_l-\rho_g)^{0.25}}{\rho_g{}^{0.5}} \qquad \text{----------} \quad (3.9)$$

Their results showed that while the Turner model had a 23.5% error and the adjusted Turner model had an 11.5% error, their model, on the other hand, was able to reduce the

error to 8.3% (see Figs. 3.1 and 3.2). Nosseir et al. (2000) also recommended that the calculations be carried out at the wellhead because that is where gas slippage and velocity is at its maximum value. Furthermore, the water properties should be used to account for the denser phase.

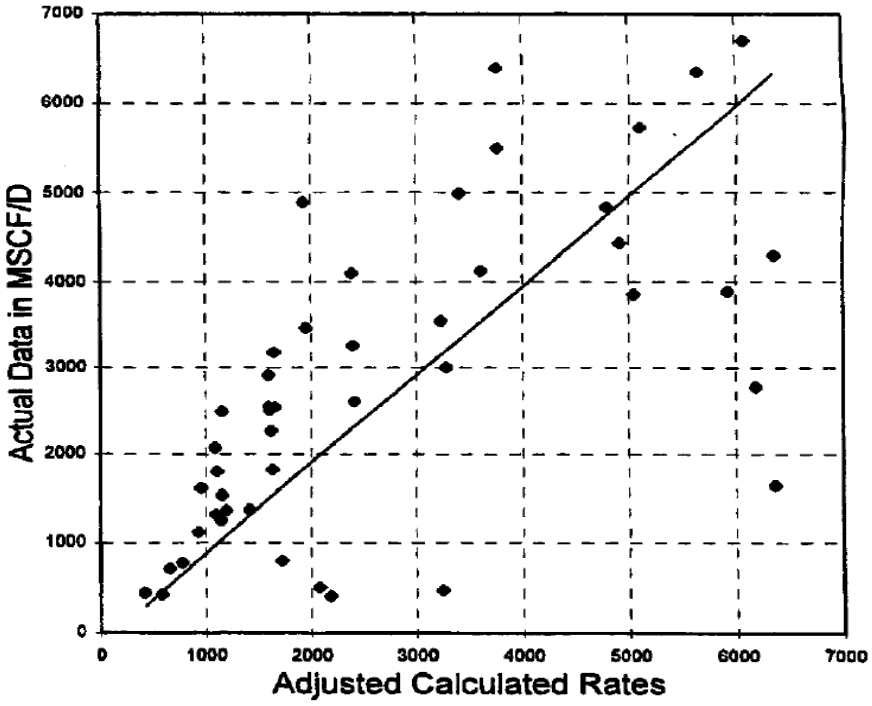

Figure 3.1: Rates from the adjusted Turner model compared to the actual Turner observations, Turner et al. (1969)

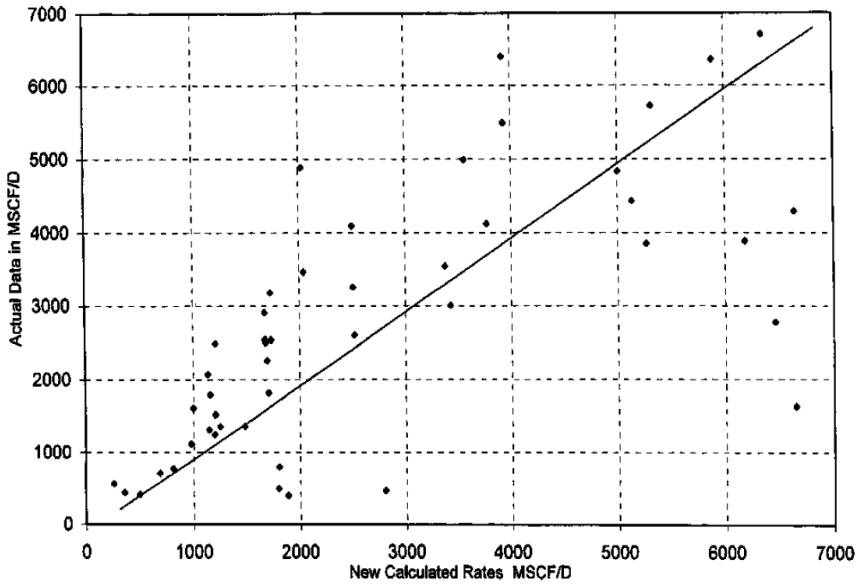

Figure 3.2: Rates from the Nosseir model compared to actual Turner observations, Nosseir et al. (2000)

Li et al. (2002) showed that a liquid droplet entrained in a high velocity gas stream will experience a pressure difference between its fore and aft regions, causing it to deform and flatten to a convex bean shape with unequal sides (see Fig. 3.3). This deformation affects the drag on the droplet as the spherical form has a lower surface area compared to flat shapes, and which requires a reduced drag to counter the force of gravity.

$$V_c = \sqrt[4]{\frac{4\,(\rho_l - \rho_g)}{C_{D\times}{\rho_g}^2} \times g \times \sigma} \qquad \text{----------} \qquad (3.10)$$

Based on the new shape, Li et al. (2002) suggested that a disk-shaped curve be used on the drag coefficient chart (Fig. 2.2) for the applicable N_{Rep} range that Turner suggested. Therefore, the drag coefficient will be close to 1. Substituting $C_d = 1$ and $g = 9.8$ m/sec^2 into Eq.3.10 which is referred to as the Li equation, we get:

$$V_c = 2.5 \times \sqrt[4]{\frac{(\rho_l - \rho_g)}{{\rho_g}^2}\,\sigma} \qquad \text{----------} \qquad (3.11)$$

where, density ρ_l in Kg/m^3, gas density ρ_g in Kg/m^3, and σ surface tension in N/m.

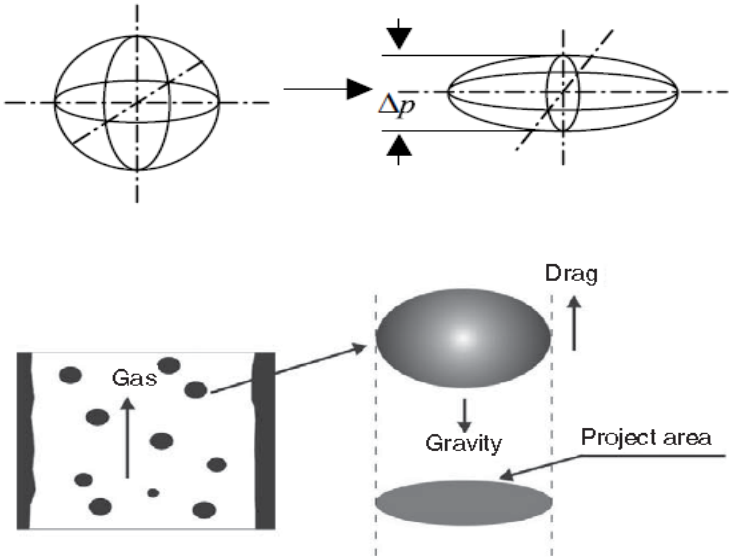

Figure 3.3: Shape of entrained drop movement in high-velocity gas, Li et al. (2002)

They also presented a simplified form of the equation in the same manner as Turner et al. that is based on fixed values of gas specific gravity, temperature, Z factor, water density, and surface tension. Li et al. (2002) compared data from 16 wells to the Turner model and concluded that the latter overestimates the critical rate while their approach has a better match which, in their view, might explain why some wells are still operating at the sub-Turner critical rate.

Unlike Li et al.'s (2002) view that Turner equation overestimates the critical gas rate, Guo et al. (2006) stated that the Turner equation underestimates the minimum critical gas rate. They presented a 4-phase kinetic energy model to estimate the minimum gas lift energy needed to maintain continuous liquid removal from the well. They started with the Turner equation and used the kinetic energy formula to arrive to the following:

$$E_k = \frac{\rho_g \times V_c}{2\, g_c} \qquad \text{----------} \qquad (3.12)$$

Equation 3.12 represents the minimum kinetic energy required to keep liquid droplets from falling. Guo et al. (2006) substituted the Turner critical velocity in Eq. 3.12 and used 0.44 as the value of the drag coefficient. They neglected the effect of gas density; therefore, the equation was reduced to:

$$E_k = 0.04\sqrt{\sigma\rho_l} \quad \text{----------} \quad (3.13)$$

where, density ρ_l in lbm/ft^{3}and σ surface tension in dynes/cm.

By assuming values for water-gas and condensate-gas interfacial tensions to be 60 and 20 dynes/cm respectively, and water and condensate densities to be 65 and 45 lbm/ft^3 respectively, Guo et al. (2006) stated that the minimum kinetic energy value for gas wells producing water should be 2.5 lbf-ft/ft^3 and for condensate, to be 1.2 lbf-ft/ft^3. Guo et al. (2006) subsequently deduced that the 20% adjustment proposed by Turner is the velocity needed to transport the particle from stagnation. Therefore, he proposed the following equation as the minimum kinetic energy needed to transport liquid droplets:

$$E_{km} = 0.0576\sqrt{\sigma\rho_l} \quad \text{----------} \quad (3.14)$$

Thus, Guo et al. (2006) proposed that the minimum required kinetic energy value for gas wells producing water to be 3.6 lbf-ft/ft^3 and for condensate, only to be 1.73 lbf-ft/ft^3. They calculated gas kinetic energy from any given gas well as compared to the minimum required kinetic energy to determine the loading status of the well. To evaluate the kinetic energy of a given well, Guo et al. (2006) proposed substituting the gas density by using the ideal gas law and refined the gas kinetic energy as follows:

$$E_k = 6.46 \times 10^{-13}\ \frac{\gamma_g \times T \times {q_g}^2}{A^2 \times P} \quad \text{----------} \quad (3.15)$$

where, γ_g is the gas specific gravity, q_g is gas rate in scf/day, A is the flow conduit cross-sectional area in ft^2, and P is the pressure in psia, and T is temperature in ^{o}R.

Equation 3.15 indicates that the controlling conditions for liquid loading calculations are bottom hole, which is contrary to Turner et al.'s view that surface conditions are in most cases the controlling point.

Guo et al. (2006) proposed a correlation to calculate pressure variation along the wellbore and used it for the critical rate calculation. Then they compared their method to the 106 data points in Turner's paper and found that their method predicted 6 loaded points in the unloaded region, as compared to 9 from the Turner method (Fig. 3.4). Therefore, they concluded that their method is more accurate in estimating the required minimum gas flow rates.

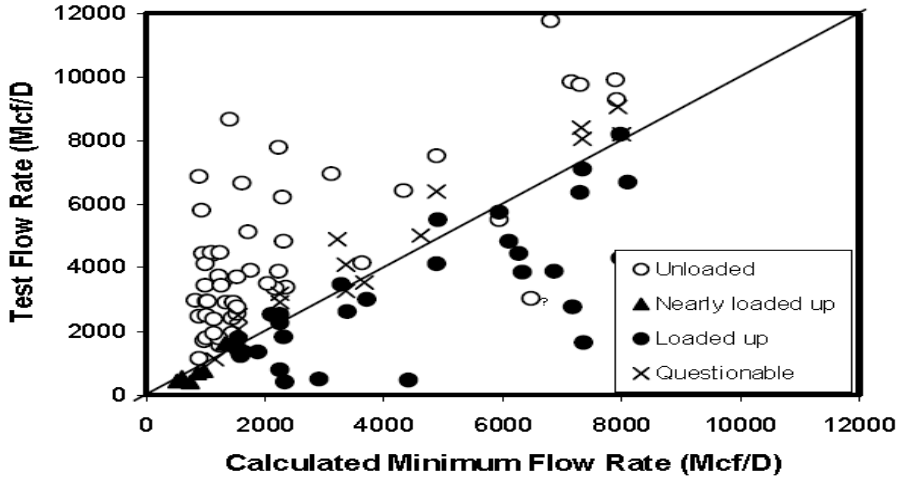

Figure 3.4: The minimum flow rate calculated using Guo et.al method mapped against the test flow rate, Guo et al. (2006)

Wang and Liu (2007) presented the shape of the liquid droplet as a disk rather than a sphere, with N_{Rep} ranging from 10^4 to 10^6, and the Morton number (a dimensionless number used to distinguish droplet shape) for the low viscosity liquid in gas wells as possibly between 10^{-10} and 10^{-12}. The corresponding drag coefficient for these

conditions is approximately 1.17. They presented their version of the critical velocity calculation as follows:

$$V_c = 0.5213\left(\frac{(\rho_l-\rho_g)}{\rho_g{}^2}\sigma\right)^{\frac{1}{4}} \qquad \text{----------} \quad (3.16)$$

where, density ρ_l in Kg/m^3, gas density ρ_g in Kg/m^3, and σ surface tension in N/m. Needless to say, their method predicts critical values significantly lower than the Turner method. Therefore, caution needs to be taken while using this method.

In 2010, Zhou et al. investigated the effect of liquid amount on the critical velocity calculation. They stated that the Turner model, even after the 20% adjustment, still underestimates the critical velocity, causing wells with liquid loading issues to continue to be loaded up. Zhou et al. (2010) stated that there is a threshold value of liquid amount in gas-liquid mixtures, above which liquid loading might appear even if the critical gas velocity of the well is higher than the calculated values by the Turner model. They stated that in high velocity gas wells, the flow is turbulent and the droplet may move irregularly in all directions, which might cause droplets to coalesce and start falling, only to break and be repeatedly picked up again by the gas stream (see Fig. 3.5).

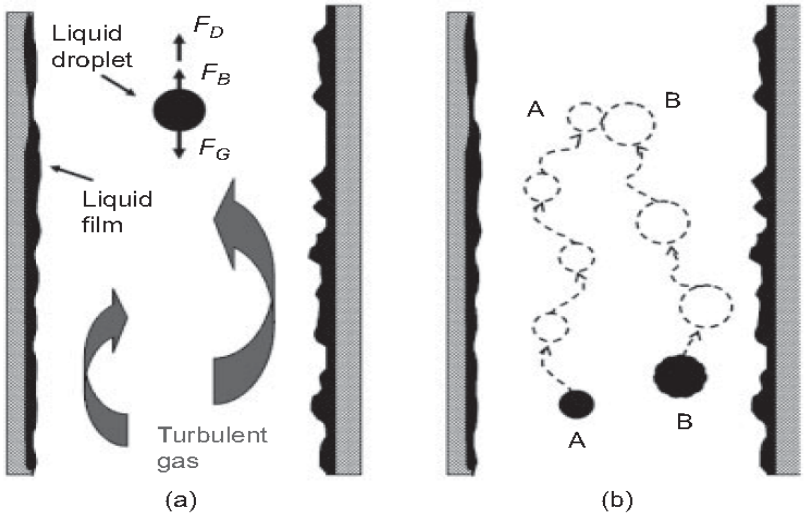

Figure 3.5: Encountering two liquid droplets in turbulent gas stream, Zhou et al. (2010)

Zhou et al. (2010) used both Turner et al. (1969) and Coleman et al. (1991) data to calculate the β_z factor as the droplet concentration and set the threshold value of 0.01. They also relied on Barnea's (1987) work, which states that the flow regime changes from mist flow to a slug or churn flow pattern when the liquid holdup value is higher than 0.24. Zhou et al. (2010) defined H_L as follows:

$$H_L = \frac{V_{sl}}{V_{sg}+V_{sl}} \qquad \text{----------} \qquad (3.17)$$

where, V_{sl} is superficial liquid velocity, and V_{sg} is superficial gas velocity.

Therefore, they stated that the Turner equation should be used when H_L is less than or equal to 0.24, and their equation should be used at values higher than 0.24. Their proposed equation included an additional term to the original Turner equation (also referred to as the Coleman equation) as follows:

$$V_{C-N} = V_{C-Turner} + ln\left(\frac{H_L}{\beta_z}\right) + \alpha_z \qquad \text{----------} \qquad (3.18)$$

where β_z = 0.01, and α_z = 0.6, as estimated from Turner's data. β_z, as mentioned earlier, is the GLR, and alpha is a curve fitting constant.

While comparing their model to Coleman's data, all calculated β_z values were less than the threshold (Fig. 3.6). Therefore, the model prediction is the same as the Turner model which, in turn, is better than the adjusted Turner model. The latter conclusion was similar to the conclusion that Coleman deduced. However, when using the original Turner et al. data, the Zhou et al. (2010) model showed an improvement in prediction from both Turner and adjusted Turner models. The Zhou model had 12 incorrectly predicted wells, as opposed to 24 from the Turner model and 13 from the adjusted Turner model (see Fig. 3.7).

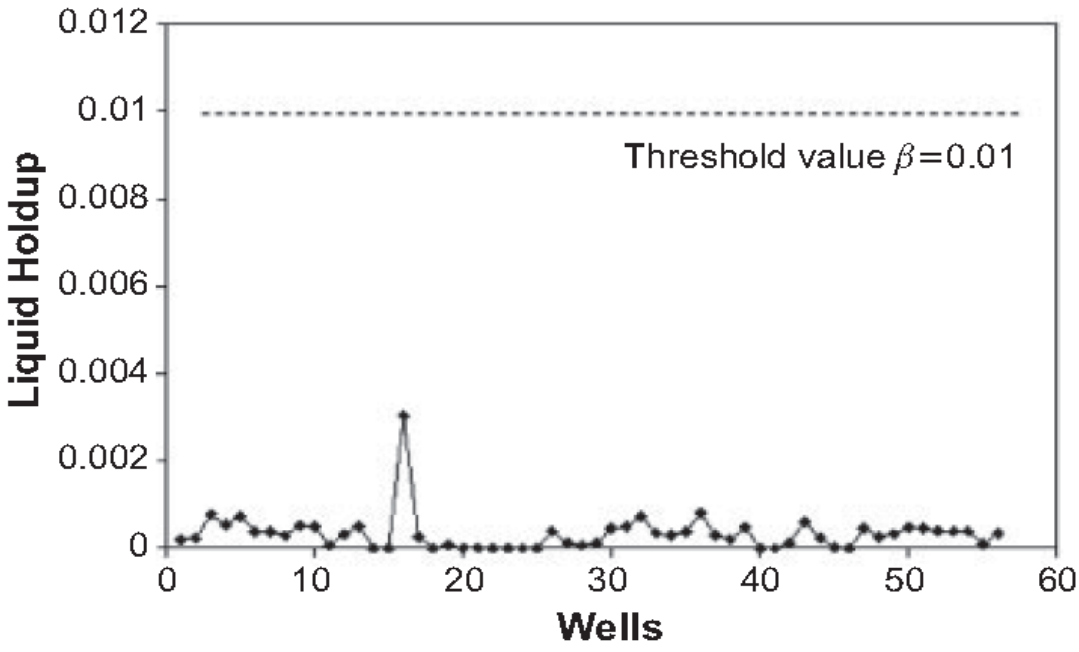

Figure 3.6: Application of the Zhou et al. model to Coleman et al. data, Zhou et al. (2010)

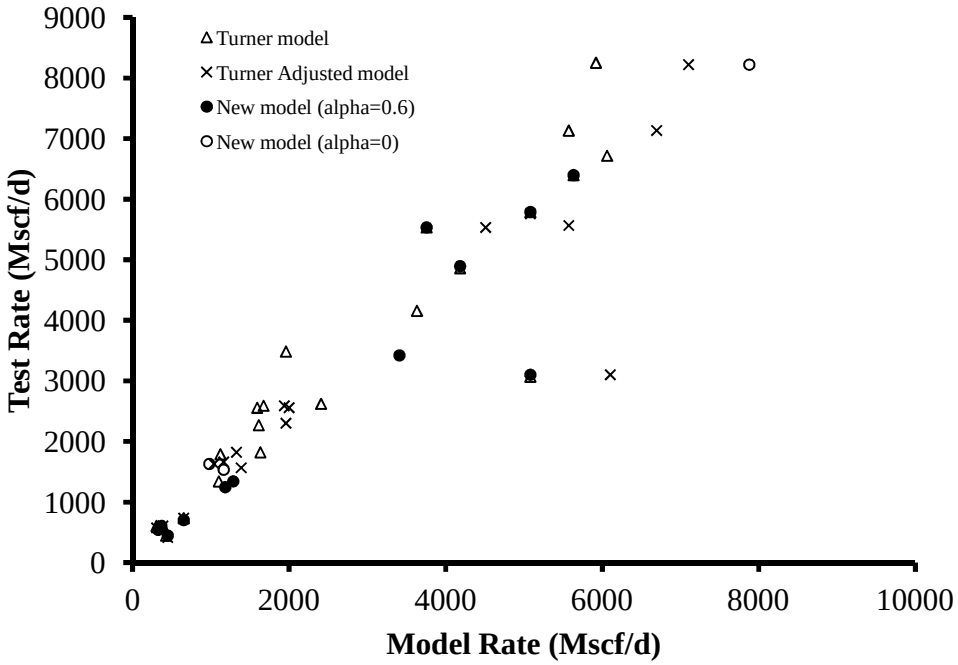

Figure 3.7: Zhou et al. model versus the Turner Model, Zhou et al. (2010)

Guohua et al. (2012) introduced an energy loss factor. To arrive at their conclusion, they started with Li's equation and relied on both Wei et al.'s (2007) experiment with high speed photographic techniques (Fig. 3.8) and Awoulsi's (2005) laboratory data (Fig. 3.9). They concluded that the reason why Turner equation over predicts the critical velocity is because Turner does not account for droplet deformation in low pressure conditions. They also invalidated Li's model, citing that it under predicts the critical gas rates because it does not take into account the rollover of the flat shaped droplet, which causes it to have a reduced bearing area. Guohua presented the following equation:

$$V_{CS} = V_{C,Li} + S \times (V_{C,Turner} - V_{C,Li}) \quad \text{----------} \quad (3.19)$$

Equation 3.19 reduces to Li's equation when the loss factor, S, is equal to zero, and the larger the S factor, the closer the model is to the Turner model.

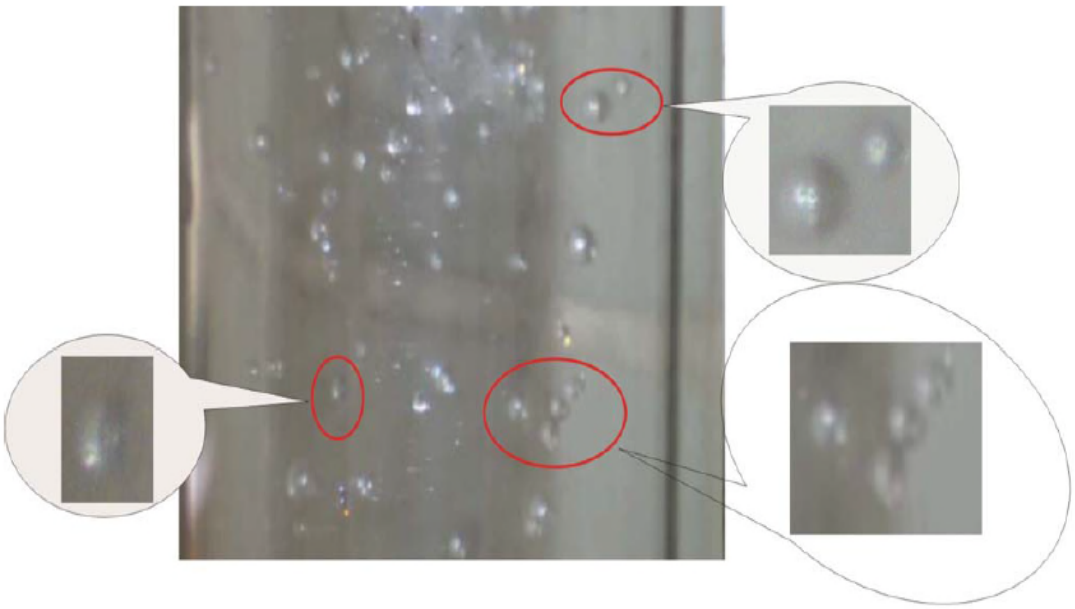

Figure 3.8: Rollover of the flat-shaped droplets in the process of rising, Wei et al. (2007)

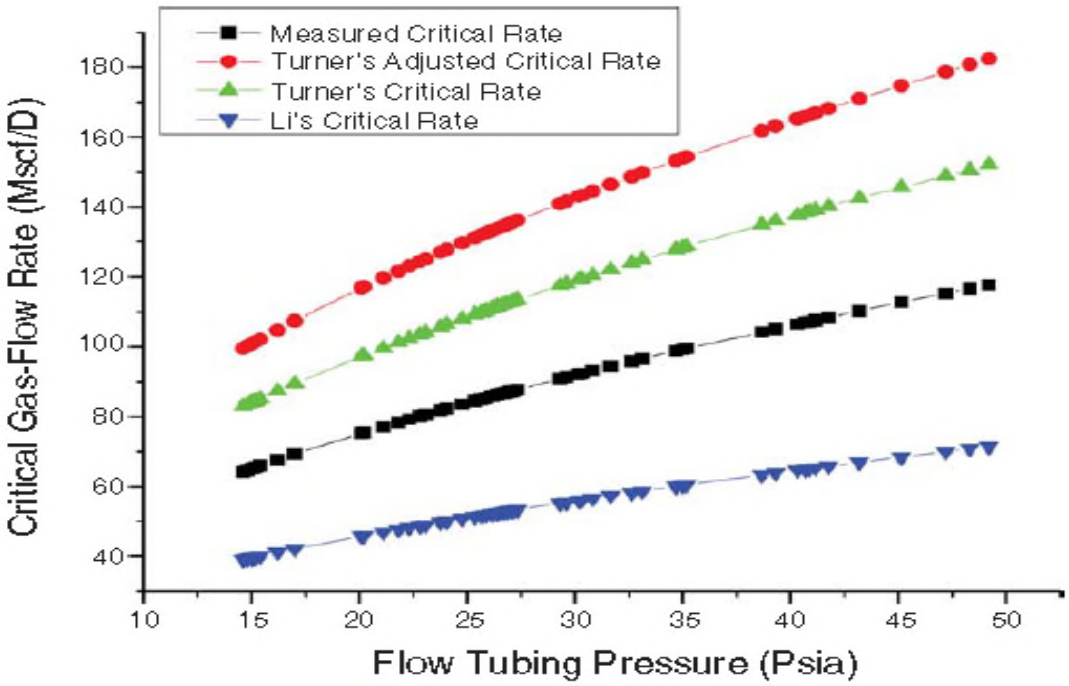

Figure 3.9: Critical gas flow rates comparison between different models, Awolusi (2005)

To determine the value of the S factor in Eq. 3.19, Guohua et al. (2012) used data from 300 wells to estimate the loading condition. They fitted their model to actual data by changing the S factor value. Their results showed that the S factor ranges from 0.75 to 0.83. Therefore, they used the upper limit of the S factor for their model as follows:

$$V_{CS} = V_{C,Li} + 0.83 * (V_{C,Turner} - V_{C,Li}) \quad \text{----------} \quad (3.20)$$

When Guohua et al. (2012) used Coleman's data to compare their model predictions to Coleman et al.'s (1991) results (Fig. 3.10), they found that their model's average absolute relative error (Table 3.2) is 0.2553, which is less than both Coleman, 0.2806, and Li, 0.4945. Therefore, they concluded that their model is more suitable for critical velocity prediction in low pressure gas wells less than 500 psi.

Table 3.2: Average absolute relative error from the Guohua et al. model using Coleman et al. data, as compared to Li and Turner models, Guohua et al. (2012)

TABLE 2—ERROR ANALYSIS OF THE THREE MODELS

Model Name	Average Absolute Relative Deviation	Correlation Coefficient
Turner's Model	0.2806	0.8033
Li's Model	0.4945	0.7750
New Model	0.2553	0.8033

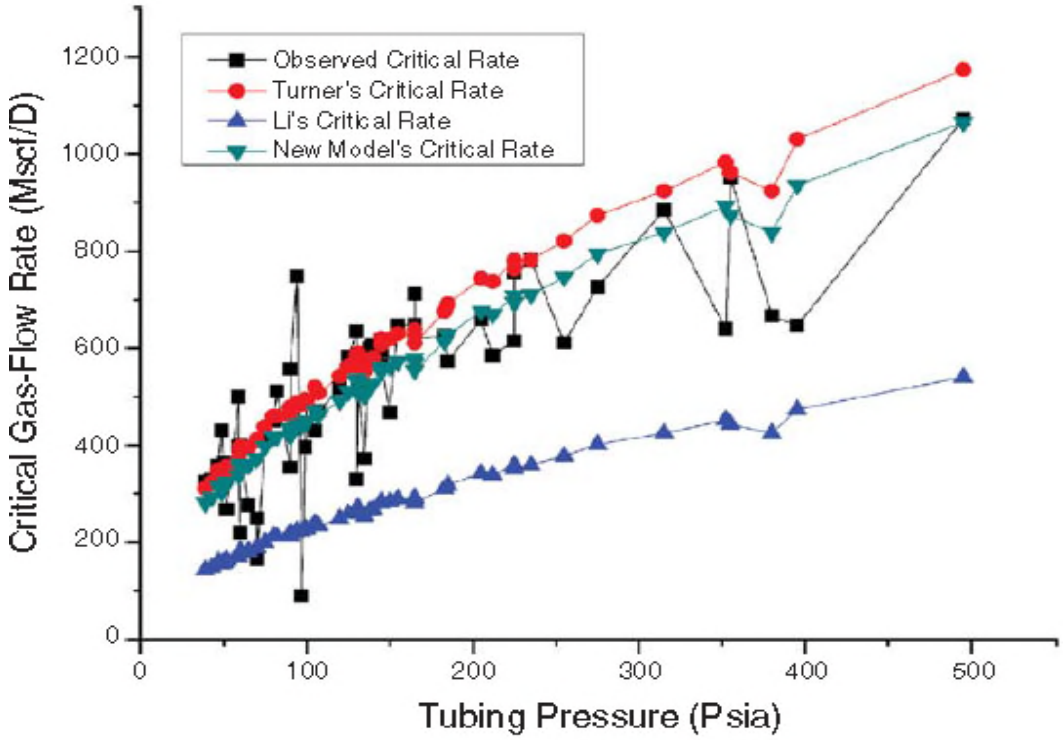

Figure 3.10: Comparison of the different models using Coleman et al. data, Guohua et al. (2012)

3.2 Horizontal well models

Veeken et al. (2009) investigated the influence of reservoir parameters and well parameters on the critical rate value. They found that the strongest correlation exists between the Turner Ratio (TR) and the observed critical rate (q_c) by using a quadratic fitting (Fig. 3.11). The Turner Ratio is expressed as follows:

$$TR = \frac{q_c}{q_{Turner}} \quad \text{----------} \quad (3.21)$$

They proposed a new equation to identify the relationship between the critical rate and the calculated Turner critical rate as follows:

$$q_c = \frac{\left\{(1-bQ_{Turner})-\left[(bQ_{Turner}-1)^2+4a.c.Q_{Turner}{}^2\right]^{0.5}\right\}}{2a.Q_{Turner}} \quad \text{----------} \quad (3.22)$$

where, a = $-2.17\text{x}10^{-6}$, b = $3.09\text{x}10^{-3}$, and c = 1.02.

Equation 3.22 is referred to as modified Turner and is limited to q_{Turner} less than $300x10^3$ m^3/d (both q_c and q_{Turner} are in $10^3 m^3/d$).

Based on their study, they stated that inflow performance has no significant effect on liquid loading, while deviation has limited influence, a 15% increase in critical rate at 30–35 degree inclination. They also concluded that the outflow performance is not affected by larger internal diameter (ID) if the length is less than 10% the total well length. Veeken's multiphase study using the modified Gray (1978) equation for BHFP calculation agreed with the modified Turner critical rate calculation and showed that the rate increase is not necessary for low gas rate wells, which is in line with the Coleman finding for low pressure wells. Lastly, based on both flow loop testing and transient multiphase flow modeling, Veeken et al. (2009) concluded that liquid loading is not controlled by droplet flow reversal, as conventionally understood, but is rather triggered by liquid film flow reversal.

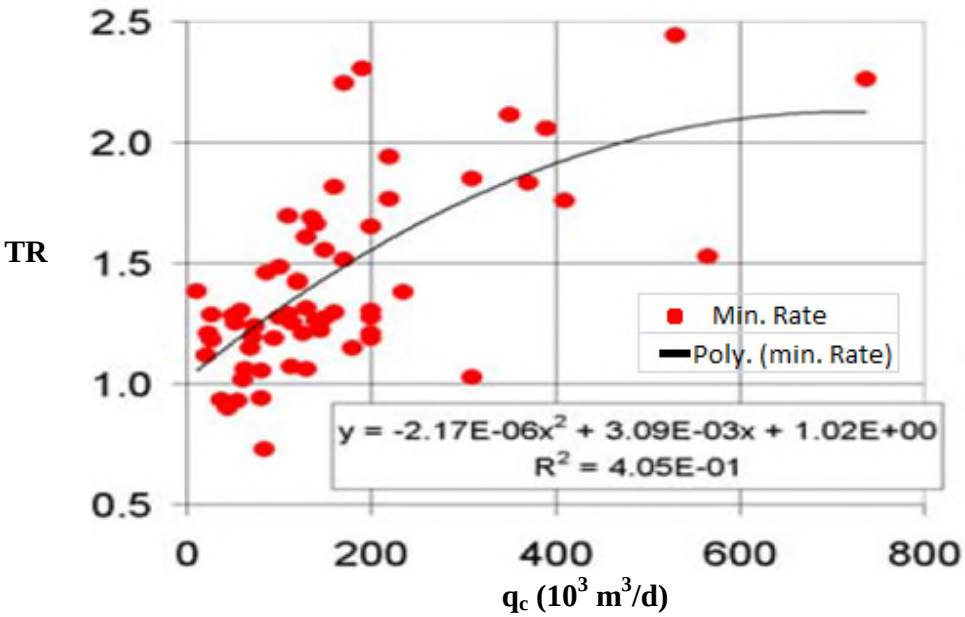

Figure 3.11: The Turner Ratio as function of observed critical rate, Veeken et al. (2009)

Belfroid et al. (2008) stated that steady state models, like Turner, underestimated the critical rate of gas wells. They discussed the effects of hole inclination, flow regime transition, and the interaction between the tubing outflow and reservoir performance on liquid loading. They used the work by C.A.M. Veeken NAM (2009) (Fig. 3.12) and the definition of the Turner Ratio (Eq. 3.21) to compare the calculated critical rate to the actual rate. They defined a reservoir parameter function, A, as a proxy of reservoir permeability and reported that high permeability wells (low reservoir parameter A) do not respond well to dynamic disturbances and may require twice the Turner criterion, while high A parameter wells seem to cope better with dynamic conditions.

Subsequently, they conducted an experiment where they subjected both high and low A parameter type wells to multiple GLR changes and then measured the liquid holdup over time. Their results showed that the high A parameter wells were able to move the liquid up the tubing while for the low A parameter wells, liquid dropped and

accumulated at the bottom of the well. The latter wells could not restart or reverse this trend, which caused them to cease flowing (Figs. 3.13 and 3.14).

As far as the influence of the inclination angle (Fig. 3.15), Belfroid et al. (2008) believed that the influence of gravity diminishes as the well moves towards a horizontal geometry. They stated that for a horizontal well, no liquid loading can occur because of the absence of forces on the liquid that can counter the gas flow. They also mentioned that the change from horizontal stratified flow to vertical distributed flow driven by inclination allows for the liquid film to be progressively thicker at the bottom compared to the top of the tube. Therefore, both the diminishing effects of gravity and the film thickening affect the critical gas rate such that it increases with medium inclination as a proxy to increased film thickness, while the lower effect of gravity is sensed at higher inclinations (Fig. 3.16). The maximum required rate is identified to occur at a 50^{o} inclination, at which the critical velocity required is 40% higher than that predicted by vertical models.

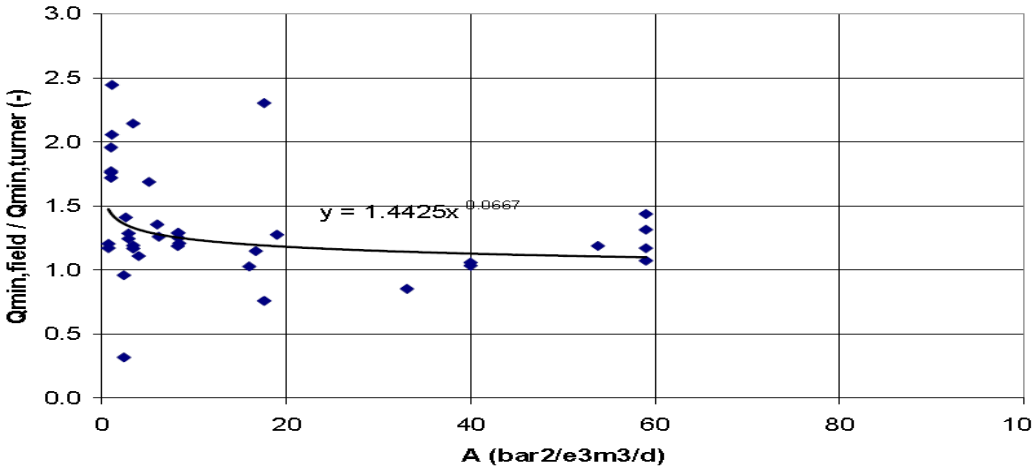

Figure 3.12: Liquid loading point made dimensionless with the Turner criterion, as function of reservoir parameter A, Veeken et al. (2009)

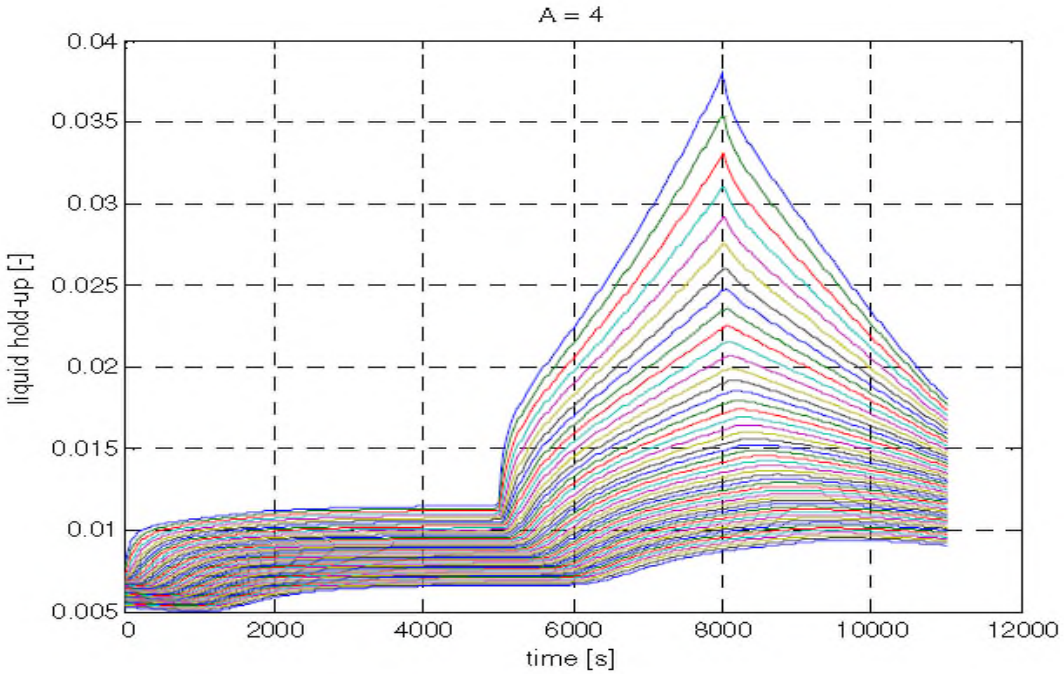

Figure 3.13: Liquid holdup as function of time for high reservoir parameter A, Belfroid et al. (2008)

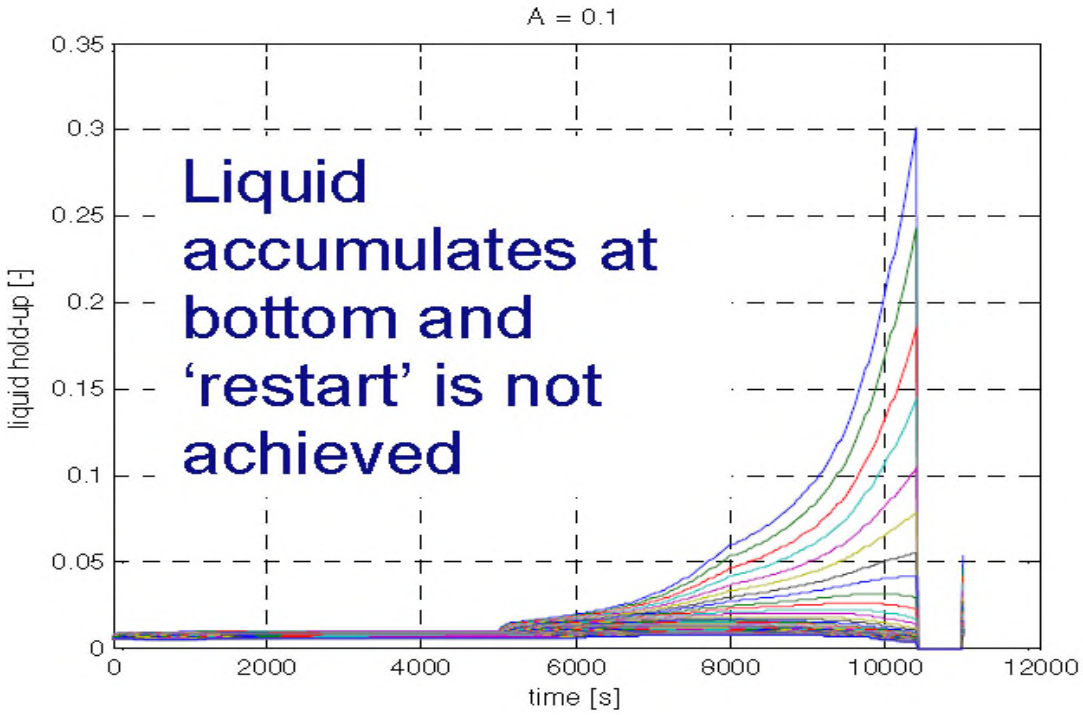

Figure 3.14: Liquid holdup as function of time in low reservoir parameter A, Belfroid et al. (2008).

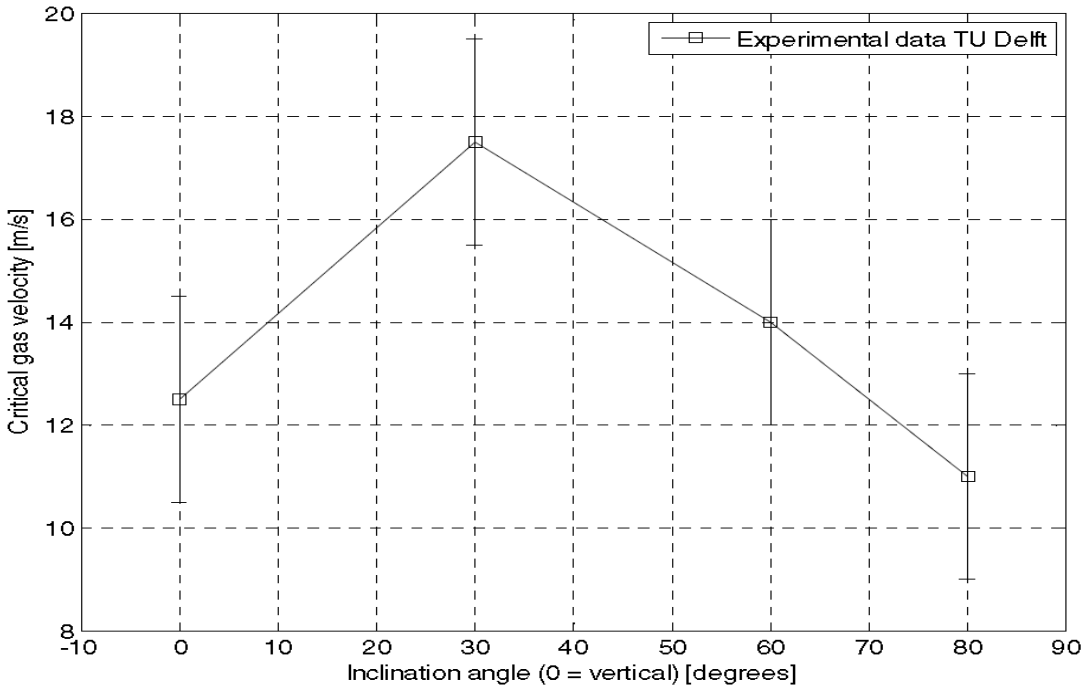

Figure 3.15: Critical gas velocity as function of inclination angle, Belfroid et al. (2008)

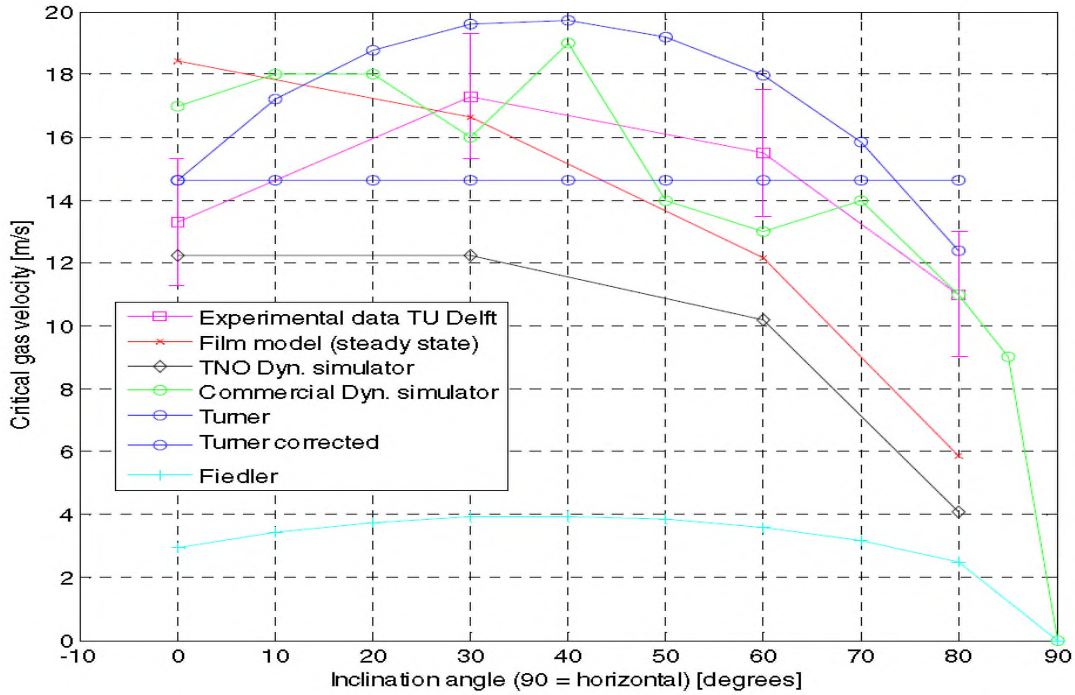

Figure 3.16: Comparison between experiment and model predictions, Belfroid et al. (2008)

In order to incorporate the inclination dependency, Belfroid et al. turned to the Fiedler shape function from flooding experiments because it captures the dependence on the inclination angle, ω. They concluded that a modified Turner model that incorporates the Fiedler shape function would be better at predicting the critical rate in deviated wells. The resulting equation is as follows:

$$V_c = 1.593\left(\frac{(\rho_l-\rho_g)}{{\rho_g}^2}\sigma\right)^{\frac{1}{4}} \times \frac{(sin\,(1.7\omega))^{0.38}}{0.78} \quad \text{----------} \quad (3.23)$$

Finally, predictions from Eq. 3.23 were compared to the experimental results from their air-water experiment and two gas wells. They found that the equation predicts the observed loading point within 20% accuracy (see Table 3.3).

Table 3.3: Comparison of the Belfroid model in the form of Turner Ratio to actual field data, Belfroid et al. (2008)

	Inclination Angle	Experiment /field data	Commercial dynamic model [-]	TNO dynamic model [-]	Turner (bottomhole, angle adapted)
Well-1	40	90000 Sm^3/day	2.1	-	1.2
Well-2	40	45000 Sm^3/day	1.6	-	0.9
Air –Water	0	13.3 m/s	1.3	0.9	1.1
	30	17.5 m/s	0.9	0.9	1.1
	60	15.5 m/s	0.9	0.7	1.2
	80	11 m/s	1.0	0.4	1.1
Error			±110%	-60%	±20%

Among all literature discussed earlier, only Belfroid et al. (2008) and Veeken et al. (2009) work specifically is focused on dealing with horizontal and deviated wells. For this study, in addition to our experimental data and the data from both of these authors will be evaluated using our method and compared to the Turner model. The change of parameters such as density, surface tension, and the Z factor with respect to pressure and temperature is significant and should be taken into account when attempting to calculate the critical rate. Therefore, this study will not rely on static values for these parameters and will instead use the Sutton et al. (2010) recommended practice of using appropriate correlations to calculate each of these components.

This study will propose a new model for critical gas rate predictions in horizontal and deviated wells and demonstrate that vertical well models should not be used in horizontal and deviated cases.

CHAPTER IV

New model development

4.1 BUR definition

Before discussing the flow in horizontal wells, it is important to understand how the geometry of this kind of wells is achieved. The subsequent discussion is a high level summary of how the curved section of a well is constructed.

Horizontal wells require drilling a curved section that connects the vertical section of the wellbore to the horizontal section where the desired reservoir is targeted. Normally, deviation does not present an issue in the vertical section (in pad drilling, deviation can present lift issues due to shallow nudges moving the well to the desired interval). However, during the drilling of the curved section, a succession of variable buildup rates (BUR) is utilized to achieve the desired horizontal target. The BUR is the rate of change in angle or deviation in the drilling path, and it is normally measured in degrees/100 ft (see Fig. 4.1). The measurement while drilling tool, MWD, is deployed as part of the drilling bottom hole assembly at a close proximity to the drill bit to provide an inclination and azimuth that, among other things, allows the real-time tracking of the well path and helps the drillers stay on course with the planned well trajectory. The degree of buildup depends on the final desired geometry and should consider both completion and production requirements to maximize the life of the well. Three types of well profiles are:

- Short radius, 5 to 10^{o}/3 ft

- Medium radius (most common), from 6 to 35^{o}/100 ft
- Long radius, 2 to 6^{o}/100 ft

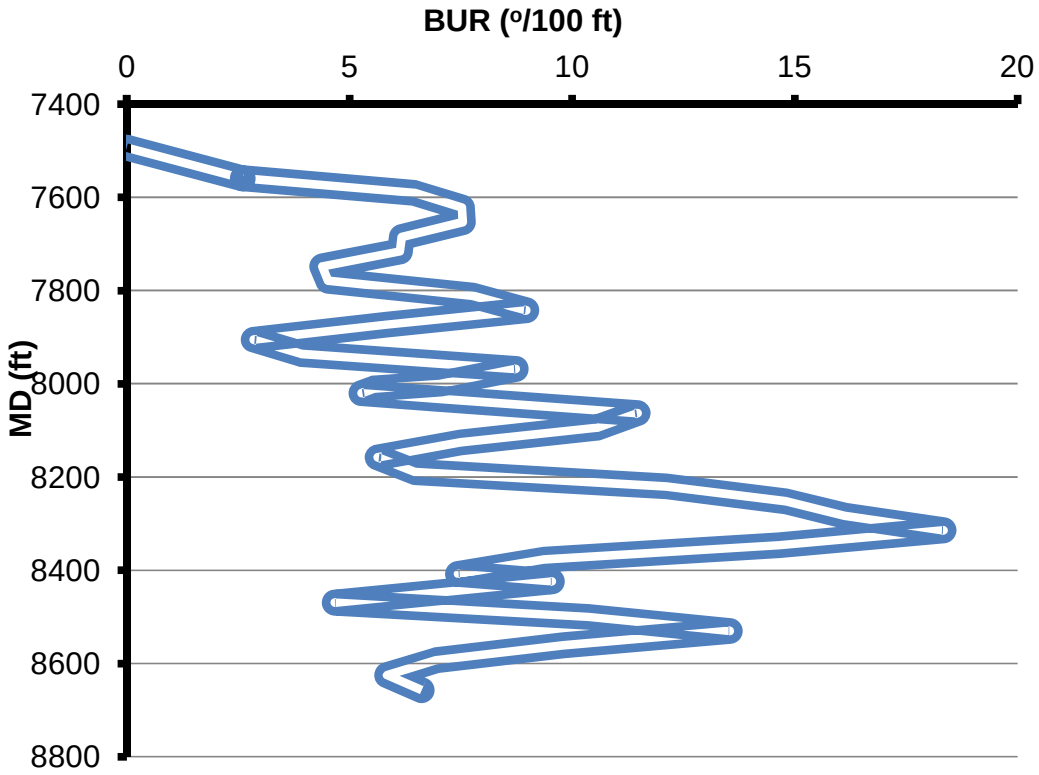

Figure 4.1: Change of BUR versus measure depth (MD) in horizontal and deviated wells

As drilling of the curved section continues, alternating between sliding, using an oriented bent downhole mud motor, and rotating, using the rotation of the entire drill string without directional orientation, allows an average BUR or dog leg severity (DLS) over a given interval. In addition to providing the three-dimensional survey data to track the wellbore progress, the MWD tool transmits the bit's orientation to the surface. Orienting the motor in a particular direction allows for steering the drill bit while in slide mode to stay on target or adjusting it to get back on target. In rotation, the bit is allowed to drift freely in any particular direction. Therefore, the desired BUR is

attained by controlling the ratio of sliding to rotating. Motors can have different bend angles, and 100% sliding gives a uniform BUR for that particular bend setting. However, rotation frequency and duration will control and adjust that theoretical 100% slide BUR down to a lower BUR due to the tangent or uncontrolled well path during that rotation period. Therefore, a 100-ft survey showing 10^o/100 ft does not necessarily mean a uniform BUR. It means that on an average, the BUR is 10^o/100 ft—part of that section could be 15^o/100 ft while sliding and 5^o/100 ft while rotating, hence, an average of 10^o/100 ft.

4.2 Effects of geometry on flow stream

The deviation and change in the wellbore geometry will affect the flow because the gas and entrained droplets stream do not react to the change in geometry until it is affected by it; in other words, the stream does not know that there is a change in geometry coming up ahead, it will only react to it once it is in it. In addition, not all the droplets in a given surface area are going to be directly affected by the change in geometry. Some droplets will be in direct contact with the wall or film, causing a series of impacts and rebounds with a restitution velocity, V_b, and then change direction (see Fig. 4.2). The latter will create a region with slower droplets positioned in the direct path of upcoming streams, which triggers other series of impacts that cause slowdowns of impinging droplets and their reorientation, allowing the whole stream to adjust to the new geometry.

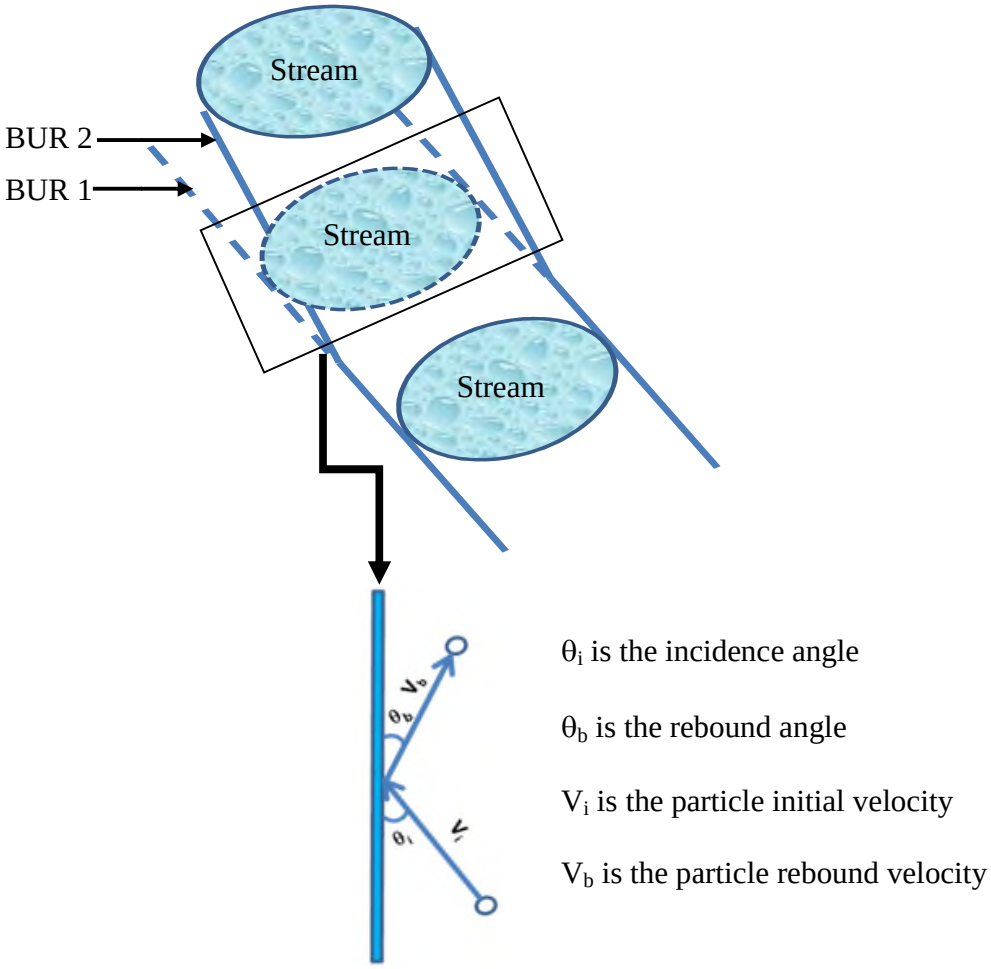

Figure 4.2: BUR effect on particle rebound after impact

Jayaratne et al. (1964) studied the coalescence and bouncing of water droplets at an air/water interface. Their experimental work indicated that for uncharged drops, regardless of the droplet diameter, the fractional energy loss increases with an increasing angle of incidence. For droplets impacting at normal incidence, the fractional energy loss converges to a limiting percentage of approximately 95% (see Fig. 4.3).

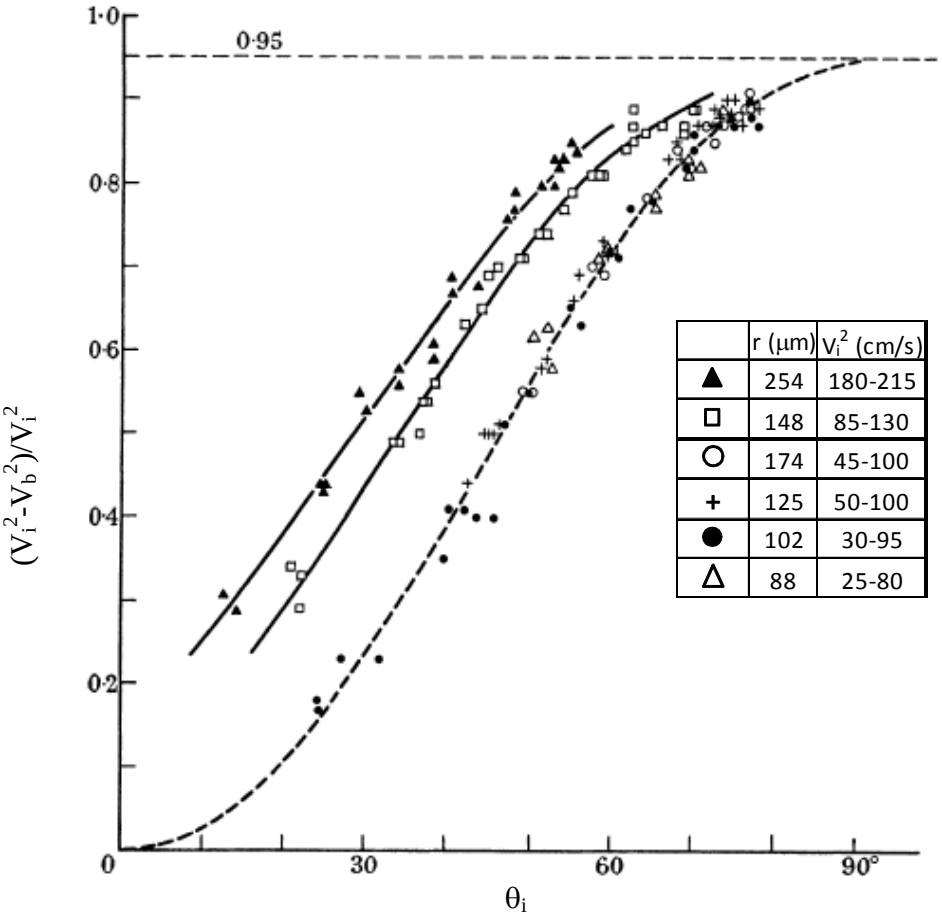

Figure 4.3: Fractional loss of energy suffered by a bouncing drop during impact as function of the angle of impact, Jayaratne et al. (1964)

Jayaratne et al. (1964) also conducted an experiment where the droplets were allowed to impinge almost tangentially on a water surface to simulate low impact angles and concluded that the fractional energy loss is smaller for low impact angles because less energy is consumed to deform the impacted surface. Data for the largest droplet used in their experiment will be used for this study to account for maximum impact. Jayaratne et al. (1964) data are fitted with a power regression model to correlate the fractional energy loss as function of the angle of incidence. Figure 4.4 shows the curve fit with R^2 of 0.98 indicating very good and adequate representation of the data. Therefore, the

fractional energy loss at different angles of incidence can be calculated and used to determine the effect of geometry changes on particle movement post impact.

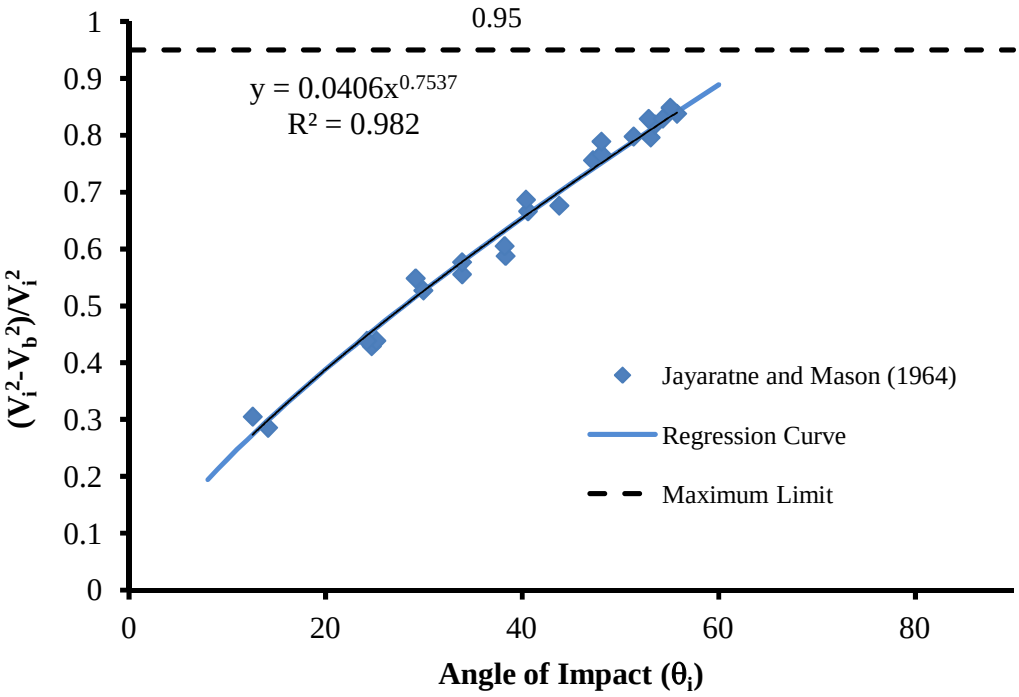

Figure 4.4: Power law fit of the fractional loss of energy suffered by a bouncing drop during impact as a function of the angle of impact

4.3 Effective velocity derivation

At the critical condition, gas is flowing at a critical velocity of $V_g = V_c$ that allows the particles to be suspended with $V_p = 0$. To understand the effect of impact and rebound, the particle will be allowed to travel at a velocity, V_g, while the gas is stationary. When the particle experiences an impact and rebound, it will slow down and have a restitution velocity that is lower than V_g. At this new condition, a stationary particle will experience a drag from the gas that is representative of the restitution condition that is lower than the critical condition; in which case will cause the particle to settle. Therefore, to offset this effect, there should be an "expandable drag" built-in to the

initial condition such that the drag will still allow for the critical condition to exist should an impact occur. Failure to maintain the critical condition will cause the droplet to settle and accumulate.

During the impact process, it is assumed that the droplet does not endure a physical change that affects the force of gravity, i.e.

$$F_{g,before} = F_{g,after} \quad \text{----------} \quad (4.1)$$

To determine the extra energy needed to maintain the critical condition, the following steps should be taken:

1. The critical gas rate should be calculated using the Turner method (Eq. 2.10). The calculated V_c will subsequently be used to calculate the effective velocity as follows:

$$V_{eff} = V_c + V_{mup} \quad \text{----------} \quad (4.2)$$

where, V_{eff} is the effective lift velocity (ft/sec), V_c is the critical velocity as expressed by Turner's derivation (ft/sec), and V_{mup} is the additional velocity above the critical velocity necessary to maintain the critical condition after a rebound (ft/sec).

2. The maximum BUR or DLS is obtained from the survey. Most surveys will have DLS.
3. The fractional energy loss at the maximum BUR or DLS is determined using Jayaratne et al. data, either graphically (Fig. 4.4) or numerically using the power fit equation as follows:

$$\frac{(V_c^2 - V_b^2)}{V_c^2} = 0.0406 \times \theta_i^{0.7537} \quad \text{----------} \quad (4.3)$$

Note that the maximum fractional energy loss is set to an upper limit of 0.95. The latter occurs at high impact angles, θ_i>70^o, which is not a typically encountered BUR in horizontal wells.

4. The restitution velocity is determined from the fractional energy loss

$$\frac{V_b}{V_c} = \alpha \; or \; V_b = \alpha \times V_c \quad \text{----------} \quad (4.4)$$

5. The drag on the particle under the new condition is then determined:

$$\mathrm{F_{d,after}} = \frac{1}{2g_c}\, \rho_g\, C_d\, A_d\, (\alpha V_c)^2 \quad \text{----------} \quad (4.5)$$

Simplifying,

$$\mathrm{F_{d,after}} = \frac{\alpha^2}{2g_c}\, \rho_g\, C_d\, A_d\, V_c^2 \quad \text{----------} \quad (4.6)$$

or,

$$\mathrm{F_{d,after}} = \alpha^2 \times \mathrm{F_{d,before}} \quad \text{----------} \quad (4.7)$$

6. The makeup drag, which is the result of the initial drag and the post impact drag that is needed to offset the fractional energy loss, can then be determined.

$$\mathrm{F_{d,mup}} = \mathrm{F_{d,before}} - \mathrm{F_{d,after}} = (1-\alpha^2)\, \mathrm{F_{d,before}} \quad \text{---------} \quad (4.8)$$

7. The makeup velocity is then obtained from the makeup drag.

$$V_{mup}^2 = (1-\alpha^2)\, V_C^2 \quad \text{----------} \quad (4.9)$$

$$V_{mup} = \beta \times V_C. \quad \text{----------} \quad (4.10)$$

where β is the effective velocity factor.

$$\beta = \sqrt{(1-\alpha^2)} \quad \text{----------} \quad (4.11)$$

8. Finally, by substituting Eq. 4.10 into Eq. 4.2, the effective velocity is calculated to incorporate the makeup velocity in the critical velocity.

$$V_{eff} = V_c + \beta V_C \quad \text{----------} \quad (4.12)$$

or,

$$V_{eff} = (1 + \beta) \times V_C. \quad \text{----------} \quad (4.13)$$

Equation 4.13 represents the critical velocity needed to offset the effect of geometry that is present in horizontal and deviated wells. Note that in vertical case where the BUR, in theory, should be or is close to zero, the model collapses back to the Turner model and no further adjustments are needed.

4.4 Example using the new model

The example presented in this section shows the steps mentioned earlier for a medium-radius horizontal well with a maximum BUR of 20°/100 ft. The droplets in their path out of the wellbore will then face that buildup section and will impact and rebound. Applying Eq. 4.3, the particle will experience a loss of 38.8% of its initial energy.

$$\frac{(V_c^2 - V_b^2)}{V_c^2} = 0.0406 \times (20)^{0.7537} = 0.388 \quad \text{----------} \quad (4.14)$$

or,

$$V_b = 0.78\, V_c. \quad \text{----------} \quad (4.15)$$

The impinging droplet is then rebounded with an effective coefficient of restitution of about 0.78.

The drag on the rebounded droplet reduces after impact; this change can be expressed as:

$$\mathrm{F_{d,after}} = \alpha^2 \mathrm{F_{d,before}} \quad \text{----------} \quad (4.16)$$

or,

$$\mathrm{F_{d,after}} = (0.78)^2 \mathrm{F_{d,before}} \quad \text{----------} \quad (4.17)$$

Simplifying,

$$F_{d,after} = 0.608F_{d,before} \quad \text{----------} \quad (4.18)$$

The needed makeup drag to reinstate the critical condition is:

$$F_{d,mup} = F_{d,before} - F_{d,after} = 0.392F_{d,before} \quad \text{----------} \quad (4.19)$$

Hence,

$$V_{mup}^2 = 0.392V_C^2 \quad \text{----------} \quad (4.20)$$

$$or, V_{mup} = 0.6258V_C. \quad \text{----------} \quad (4.21)$$

Therefore, Eq. (4.2) becomes:

$$V_{eff} = V_c + 0.6258V_c \quad \text{----------} \quad (4.22)$$

$$V_{eff} = 1.6258V_c. \quad \text{----------} \quad (4.23)$$

Substituting Eq. 2.10 into Eq. 4.23 leads to:

$$V_{eff} = 1.625 \times \left[1.593\left(\frac{(\rho_l - \rho_g)}{\rho_g{}^2}\sigma\right)^{\frac{1}{4}}\right] \quad \text{----------} \quad (4.24)$$

Thus,

$$V_{eff} = 2.589\left(\frac{(\rho_l - \rho_g)}{\rho_g{}^2}\sigma\right)^{\frac{1}{4}} \quad \text{----------} \quad (4.25)$$

Finally,

$$q_c = \frac{3.067 \times P \times A \times V_{eff}}{T \times Z} \quad \text{----------} \quad (4.26)$$

In Eq. 4.26, V_{eff} is the effective gas velocity in ft/sec, ρ_l is the liquid density in lbm/ft^3, ρ_g is the gas density in lbm/ft^3, σ is the surface tension in dynes/cm, A is the conduit cross sectional area in ft^2, P is the pressure at the evaluation point in psi, T is the temperature at the evaluation point in ^{o}R, and Z is the gas compressibility factor.

It is noteworthy to mention that a particle, when it falls in a vertical geometry, will go an ample distance before it reaches the bottom. The case is different for horizontal and deviated geometries because, after the impact and rebound, the particle reaches the bottom very quickly. The latter case can create favorable conditions of coalescence either with other particles to start forming a film or as a part of the existing film.

Coalescence occurs if the impact exceeds the force required to expel the thin air film acting as a barrier between the two colliding droplets. Jayaratne and Mason (1964) observed in their study that as the droplet size increases, the critical velocity and impact angle required for coalescence decrease. It is not desirable for coalescence to occur because it significantly affects the force balance for the critical condition, therefore causing a large change in the required critical velocity. For example, in the case of two identical droplets coalescing, the mass of the resulting droplet is double the original droplet, which in turn causes the force of gravity to double. On the other hand, because the newly formed droplet will have a higher volume and, by default, a larger surface area than the original droplet, the drag force will only increase by a factor of $2^{2/3}$, which is not quite as much of an increase on the gravity force, assuming a direct relationship between the two forces. This imbalance would allow the force of gravity to dominate and cause the droplet to fall.

CHAPTER V

New model comparison using literature data

5.1 Horizontal wells

As discussed in the literature review, two authors, Belfroid et al. (2008) and Veeken et al. (2009), have presented data from horizontal wells and the observed critical flow rates associated with them. In this section, the predictions of the effective flow rate from the new model are presented and compared to the critical rate of other models available from the literature.

5.1.1 Comparison at 20^o/100 ft

The first set of data used was taken from the Veeken et al. (2009) paper. They provided 67 data points, including well parameters and their observed critical rates. The new model was applied to data sets of each well. Table B1 in Appendix B shows the wells' data and the calculated predicted critical rates, along with a comparison to the observed critical rates. Conventional vertical models were also used to test their validity in horizontal and deviated wells.

Figure 5.1 shows the deviation of the new model and the Veeken model from the actual observed data. The new model appears to have closer predictions to the observed data with an overall deviation of 19% compared to Veeken model which has 21% deviation. The latter observation is especially true for gas rates less 10,000 Mscf/d where the new model shows even better performance and a reduced deviation of 17.5% from actual. However, For rates higher than 10,000 Mscf/d , the Veeken model shows less deviation

from the observed data than the new model. Under the latter condition, the absolute deviation from the new model is 34% versus 25% for the Veeken model.

The underlying cause behind the shift above 10,000 Mscf/d rate can be due to the fact that at higher flowing gas rates the droplets are broken down and become very small that the effect of gravity becomes minimal and therefore, even after impact and rebound the drag force can still outweighs the gravity force.

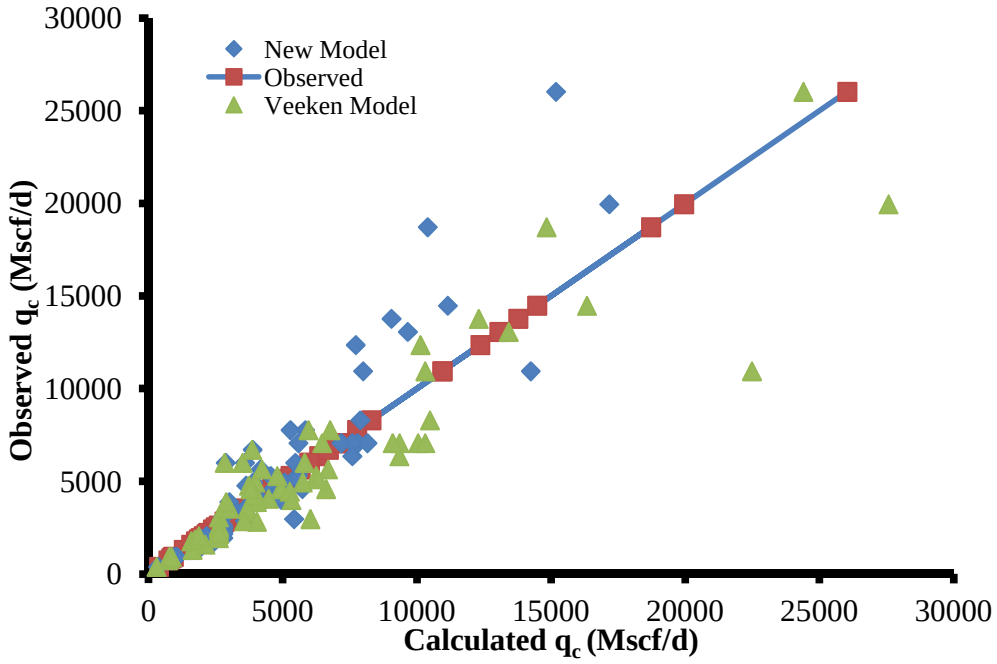

Figure 5.1: Veeken model versus the new model using observed Veeken et al. data at 20°/100 ft BUR

Table 5.1 summarizes the critical gas rate predictions in the form of absolute average percent deviation that each model yields for all 67 wells provided by Veeken et al. (2009). While Table 5.2 shows the results only using wells flowing below 10,000 Mscf/d. The new model is shown to more accurately predict the critical gas rates in both cases compared to all other models. It is also demonstrated that the conventional models, Turner and Coleman, both under-predict the critical gas rate and respectively

have 26% and 39% deviation while using all data, and 24% and 36% deviation while using only data less 10,000 Mscf/d. Therefore, these conventional models are unfit for usage in horizontal and deviated wells.

Table 5.1: Absolute average deviation using all Veeken et al. data at 20^{o}/100 ft

	Turner	Coleman	New model	Veeken
Absolute Average Percent Deviation %	26	39	19	21

Table 5.2: Absolute average deviation using rates less than 10 MMscf/d from Veeken et al. data at 20^{o}/100 ft

	Turner	Coleman	New model	Veeken
Absolute Average Percent Deviation %	24	36	17.5	21

The second set of data is obtained from the Belfroid et al. (2008) paper. They observed and reported the critical gas rates for two gas wells and provided their own predicted critical rates in a dimensionless form as a ratio of the observed critical gas rate and their predicted critical gas rate. They referred to the ratio as a modified Turner Ratio, bottom hole angle adapted by using the Fiedler shape function. For the first well they reported a TR of 1.2, and for the second well they reported 0.9. These ratios translate to a predicted critical gas rate of 2,648 Mscf/d for Well 1 and 1,766 Mscf/d for Well 2. Table 5.3 shows the reported data of the two wells included in the Belfroid et al. (2008) paper, including well parameters, fluid parameters, and the observed critical gas rate. These data were used to calculate the predicted critical gas rate for each well using the

new model. Table 5.4 shows the comparative results between the new, Belfroid, and Turner models prediction for both wells. For Well 1, the new model predicts a model TR of 1.0, while both the Belfroid and Turner models predict a TR of 1.2. For Well 2, both the new model and Belfroid model predict a TR of 0.9, while the Turner model predicts a ratio of 1.1. These results indicate that the new model has better prediction capabilities of the critical gas rates than the Belfroid model, and the Turner model has the lowest prediction accuracy of the three models. Thus, based on the comparison of data from both Veeken et al. (2009) and Belfroid et al. (2008), it is clear that the new model shows an improvement in predicting the critical gas rates in horizontal and deviated wells.

Table 5.3: Belfroid et al. data (2008)

	Well 1	Well 2
Inner Diameter [m]	0.112	0.074
Length [m]	3743	3545
Inclination Angle [°]	Variable	Variable
Gas [glmole]	18.6	17.5
Wellhead Pressure [bara]	14	21
Wellhead temperature [°C]	45	30
Reservoir temperature [°C]	120	110
Water density [kg/rn^3]	1020	1050
Gas Rate [m^3]	90000	45000

Table 5.4: Comparing different models using Belfroid et al. data at 20^o/100 ft

	Turner Ratio, TR		
	New model	Belfroid	Turner
Well 1	1.0	1.2	1.2
Well 2	0.9	0.9	1.1

5.1.2 Comparison at 12^o/100 ft

To enforce the conclusion from the previous comparison at 20^o/100 ft, the model was also tested at a different condition. This time, a BUR of 12^o/100 ft was used to predict the critical gas rate for the 67 wells from Veeken's work and the two wells from Belfroid's work. Table B2 in Appendix B shows the well data and the calculated predicted critical rates, along with a comparison of the predicted and observed critical rates.

Figure 5.2 shows the deviation of the new model and the Veeken model from the actual observed data. Once again, the new model appears to have closer predictions to the observed data with an overall deviation of 18% compared to Veeken model which has 21% deviation. The latter observation is especially true for gas rates less 10,000 Mscf/d where the new model shows even better performance and a reduced deviation of 15.7% from actual.

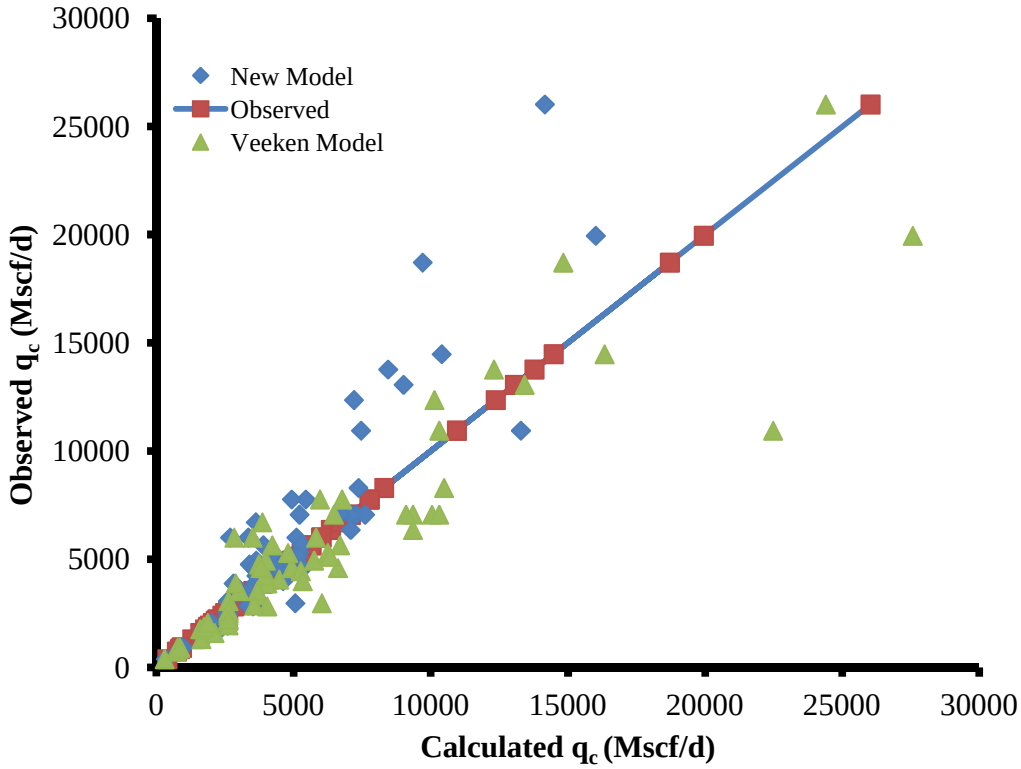

Figure 5.2: Veeken model versus the new model with observed Veeken et al. data using 12°/100 ft BUR

Table 5.5 summarizes the critical gas rate predictions using a BUR of 12°/100 ft in the form of absolute average percent deviation that each model yields for all 67 wells provided by Veeken et al. (2009). Table 5.6 shows the results using only wells flowing below 10,000 Mscf/d. In both cases the new model is shown to more accurately predict the critical gas rates when compared to all other models.

Table 5.5: Absolute average deviation using all Veeken et al. data at 12°/100 ft

	Turner	Coleman	New model	Veeken
Absolute Average Percent Deviation %	26	39	18	21

Table 5.6: Absolute average deviation using rates less than 10 MMscf/d from Veeken et al. data at 12^{o}/100 ft

	Turner	Coleman	New model	Veeken
Absolute Average Percent Deviation %	24	36	15.7	21

The comparison of the new model predictions with the Belfroid et al. (2008) model in Table 5.7 shows that for Well 1, the new model predicts a ratio of 1.1, while both the Belfroid and Turner models predict a ratio of 1.2. In the meanwhile, for well 2, both the new model and Belfroid model predict a ratio of 0.9, while the Turner model predicts a ratio of 1.1. Again, the new model shows that it has better prediction capabilities of the critical gas rates than both the Belfroid model and the Turner model.

Table 5.7: Comparing different models using Belfroid et al. data at 12^{o}/100 ft

	Turner Ratio		
	New model	Belfroid	Turner
Well 1	1.1	1.2	1.2
Well 2	0.9	0.9	1.1

5.1.3 Comparison at different buildup rates

In order to determine the extent of improvement and usage range, the new model was applied to a range of BUR from 3 to 30 ^{o}/100 ft. Figure 5.3 shows the results of the comparison of the new model's critical gas rate predictions to the Veeken model. The

model appears to have better performance from 4 to 29 ^{o}/100 ft, while Veeken's model is better at less than 4 ^{o}/100 ft and more than 29 ^{o}/100 ft.

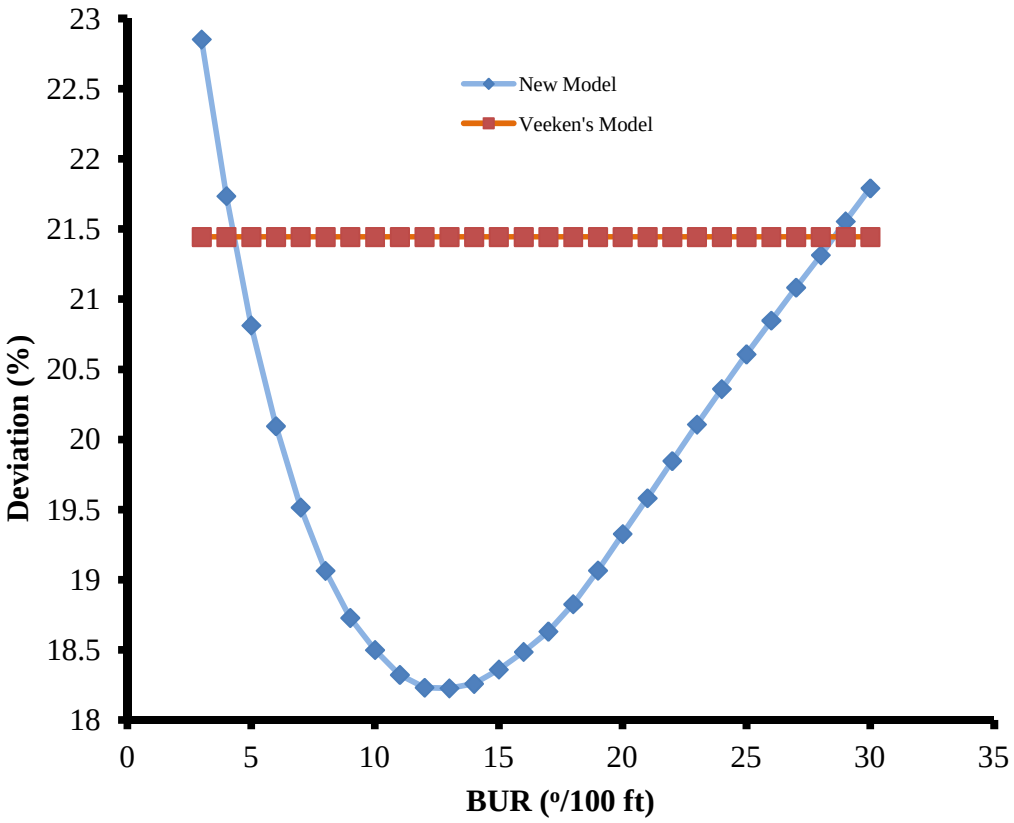

Figure 5.3: Veeken model versus the new model with observed Veeken et al. data at different ^{o}/100 ft BUR

For flow rates less than 10 MMscf/d, Fig. 5.4 shows that the model performance significantly outperforms Veeken's model throughout the investigated range of BUR from 3 to 30 ^{o}/100 ft. The possible underlying cause behind the improved performance of the new model at rates less than 10 MMscf/d was discussed earlier.

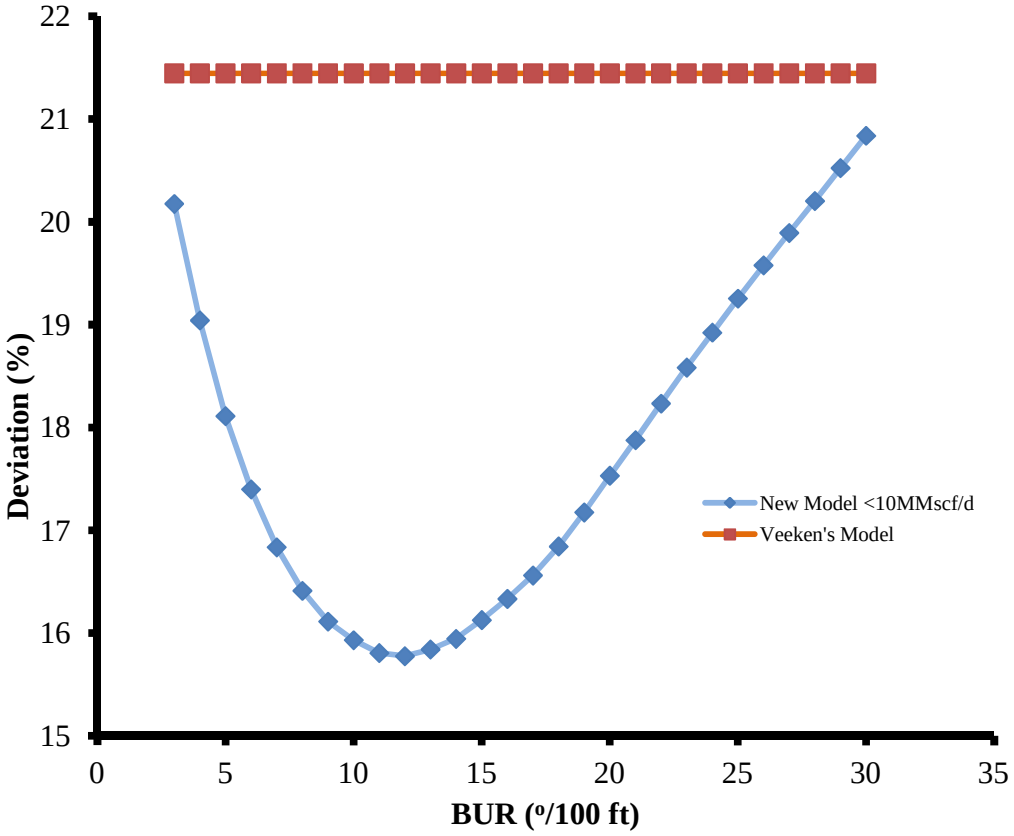

Figure 5.4: Veeken model versus the new model with observed Veeken et al. data less than 10 MMscf/d at different °/100 ft BUR

Similar to the comparison with Veeken's model, Fig. 5.5 shows the result of the comparison of the new model critical gas rate predictions to the Belfroid model. The new model appears to have better performance from 4 to 30 °/100 ft, while Belfroid's model is more accurate at less than 4 °/100 ft.

Therefore, it is recommended to use the new model only within BUR range values of 4 to 30 °/100 ft. This range covers most of the medium radius wells, which are the most common type of wells currently drilled. Thus, based on the comparison of data from both Veeken et al. (2009) and Belfroid et al. (2008), it is clear that the new model shows an improvement in predicting the critical gas rates in horizontal and deviated wells.

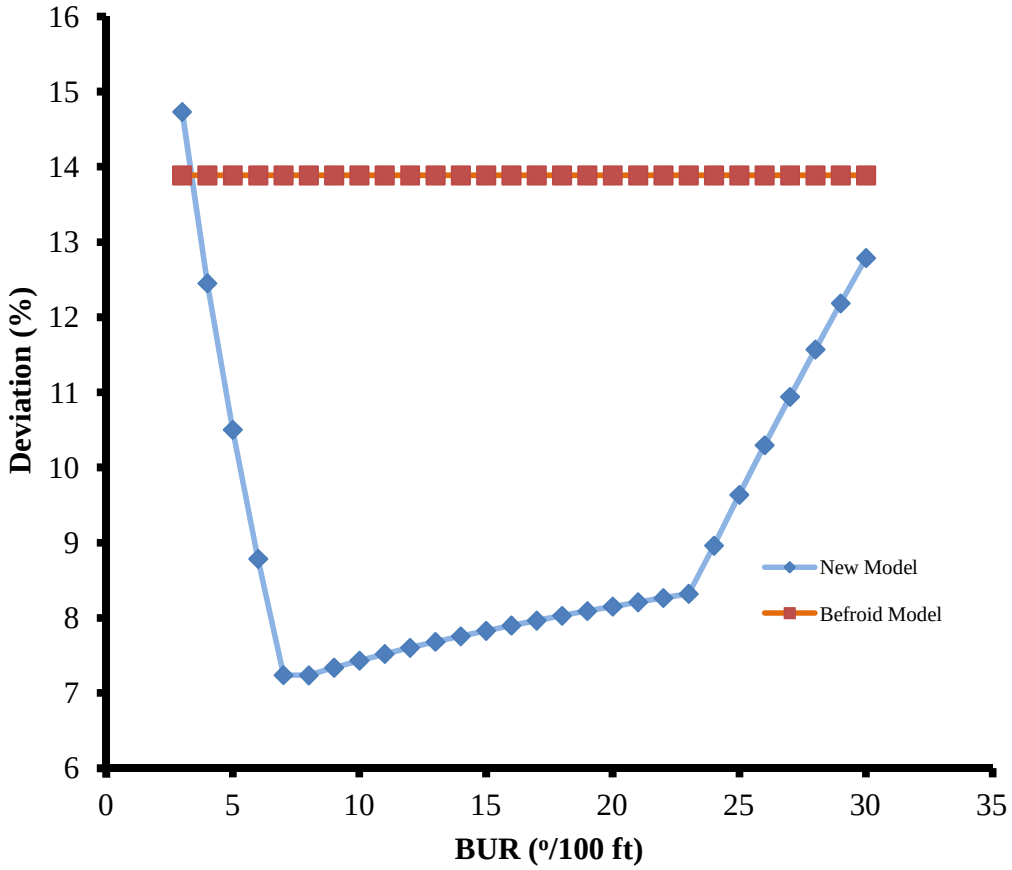

Figure 5.5: Belfroid model and the new model versus observed Belfroid et al. data at different ^{o}/100

5.2 Vertical wells

In vertical wells, the new model collapses to the Coleman model. However, it was desired to compare the model results with a 20 ^{o}/100 ft BUR to the vertical case. In other words, it is desired to predict what the critical gas rate should be if the same vertical well were horizontal. This can occur if a sidetrack program is started in a vertical well's field. Understanding the critical gas rates needed prior to sidetracking a vertical well's field is important when planning to upgrade the infrastructure, especially if gas lift will be implemented. Both Coleman and Turner presented data sets for vertical wells in their work. Table 5.8 shows the data from the 56 wells presented by

Coleman et al. (1991), and Table 5.9 shows the deviation of the new model compared to both the Coleman and Turner models. It is clear that both traditional vertical models show better predictions than the new model for vertical wells (see Fig. 5.6).

Table 5.8: New model versus Coleman model predictions using Coleman data

		Critical Rate (Mscf/d)			
Test	WHFP (psia)	Observed	Coleman	Turner	New model
1	275	726	874	977	1017
2	205	660	744	844	867
3	212	585	737	858	859
4	150	468	618	722	720
5	185	573	691	802	806
6	145	593	619	710	723
7	145	617	619	710	723
8	70	250	412	494	481
9	140	607	580	698	675
10	138	600	575	693	670
11	130	635	586	673	684
12	125	583	563	660	657
13	165	649	628	758	732
14	395	647	1,031	1169	1199
15	255	612	821	941	957
16	355	952	962	1109	1119
17	105	430	520	605	605
18	99	396	494	587	577
19	70	164	410	494	481
20	43	329	323	387	377
21	52	267	356	426	416
22	352	640	983	1104	1143
23	225	615	780	884	909
24	495	1072	1,174	1307	1363
25	94	748	488	572	571
26	65	276	395	476	460
27	59	500	371	454	432
28	50	366	348	418	407
29	39	324	311	369	364
30	97	90	484	581	565

Test	WHFP (psia)	Observed	Coleman	Turner	New model
31	60	220	389	457	454
32	90	355	478	560	556
33	50	338	341	418	397
34	60	401	398	457	464
35	80	450	460	528	537
36	107	471	508	610	591
37	135	372	553	686	644
38	131	518	590	675	688
39	130	330	562	673	654
40	82	511	460	535	536
41	90	558	461	560	537
42	100	493	491	590	572
43	183	627	676	798	789
44	120	518	542	646	632
46	47	358	349	405	407
46	315	885	924	1045	1075
47	165	712	638	758	743
48	75	408	438	511	511
49	380	666	924	1147	1072
50	155	648	630	734	734
51	145	564	608	710	710
52	235	781	782	903	910
53	225	755	764	884	890
54	165	620	610	758	710
55	49	430	335	413	392
56	59	397	372	454	434

Table 5.9: Absolute average percent deviation comparison for Coleman's 56 wells

Absolute Percent Deviation %		
Coleman	**Turner**	**New model**
28	45	77

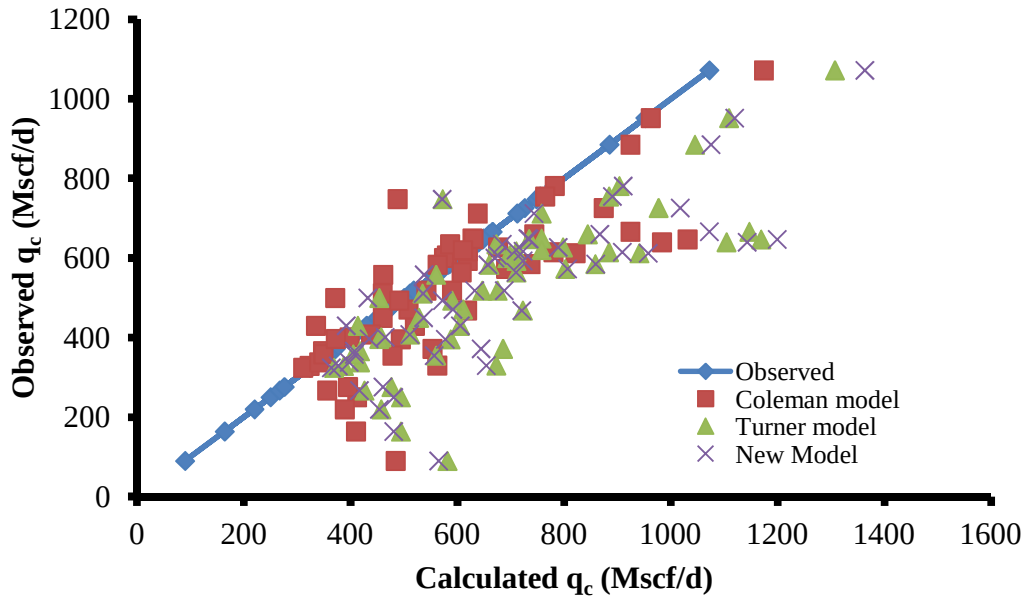

Figure 5.6: New model versus conventional models predictions using observed Coleman data

In the case of Coleman's 56 data points, the absolute average percent deviation for the new model is 77%, while Coleman is 28% and Turner is 45% (see Table 5.9). Coleman data represents low pressure wells, i.e. less than 500 psi. This finding agrees with Coleman's statement that the 20% adjustment suggested by Turner is not necessary. Similar conclusions as those from the Coleman comparison are drawn when comparing the new model with the Turner model using Turner et al. data. Figure 5.7 and Table B3 in Appendix B show the data from the comparison. Out of 106 data points, 16 were reported by Turner as questionable, while 6 were reported as near loaded, 30 as loaded up, and 54 as unloaded. If the questionable data are disregarded from the comparison, the Turner model missed 26 data points out of 90 (see Fig. 5.8). On the other hand, the new model missed 34 out of 90, with most predictions being overestimated (see Fig. 5.9).

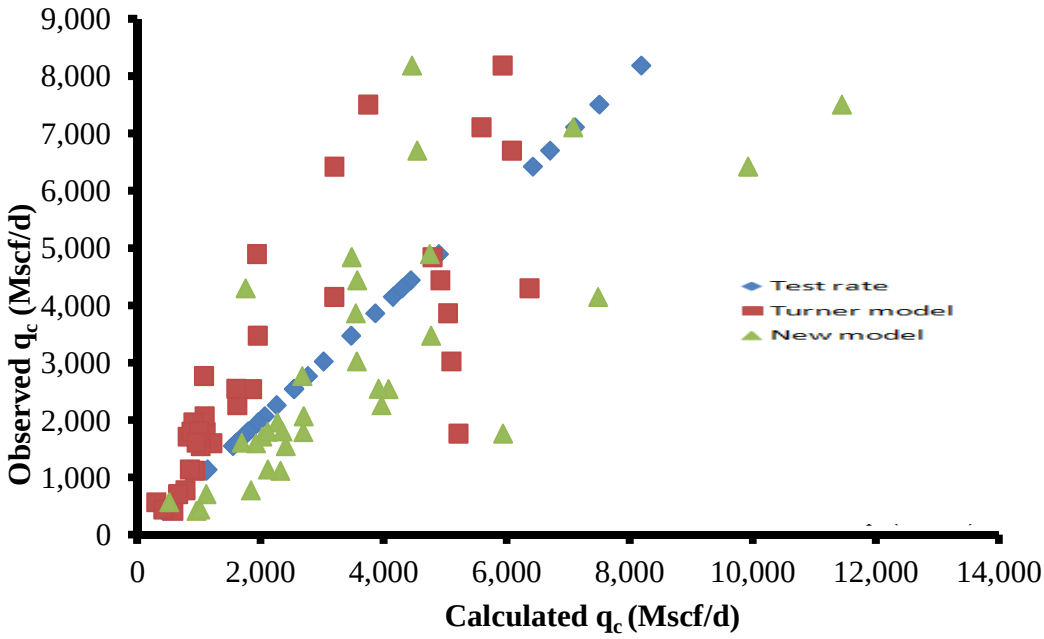

Figure 5.7: The new model versus the Turner model predictions using observed Turner data

These results show that the Turner model has better prediction capabilities than the new model in vertical wells. The reason why both traditional vertical models outperform the new model is because, when using a deviation, the new model overestimates the gas critical rate. Also, it is important to note that the tested wells are all vertical in which the effects of geometry are quasi-absent.

In conclusion, vertical well models are suitable for vertical wells only and the new model collapsing back to the vertical models in vertical well cases is appropriate. However, if a vertical well geometry is changed, i.e. sidetrack, the new model will provide better solution to account for the required increase in gas volumes and plan the appropriate infrastructure to account for the changed condition.

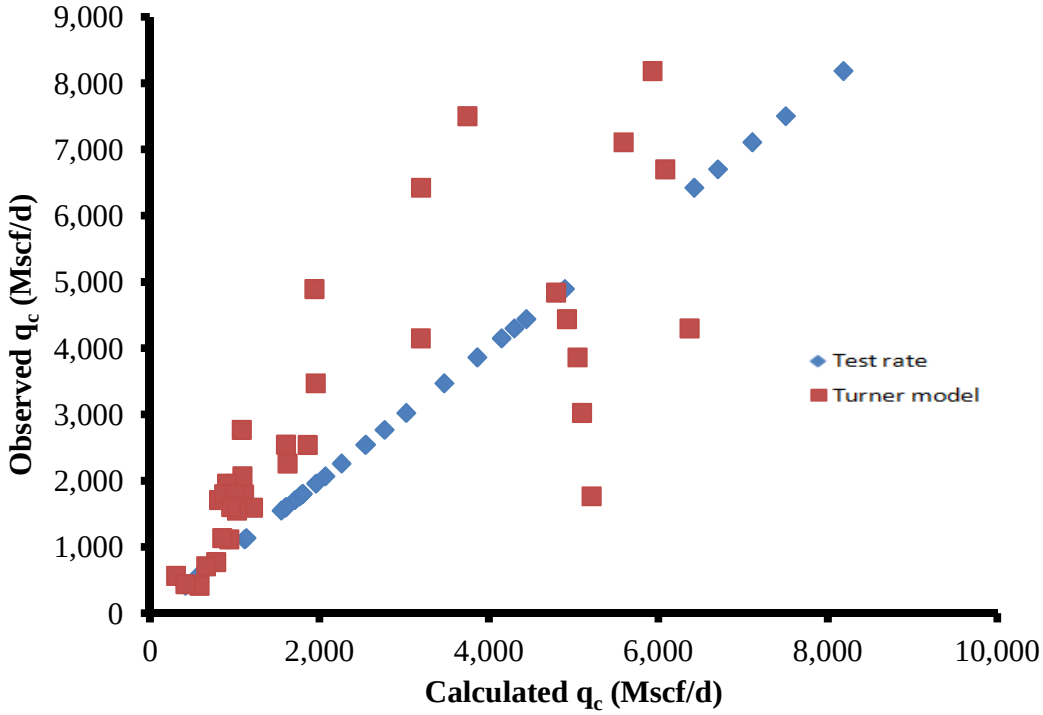

Figure 5.8: Turner model missed data compared to observed Turner data

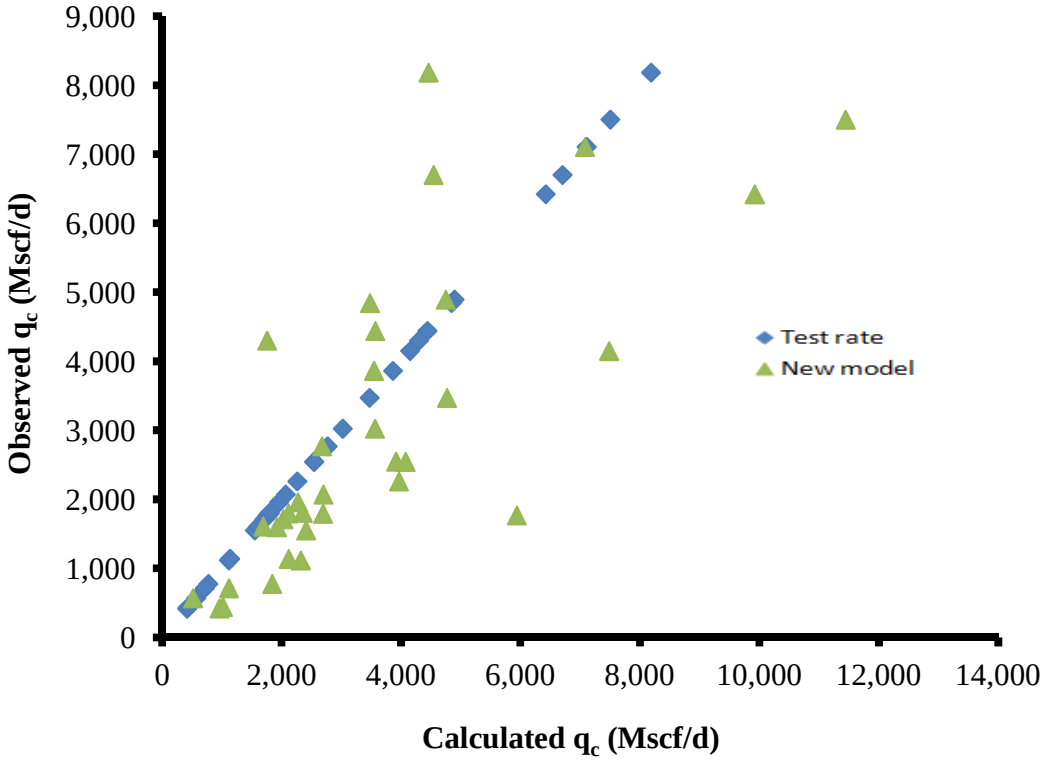

Figure 5.9: New model missed data compared to observed Turner data

CHAPTER VI

Experimental setup

To identify the critical rate needed to maintain continuous production from the wells, experimental work on two horizontal wells operating at an intermittent state below the critical gas rate was conducted. Overall, two different types of setups were used depending on different factors, including usability, availability, and proximity of the source gas, compressor type and availability, line pressure, and economics. The objective, however, remained the same—to know the total gas rate at which these wells will start flowing continuously in a stable condition. This is accomplished by using continuous gas circulation techniques. In the latter operation, compressed gas is injected down the tubing-casing annulus through open-ended tubing, preferably set just above the producing interval, where the injected gas will assist formation gas in lifting the liquids. The increased Gas Liquid Ratio (GLR) reduces the hydrostatic backpressure on the formation and allows more reservoir contribution therefore, helping lift the liquids. The injection gas rate is then varied until a total gas rate that causes the production rate to stabilize is identified. That rate is then considered to be the critical rate.

6.1 First setup

The setup shown in Fig. 6.1 consists of a gas makeup source connected through a poly pipe to the inlet of a gas-powered compressor where the supply gas goes through three stages of compression to obtain the desired discharge pressure before exiting through the compressor discharge line to the casing–tubing annulus. The desired injection rates

and pressures are controlled and automated using equal percentage motor valves (see Figs. 6.2 and 6.3) through the SCADA system that uses an Electro-Pneumatic Transducer, current to pressure (I2P) (Fig. 6.4). The discharge, in this case, has a bifurcation where the first line is connected to the casing tubing annulus, referred to as the backside or injection line, and the second line is connected to the sales line. A rate controlled valve is set on the injection line to allow the desired flow through the gas injection meter. For example, if the desired injection rate is 500 Mscf/d, the valve will provide a flow area large enough to allow that gas volume to flow through it, and if the rate becomes increasingly higher, the valve will automatically adjust and reduce the flow area to reduce the flow rate back to the desired rate. The pressure control valve was installed to maintain the desired discharge pressure from the compressor. This was necessary to allow continuous operation above the line pressure, which was routinely high, i.e., more than 600 psi. Both I2P controlled valves have bypass in case of malfunction. The bypass allowed for manual control over the operation by means of a choke. This, however, is not ideal because the rate through the choke cannot be maintained constant and will fluctuate with pressure. A valve was set downstream of the separator and upstream of the sales line to act as a relief valve to the sales line in case the gas intake was higher than the desired suction pressure in the compressor.

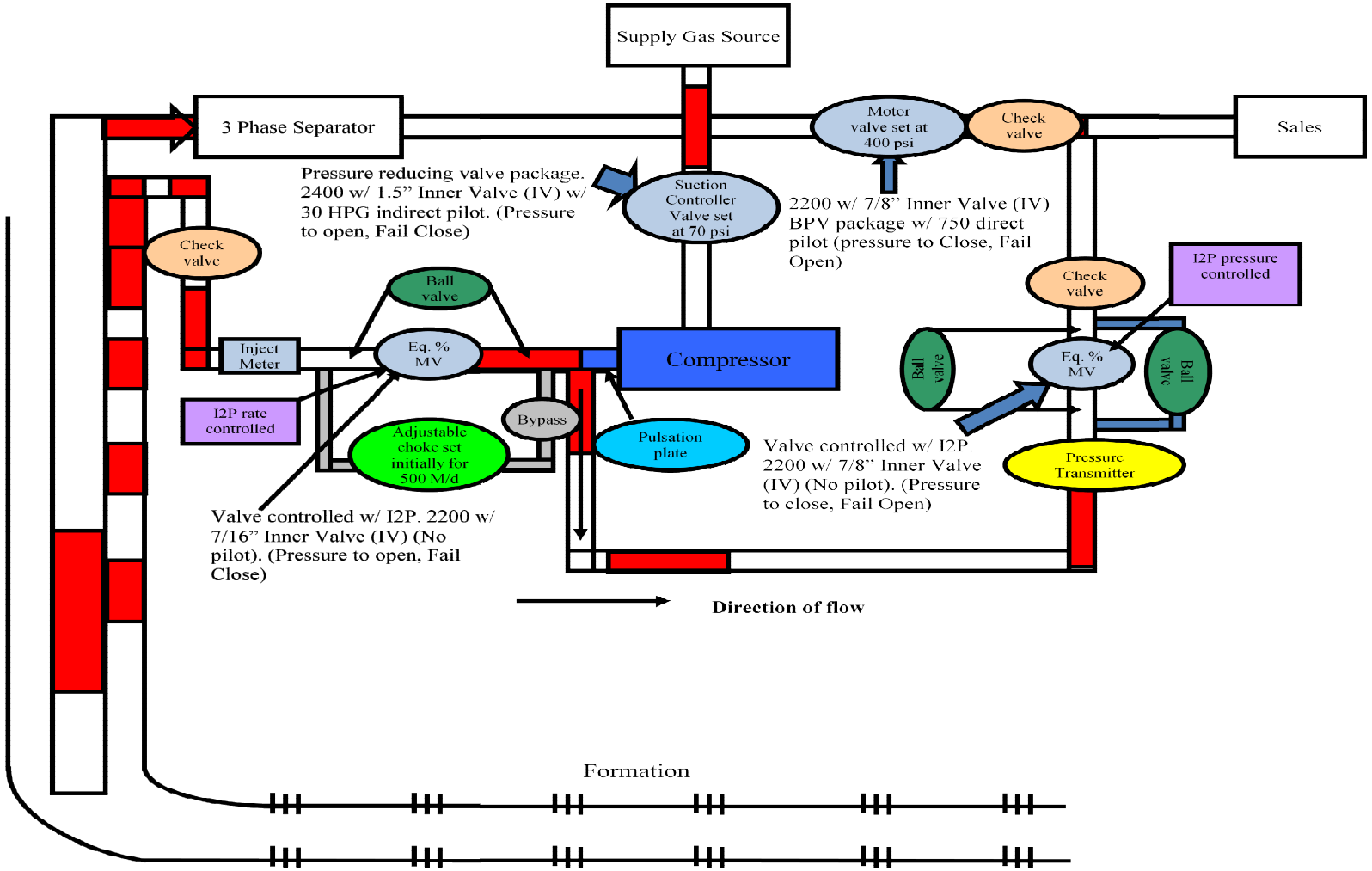

Figure 6.1: The first experimental setup

Figure 6.2: The control valve used for pressure and rate control, Courtesy of Kimray

Figure 6.3: Cutaway of the control valve, Courtesy of Kimray

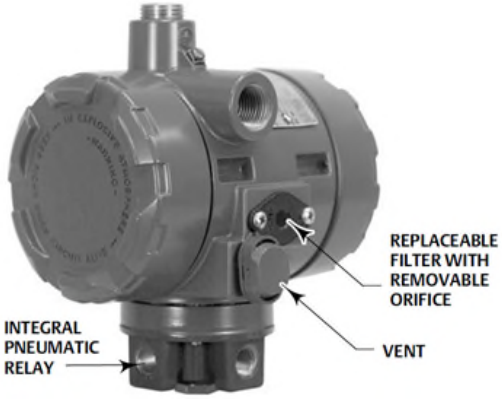

Figure 6.4: Electro-pneumatic transducer, current to pressure (I2P), Courtesy of Fisher

Figure 6.5: High-speed 3-stage compressor, Courtesy of NGSG

All piping is 2 inches ID schedule 80. The installation of the pulsation plate helped to reduce the vibration on the line caused by the compressor, especially with the sensitive telemetry equipment at proximity of the discharge line. This setup enabled better and more accurate control over the operation because it ensured a stable rate and pressure with minimum operational fluctuations. On the other hand, it required good telecommunication infrastructure in addition to reliable equipment.

The compressor used in this case was a 3-stage reciprocating high speed compressor (Fig. 6.5). Injection gas came in from the supply source through the poly pipe, and its pressure was regulated down to the desired suction pressure using the suction controller

valve. The reduced pressure gas then entered the suction scrubber to dry off by knocking off as much liquid as possible. The stripped liquids were dumped from the bottom of the scrubber to the producing tanks while the dry gas exited the top of the scrubber towards the first stage of compression. The dual reciprocating piston compressed the gas until it reached the discharge pressure from the first stage. The hot compressed gas was sent towards the cooler to go through series of heat exchangers to dissipate the heat from first compression stage. As the gas temperature dropped, it reached the dew point and started dropping liquids. This is not desired, and therefore, the gas was sent to a second scrubber where these liquids were accumulated at the bottom of the vessel and sent to the producing tanks while the dryer gas once again exited at the top of the scrubber and flowed towards the second stage of compression. The gas entered the compression chamber at a higher pressure than the in first stage and was compressed further until it reached the discharge pressure of the second stage.

At this point, the gas was flowing at a higher pressure and temperature than the inlet pressure at the second stage. Following the second stage of compression, the gas was sent towards the cooler again to reduce its temperature and then continued, along with the dropped liquids, towards the scrubber for the third stage. The remaining liquids were again accumulated at the bottom of the scrubber and dumped into the producing tanks, while the gas exited at the top and continued flowing towards the third stage of compression where it was further compressed until it reached the final desired discharge pressure. At this point, the gas was hotter and was flowing at higher pressure than the first and second stages. This high pressure gas exited the compressor skid towards the well and was injected down the tubing-casing annulus.

The set up is build to handle the occasional high line pressure through the use of flaring system that is activated when line pressure reaches s certain threshold. Gas is re-routed to the flare system to avoid venting it to atmosphere.

Also, there might be periods of low gas supply towards the compressor. In the latter case, the fuel recycle valve will open and continues supplying fuel gas to the compressor engine in order to keep it from shutting down until the gas supply reached its normal level once again. If supply gas levels remain low for an extended time period, the compressor engine temperature will continue rising and will eventually reach high enough level that will force the compressor to shut down. Safe guards to protect the compressor from exceedingly high temperatures that can damage it are put in place and will be triggered if such event occurs.

6.2 Second setup

The second setup, as shown in Fig. 6.6, is more basic and did not have the injection meter or the rate and pressure control valve as part of the installation. In this case, supply gas came from an offset well where it went through compression to reach higher pressure; then it was discharged to the injection well tubing-casing annulus to assist in the lifting operation.

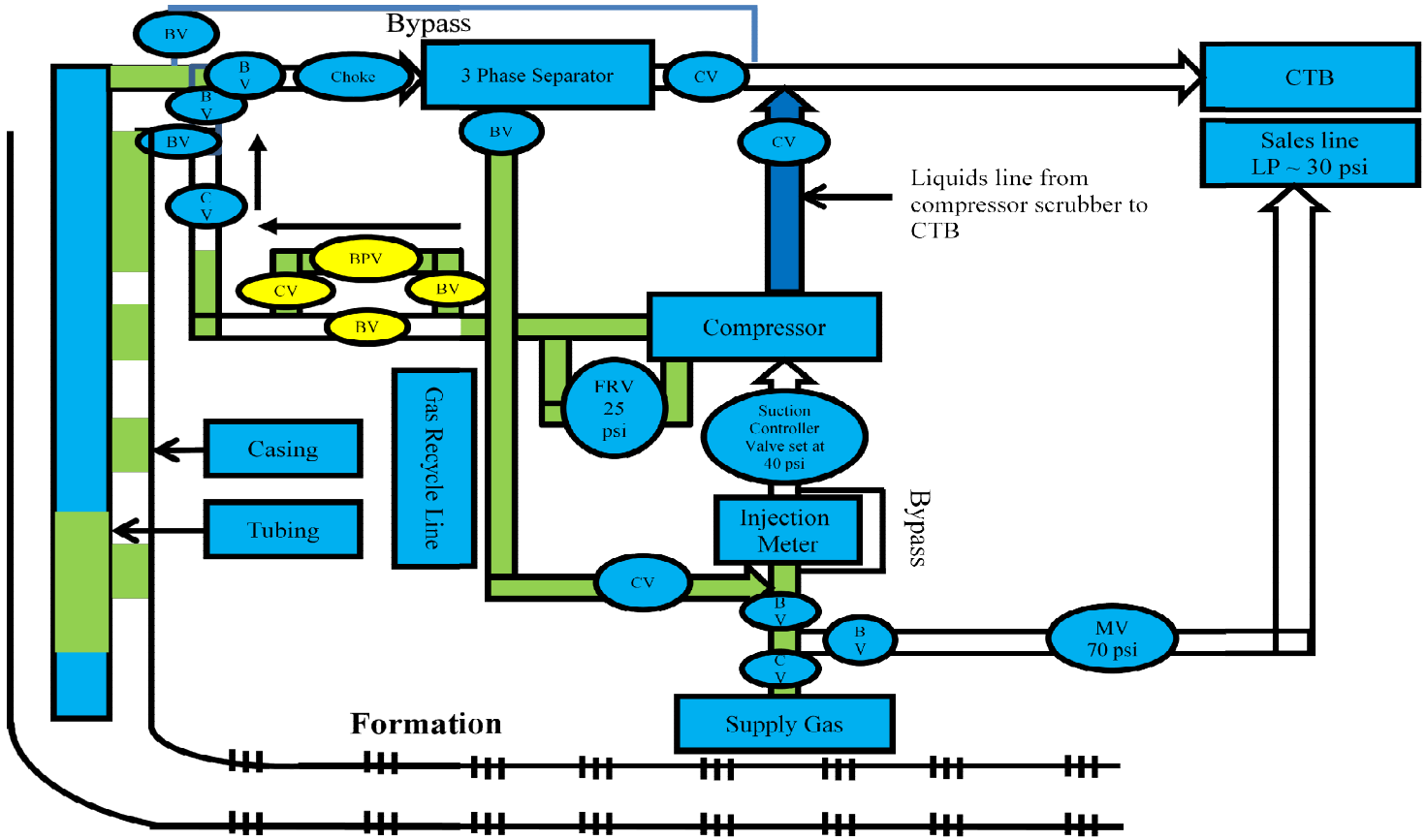

Figure 6.6: Second experimental setup

NB: BPV: back pressure valve; BV: ball valve; MV: motor valve; and CV: check valve. With the exception of the 3" poly pipe suction line, all piping was 2" Schedule 80.

Not all types of gas can be used for injection. There are stringent specs of gas that need be met before it is suitable (see Table. 6.1). The source gas has to be sweet gas, that is, it has to contain less than 50 ppm of H_2S. Gas at higher concentrations than that will cause damage to the engine. Also, it is preferable that the gas heating value is less than 1400 BTU; otherwise, residue will be deposited from inefficient burning of the rich gas.

Table 6.1: Typical gas analysis needed for compression design and selection

FRACTIONAL ANALYSIS
CALCULATED @ 14.650 PSIA AND 60F

	MOL%	GPM (REAL)	
HYDROGEN SULFIDE...	0.008		
NITROGEN.....	1.915		
CARBON DIOXIDE.....	1.330		
METHANE.....	81.197		
ETHANE.....	9.378	2.502	CORRECTED H2S PPMV = 75
PROPANE.....	3.902	1.072	
ISO-BUTANE.....	0.360	0.117	
NOR-BUTANE.....	1.099	0.346	
ISO-PENTANE.....	0.179	0.065	'Z' FACTOR (DRY) = 0.9969
NOR-PENTANE.....	0.255	0.092	'Z' FACTOR (WET) = 0.9965
HEXANES	0.178	0.077	
HEPTANES + ...	0.199	0.086	
	-------	------	26 LB. R.V.P. = 0.495
TOTALS	100.000	4.357	

..CALCULATED SPECIFIC GRAVITIES..		..CALCULATED GROSS HEATING VALUES..	
IDEAL, DRY.....	0.6976	BTU/CF - IDEAL, DRY	1165
IDEAL, WET	0.6963	BTU/CF - IDEAL, WET	1145
REAL, DRY	0.6995	BTU/CF - REAL, DRY	1169
REAL, WET	0.6984	BTU/CF - REAL, WET	1149

The supply of gas from the offset well will eventually phase away and be used only for restart operations. Because the well-produced liquids and both formation and injection gas, the total stream was taken to a 2-phase separator where the liquids dropped to the bottom of the vessel and were sent to the central tank battery. The gas was taken out of the outlet of the scrubber and plumbed back to the suction line where the pressure was regulated before it entered the compressor. Another line was laid from the separator to carry the excess gas to the sales line to avoid backups due to higher than anticipated gas volumes that exceeded the compressor capacity or unplanned shut downs and

upsets of the compressor. In absence of automation, the injection rate was inferred from the compressor performance curves and was manipulated by varying suction and discharge pressures. Figure 6.7 shows the compressor performance curve used in this experiment (Courtesy of Compresco Partners L.P.).

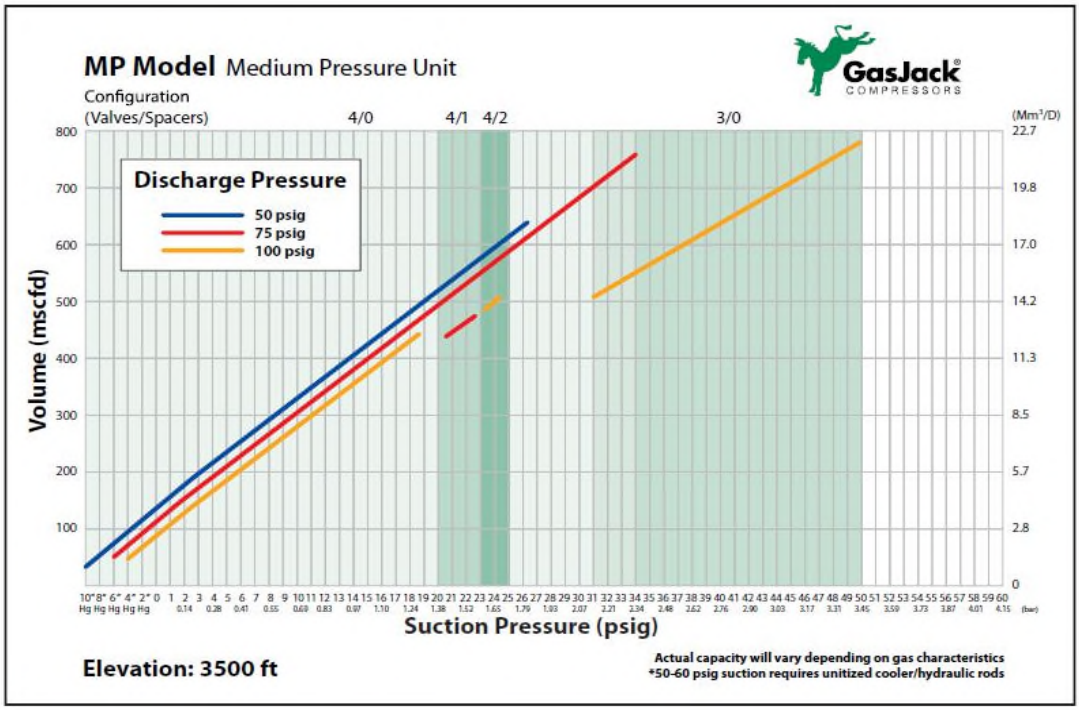

Figure 6.7: Compressor performance curves

6.3 Operational issues and solutions

Few issues can arise during this operation. They could be surface or bottom hole related. Following is a list of potential problems and solutions to rectify them.

6.3.1 Compressor down on maximum discharge pressure

In case the compressor repeatedly goes down on high discharge, the following causes should be investigated. The volume of liquid accumulated in the wellbore may be high. This can be resolved by reducing the liquid volume in the well before starting the compressor injection, which can be done either by swabbing the well or using the

compressor injection down both the casing annulus and tubing to push the fluid level back to the reservoir. This could also be caused by the lifting point in the wellbore being too deep; in which case, it is necessary to move the injection point to a shallower depth by introducing new tubing perforations. This solution is not optimal because it still leaves the section below the injection point exposed to the potential of liquid loading. If this issue keeps occurring, then conventional gas lift might be a better solution. Other causes could be as simple as a malfunctioning discharge valve can. In that case, a routine check and maintenance of the valve to ensure proper functioning would suffice.

6.3.2 Compressor down on low suction pressure

Issues such as low gas supply to the compressor or a malfunctioning suction valve will cause the compressor to continuously go down on low suction. To avoid these interruptions to the operation, it is important to keep the supply gas steady by adding a recirculation line or gas buyback meter in addition to having a maintenance program to routinely check the suction control valve to ensure proper functioning. Hydrate formation, especially in cold weather conditions, will cause an interruption in supply gas or freeze the controls of the valve. In the latter case, heat tracing the lines and valves and/or injecting methanol will help the lines stay clear and ensure that the valve functions normally.

6.3.3 Monitoring pressure

Monitoring casing and tubing pressure was also used to evaluate the effectiveness of the process. The following are some observations noted during the operation:

- Equalized casing and tubing pressures

- Equalized or quasi-equalized volume of both injection and produced gas
- Low to no fluid production observed at the surface
- Low fluid level in the well, confirmed by a pressure gradient survey or fluid shot.

The combination of the conditions described above is typically an indication of reduced inflow performance due to either “in-reservoir conditions” such as low reservoir deliverability caused by depletion or skin, or “in-wellbore conditions” caused by blockage due to scaling from incompatible water sources, paraffin, or sand from the fracturing treatment or formation. lowering the tubing to reach a new fluid level or cleaning the well out and/or re-stimulating it to re-establish reservoir deliverability are all potential solutions to resolve the low deliverability issue. Another issue that can be encountered, especially after the initial startup, is climbing casing and tubing pressures. The latter issue is mainly caused by higher injection volume and discharge pressure than necessary and/or the presence of restrictions causing back pressure. To resolve this issue, it is recommended to reduce the injection volume or reduce the discharge pressure. The latter can be done if a back pressure valve is set downstream from the compressor discharge. The restrictions and/or pressure drop points could also be reduced, i.e. by opening the choke and reducing elbows. Low casing and tubing pressures can also occur, especially in the presence of a thief zone or injection line leaks. Typically, raising the tubing above the thief zone or inserting circulating holes above it while reducing the discharge pressure and/or injection rate can resolve the low pressure problem. As for injection line leaks, implementing routine maintenance and visual inspections is the first line of defense to resolve the issue.

CHAPTER VII

Experimental results

The previous chapter described the experimental setup and equipment used in order to execute the procedure to identify the effective lift rate. In this chapter, data gathered from the experiment are analyzed and compared to the predictions from the critical gas rate models including the new model, the horizontal well models, Veeken model and Belfroid model, and the conventional vertical well models, Turner model and Coleman model. As discussed in the literature review chapter, Belfroid's model is a merger between the Turner model and the Fiedler shape function which attaches a dependency of the model to the deviation angle ω. The latter dependence results in a maximum of 35% rate increase over the critical gas rate calculated using the Turner model and this peak increase occurs at 53^{o} inclination. At the latter inclination, the Belfroid model critical gas rate prediction is almost similar to the new model. However, the error from the Belfroid model can have a large range depending on the inclination angle of the evaluation point. For example in Horizontal Well 1, the range is from zero to 37%, and for Horizontal Well 2, it is from 5 to 41%. For the purpose of this work, the maximum build up angle of each of the two horizontal wells is implemented when using the Belfroid model. Table 7.1 shows the properties of the two horizontal wells. The actual production data from these wells were recorded and only days with valid data were used. Valid data means data collected for days when the wells did not experience any problems and had 100% run time without compressor problems, such as mechanical problems, gas supply issues, or freezing due to weather conditions. Also, after the

injection rate was changed, the well was allowed to become stable before the data were recorded so that the results were not skewed by unsteady state conditions.

Table 7.1: Data from Horizontal Wells 1 and 2

		Horizontal Well 1	Horizontal Well 2
Production Data	q_o (BO/d)	2.39	61.50
	q_w (BW/d)	19.52	2.00
	q_g (Mscf/d)	273	181
	FTP (psia)	110	92
	$T_{surface}$ (^oF)	80	60
	$T_{formation}$ (^oF)	223	130
	OGR (bbls/MMscf)	3.3	90
	WGR (bbls/MMscf)	27	3
	WOR	8.18	0.03
Tubular Data	Tubing OD (in.)	2.875	2.875
	d (in.)	2.441	2.441
	Casing OD (in.)	5.5	7
	Casing ID (in.)	4.892	6.276
	Liner Top (ft)	12,950	8,177
	Liner OD (in.)	3.5	4.5
	Liner ID (in.)	2.992	4
	Absolute roughness (in.)	0.0006	0.0006
	Depth (ft)	12,863	8,306
	Max BUR ^{o}/100 ft	12.34	18.34
PVT	API	65	40
	N_2 Mol %	0	1.686
	CO_2 Mol %	0	0.843
	H_2S Mol %	0	0.003
	Specific gas gravity	0.65	0.7
	Specific water gravity g_w	1.02	1.02
	Specific oil gravity g_o	0.72	0.83

7.1 Horizontal Well 1

The recorded production data for the first horizontal well are captured and presented in Table 7.2. Figure 7.1 depict the data in graphical form showing Well 1 response to the different injection rates applied to determine the gas rate needed to keep it unloaded.

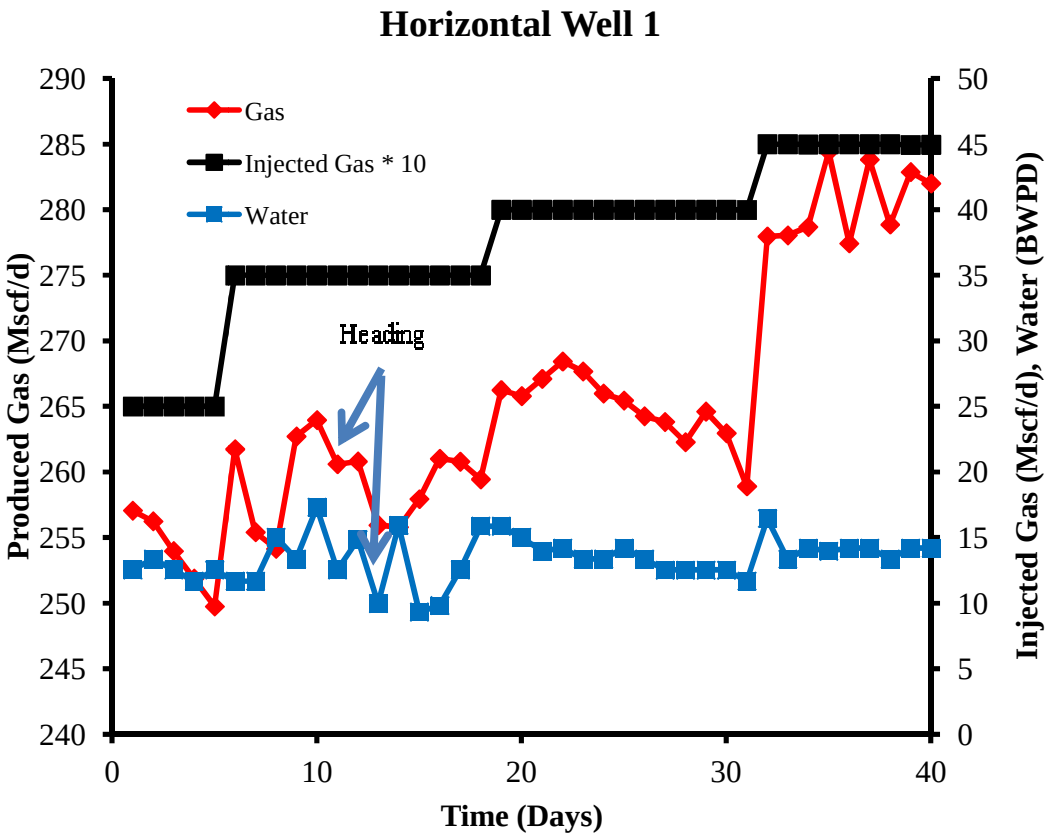

Figure 7.1: Critical gas rate for the Horizontal Well 1

Table 7.2: Horizontal Well 1 production data

Days	Oil (BOPD)	Gas (Mscf/d)	Water (BWPD)	Casing Pressure (psia)	Tubing Pressure (psia)	Injected Gas (Mscf/d)	Total Gas (Mscf/d)
1	1.7	257	13	637	111	250	507
2	2.5	256	13	631	111	250	506
3	1.7	254	13	637	112	250	504
4	1.7	252	12	643	114	250	502
5	2.5	250	13	637	114	250	500
6	2.5	262	12	540	120	350	612
7	2.5	255	12	562	120	350	605

Days	Oil (BOPD)	Gas (Mscf/d)	Water (BWPD)	Casing Pressure (psia)	Tubing Pressure (psia)	Injected Gas (Mscf/d)	Total Gas (Mscf/d)
8	0.8	254	15	566	120	350	604
9	0.0	263	13	551	116	350	613
10	1.7	264	17	542	116	350	614
11	1.7	261	13	542	118	350	611
12	0.1	261	15	542	118	350	611
13	0.0	256	10	543	118	350	606
14	2.6	256	16	557	118	350	606
15	5.8	258	9	883	116	350	608
16	0.8	261	10	781	116	350	611
17	1.7	261	13	802	116	350	611
18	1.7	259	16	802	114	350	609
19	2.5	266	16	473	120	400	666
20	1.7	266	15	467	120	400	666
21	1.7	267	14	457	120	400	667
22	1.7	268	14	452	120	400	668
23	2.5	268	13	452	120	400	668
24	1.7	266	13	452	120	400	666
25	1.7	265	14	495	120	400	665
26	2.5	264	13	491	120	400	664
27	2.5	264	13	485	120	400	664
28	1.7	262	13	493	120	400	662
29	1.7	265	13	493	120	400	665
30	1.7	263	13	496	120	400	663
31	0.8	259	12	491	120	400	659
32	1.7	278	16	412	120	450	728
33	2.5	278	13	403	114	450	728
34	0.0	279	14	393	118	450	729
35	0.8	284	14	301	120	450	734
36	1.7	277	14	305	114	450	727
37	1.7	284	14	299	116	450	734
38	0.8	279	13	305	114	450	729
39	0.8	283	14	280	99	449	732
40	1.7	282	14	293	114	450	732

An initial total rate of 500 Mscf/d (250 Mscf/d sold and 250 Mscf/d injected) did not help stabilize the well, and the production rate showed a continuous decline. The rate was increased to 610 Mscf/d (260 Mscf/d sold and 350 Mscf/d injected). At this rate, the wells started cycling, as is evident in both the water and gas rates. Note that at day 13, the gas rate dropped, followed by a drop in water production the following day; then

at day 14, a surge in water production was followed by an increase in gas rate. The heading behavior was indicative of the well operating below its critical rate. The total rate was increased again to 670 Mscf/d (270 Mscf/d sold and 400 Mscf/d injected). At that rate, the cycling effect started to wane; however, the total production trend was still descending. The latter observation indicates that the critical rate condition was almost achieved. Therefore, the total rate was further increased to 730 Mscf/d (280 Mscf/d sold and 450 Mscf/d injected). At this rate, the production started to show signs of stability for both water and gas. Therefore, a total rate of 730 Mscf/d was considered to be the critical rate.

Table 7.3: Observed critical gas rates and percent deviation for Horizontal Well 1

Actual Lift Rate, Mscf/ d	730	Absolute Percent Deviation, %
Coleman CR, Mscf / d	455	38
Turner, Mscf / d	541	26
New model, Mscf / d	**692**	**5**
Belfroid, Mscf / d	495	32
Veeken, Mscf / d	579	21

Table 7.3 shows the calculated critical rates and deviations with respect to the actual observed critical rate from both conventional vertical and horizontal models. Compared to the vertical models, Coleman (455 Mscf/d and 38% deviation), Turner (541 Mscf/d and 26% deviation), it is clear that the new model shows better prediction of the critical rate. Also, when compared to the horizontal models, Veeken (579 Mscf/d and 21% deviation) and Belfroid (495 Mscf/d and 32% deviation), the new model (692 Mscf/d and 5% deviation) clearly outperforms both in predicting the critical rate.

7.2 Horizontal Well 2

A similar process to that described for Horizontal Well 1 was applied to the second horizontal well. The production data is presented in Fig. 7.2 and Table 7.4.

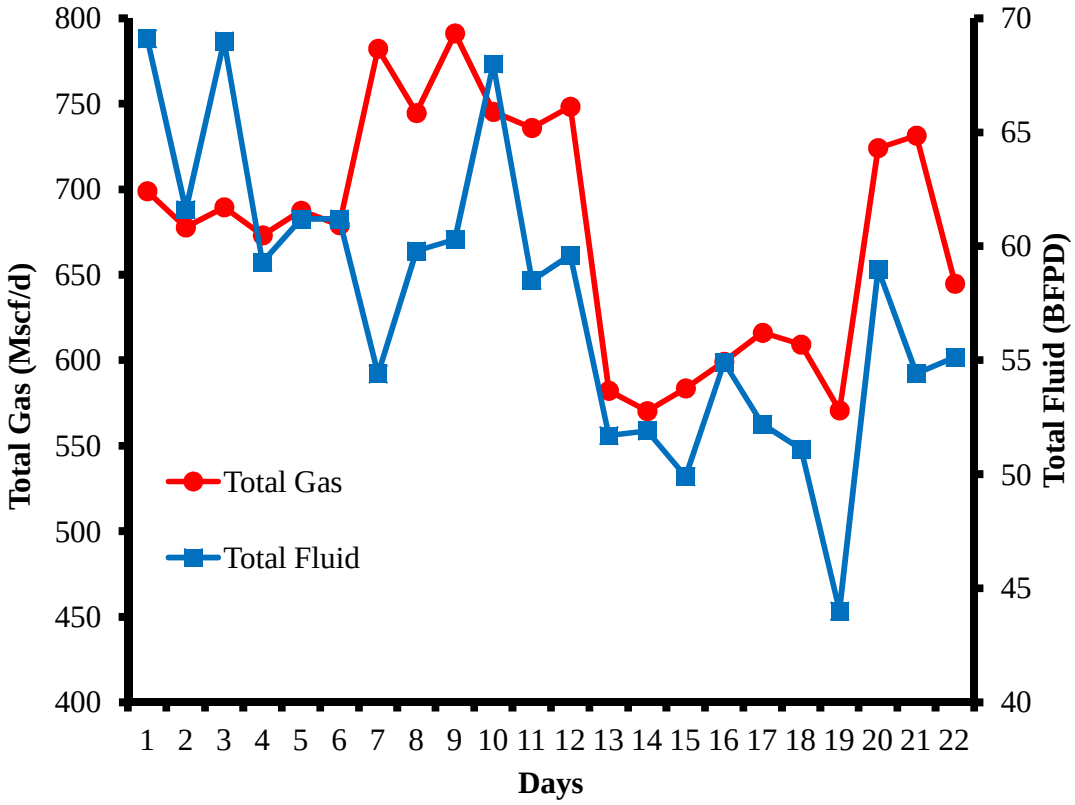

Figure 7.2: Critical gas rate for Horizontal Well 2

Table 7.4: Horizontal Well 2 production data

Days	Gas (Mscf/d)	Oil (BOPD)	Water (BWPD)	Fluid (BFPD)	Injection Rate (Mscf/d)	Total Gas (Mscf/d)	Avg Csg (psi)	Avg Tbg (psi)
1	190	44	25	69	509	699	419	94
2	174	62	0	62	503	678	420	91
3	187	69	0	69	503	690	416	94
4	172	59	0	59	501	673	412	91
5	184	48	13	61	504	688	411	92
6	181	56	6	61	498	679	406	91
7	194	54	0	54	588	782	393	99
8	157	60	0	60	587	745	397	98

9	182	60	0	60	610	791	394	101
10	157	68	0	68	588	745	392	96
11	148	59	0	59	588	736	393	96
12	137	60	0	60	611	748	391	99
13	150	51	1	52	432	582	390	83
14	141	52	0	52	429	570	391	72
15	154	49	1	50	430	584	385	78
16	165	53	2	55	434	599	387	74
17	162	51	1	52	454	616	381	79
18	158	50	1	51	451	609	382	81
19	160	40	4	44	411	571	387	24
20	189	55	4	59	535	724	382	84
21	155	52	2	54	576	731	371	90
22	125	55	0	55	520	645	363	80

The initial total rate of 684 Mscf/d (181 Mscf/d sold and 503 Mscf/d injected) yielded an average of 64 BFPD with a Flowing Tubing Pressure (FTP) of 92 psi. Increasing the injection rate to a total rate of 758 Mscf/d (162 Mscf/d sold and 595 Mscf/d injected) did not yield an increase in production; in fact, it reduced the total average liquid rate to 60 BLPD. This was an indication of over-injection, which is also evident in the increase in FTP to 98 psig. The injection rate was subsequently dropped to simulate lower total gas closer to the predicted flow rates from vertical models. The production response at a rate of 590 Mscf/d (156 Mscf/d sold and 434 Mscf/d injected) was not favorable and dropped to an average liquid rate of 51 BFPD, a loss of 13 BOPD and 26 Mscf/d. To verify the reversibility of the production drop and the dependence of production rate on total gas rate, the injection rate was subsequently increased. The production response was clear and swift, as the liquid rate increased back up to 55 BFPD, which is clear evidence that at lower gas rates, the liquid drop inside the wellbore is due to low lift force as a proxy to the lack of critical gas velocity. This confirms Wallis (1969) work,

which states that at very high velocities the liquid film thickness approaches zero and all liquids are entrained in the gas stream. As the gas velocity decreases, fluids accumulate to form a thicker film surrounding a gas core with entrained droplets. If the latter condition continues or worsens, the well will eventually load up.

Based on the results discussed earlier, a total rate of 684 Mscf/d is considered to be the critical rate. Table 7.5 shows the calculated critical rates and deviations with respect to the actual observed critical rate from both conventional vertical models and two horizontal models. Compared to the vertical models, Coleman (404 Mscf/d and 41% deviation), and Turner (481 Mscf/d and 30% deviation), it is clear that the new model shows better predictions of the critical rate. Also, when compared to the horizontal models, Veeken (512 Mscf/d and 25% deviation) and Belfroid (506 Mscf/d and 26% deviation), the new model (648 Mscf/d and 5% deviation) clearly outperforms both in predicting the critical rate.

In conclusion, it is recommended that the conventional models of Turner and Coleman not be used outside the vertical application and the new model presented here should be applied for horizontal and deviated wells.

Table 7.5: Observed critical gas rates and percent deviation for Horizontal Well 2

Actual Lift Rate, Mscf / d	684	Absolute Percent Deviation, %
Coleman CR, Mscf / d	404	41
Turner, Mscf / d	481	30
New model, Mscf / d	**648**	**5**
Belfroid, Mscf / d	506	26
Veeken, Mscf / d	512	25

CHAPTER VIII

Liquid holdup theory

8.1 Pressure traverse and liquid holdup

Liquid holdup, H_L, refers to the fraction of liquid present in a cross sectional area of a pipe. Multiple correlations are currently used by the industry to calculate the liquid holdup. Some of these correlations consider slippage and some do not. Brill et al. (1999) classified the current empirical pressure gradient correlations into three categories:

- Category a: no slip, no flow pattern
- Category b: considers slip, but no flow pattern
- Category c: considers both slip and flow pattern

Slippage occurs because there are differences in flowing velocities between the different flowing phases. Therefore, the H_L is typically different from the input liquid fraction. The liquid fraction at a given depth is defined as follows:

$$H_L = \frac{A_L}{A} \qquad \text{----------} \qquad (8.1)$$

where A_L is the cross-sectional area occupied by the liquid phase, and A is the total cross-sectional area of the pipe.

It is important to determine the liquid holdup because it is used to compute the pressure gradient throughout the wellbore and to define how the flow patterns should be mapped. The governing equation for the pressure gradient is determined by applying the

concepts of conservation of mass and conservation of linear momentum for steady state flow. The resulting mechanical energy balance is as follows:

$$\Delta P_{Total} = \Delta P_{Hydrostatic} + \Delta P_{Friction} + \Delta P_{acceleration} \quad \text{----------} \quad (8.2)$$

Equation 8.2 has three components—the friction pressure loss component, the hydrostatic pressure component, and an acceleration component. The friction and hydrostatic components are the most influential, with gravity being the dominant player, while the acceleration component is typically negligible.

8.1.1 The friction component

The friction component is a function of the friction factor, fluid density and velocity, and conduit diameter and is defined in psi using the Fanning friction factor as follows:

$$\Delta P_{friction} = \frac{2 f \rho_n V_m^2 h}{g_c d} \quad \text{----------} \quad (8.3)$$

where f is the Fanning friction factor, ρ_n is the non-slip mixture density, V_m is the mixture velocity, h is the elevation, g_c is gravitational correction factor constant, and d is the flow conduit inside diameter.

The single phase flow friction factor, for gas or liquid, is determined either graphically or numerically. Figure 8.1 shows the Moody diagram used to determine the Moody friction factor for a given N_{Re} and pipe relative roughness. Note that the Moody friction factor is four times the Fanning friction factor.

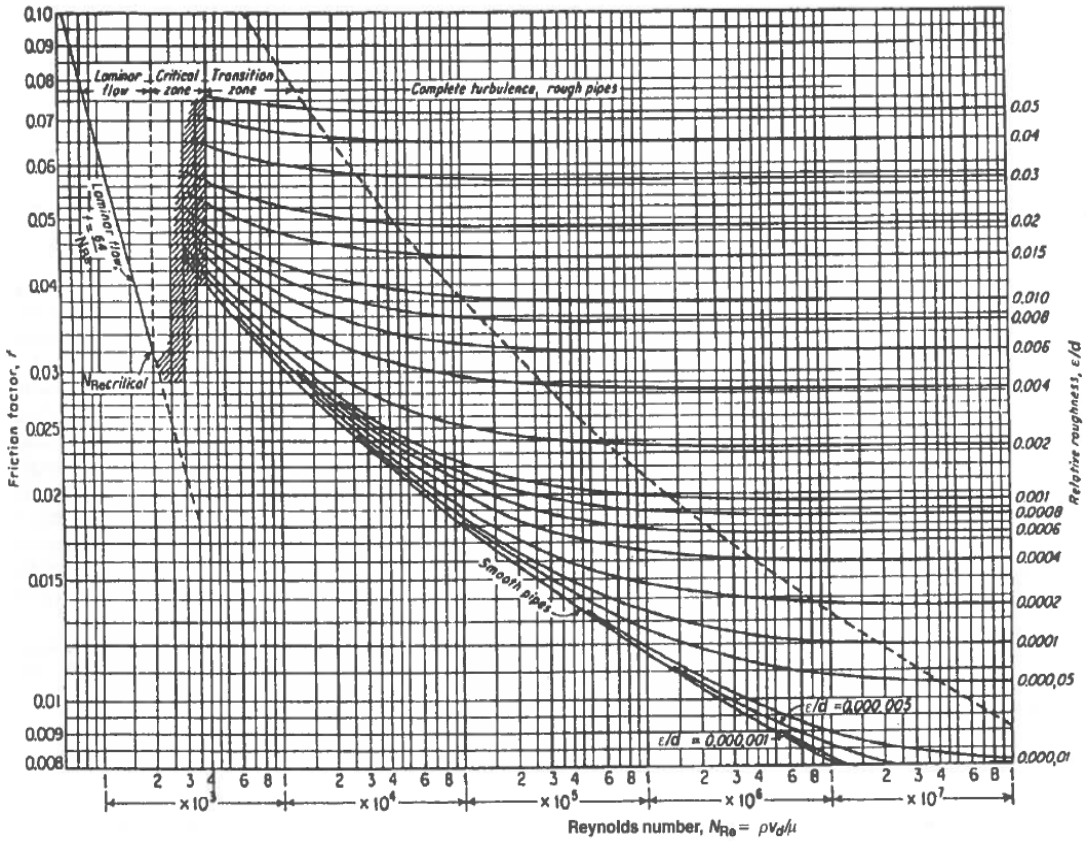

Figure 8.1 Moody friction factor diagram for pipes

An empirical equation to compute the Fanning friction factor was presented by Chen (1979) as follows:

$$\frac{1}{\sqrt{f}} = -4\log\left[0.2698\left(\frac{k}{d}\right) - \frac{5.0452}{N_{Re}}\log\left\{0.3539\left(\frac{k}{d}\right)^{1.1098} + \frac{5.8506}{N_{Re}^{0.8981}}\right\}\right] \quad \text{---------} \quad (8.4)$$

where, f is the Fanning friction factor, k is the pipe absolute roughness, k/d is the relative roughness, and N_{Re} is the Reynolds number, defined as follows:

$$N_{Re} = \frac{\rho V d}{\mu} \quad \text{----------} \quad (8.5)$$

where, ρ is the mixture density, V_m is the mixture velocity, d is the flow conduit inside diameter, and μ is the mixture viscosity.

For multiphase flow cases, the single phase friction factor is still adapted. This adaptation differs from one correlation to another. For example, Gray (1978) uses a pseudo-wall-roughness to incorporate the effect of H_L on friction loss, while Hagedorn and Brown (1965) uses a two-phase N_{Re} to determine the friction factor.

8.1.2 The hydrostatic component

The hydrostatic component is a function of the fluid density and the change in elevation. It is defined as follows:

$$\Delta P_{Hydrostatic} = \rho_m g h \qquad (8.6)$$

where, h is the elevation, ρ_m is the mixture density, and g is acceleration of gravity.

For multiphase flow cases, the mixture density is obtained after H_L is identified, which represents the in-situ condition. The no-slip density is not used in this case because it represents the input condition, not the in-situ. The mixture density is identified as follows:

$$\rho_m = \rho_L H_L + \rho_g (1 - H_L) \qquad (8.7)$$

where, H_L is the in-situ liquid volume fraction (liquid holdup), ρ_m is the mixture density, ρ_L is the liquid density, and ρ_g is the gas density.

8.2 Liquid holdup adjustment

The effect of buildup rate (BUR) and dog leg severity (DLS) is manifested through a change in the liquid holdup. As droplets exit one section of the pipe towards a new section with a different BUR, they will experience an impact and rebound that positions them in the way of upcoming droplets. That situation will cause droplets to collide with

each other and change direction, resulting in gradual reorientation of all droplets to the new geometry. The latter process will be repeated throughout the build section as the BUR changes until the vertical section above the kick off point is reached. At that point, the changes in BUR are usually insignificant, typically less than 3 degree deviation (see Fig. 8.2).

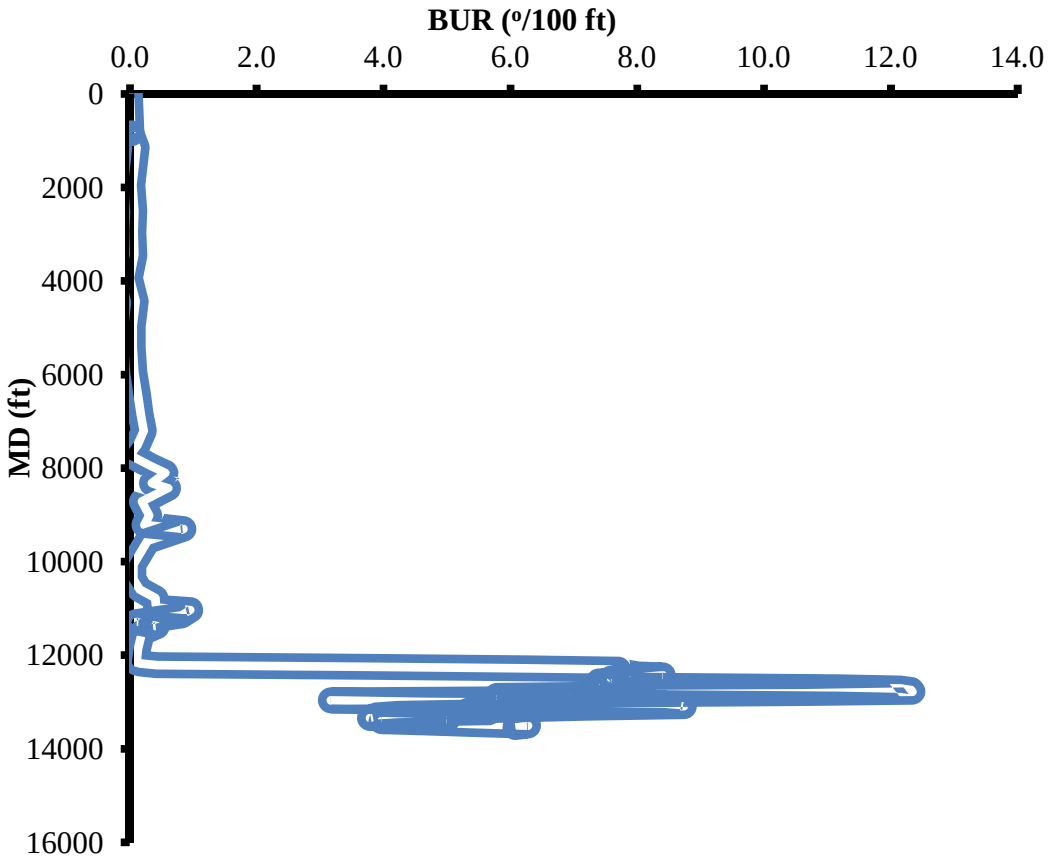

Figure 8.2: Change of inclination versus MD in horizontal and deviated wells

The effect of impact and rebound is more stringent in horizontal and deviated wells, especially at the curve or build section, than it is in vertical wells. This can be explained by the available distance the droplet has to travel downward before it reaches a rest surface, i.e., wall or plug back true depth. In vertical wells, that distance can be

significant, tens to thousands of feet. The case is different for horizontal and deviated wells because of the very limited time and space the droplet might have before it can reach a rest surface, typically inches to tens of feet.

To illustrate the influence of the BUR, Fig. 8.3 shows the lowest portion of the cross sectional area at the pivot point where change in geometry occurs. The reduction of the droplets' velocity at these locations makes these areas act as a collection ground for droplets. If the droplet collection process continues, it will eventually gather enough liquid to fill up the pivot point and use it as a liquid buildup base. Having water occupying that portion of the pipe affects the liquid holdup. Therefore, a new liquid holdup that takes into account the presence of a watered out portion of the cross sectional area will need to be considered.

A few steps are taken to determine the new H_L:

1. Identify the portion of the cross sectional area that is submerged under liquid. That area, A_α, is a direct function of the BUR angle α and can be computed from the deviation survey.
2. Compute the liquid holdup using one of the many available correlations. For this study, the Gray correlation (1978) was used.
3. Finally, the calculated H_L is adjusted to account for the liquid accumulation, and a new H_L, referred to as H_{Lnew}, is computed.

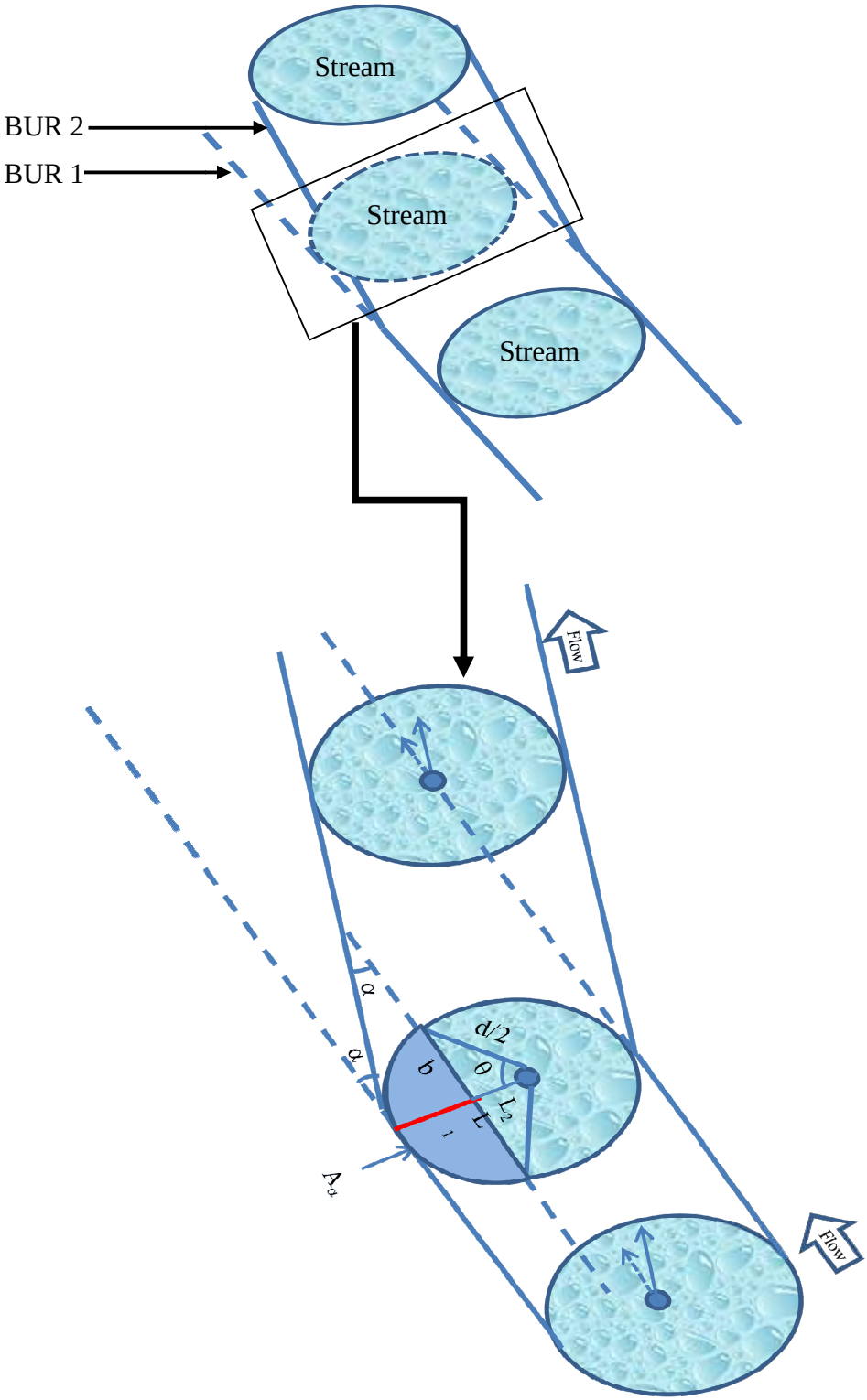

Figure 8.3: The effect of BUR on liquid holdup

In order to determine A_α, first we need to determine the height, L_1, of the cross sectional area that is filled up with water. For any given α, using one projection of the flow conduit diameter, d, L_1 is calculated as follows:

$$L_1 = d \times sin\alpha \qquad (8.8)$$

L_2 is the length difference between the flow conduit radius and the wet chord peak L_1 defined as follows:

$$L_1 + L_2 = \frac{\mathrm{d}}{2} \qquad (8.9)$$

or,

$$L_2 = \frac{d}{2} - L_1 \qquad (8.10)$$

Once L_1 is identified, the area A_α can be computed as the resultant of the internal flow conduit area and twice the area of the triangle A_t defined as $\left(b\hat{\theta}(d/2)\right)$ as follows:

$$A_\alpha = (\frac{2\theta}{2\pi} \times \frac{\pi}{4} d^2) - 2\mathrm{A}_t \qquad (8.11)$$

or,

$$A_\alpha = \left(\frac{\theta}{4} \times d^2\right) - 2\,A_t \qquad (8.12)$$

where,

$$Cos\ \theta = \frac{L2}{d/2} = 1 - \frac{2L1}{d} \qquad (8.13)$$

Replacing Eqs. 8.8 and 8.10 into Eq. 8.13 and solving for θ leads to:

$$\theta = Acos(1 - 2sin\alpha) \qquad (8.14)$$

The area of the triangle A_t is defined as:

$$A_t = \frac{1}{2} b \times L_2 \qquad (8.15)$$

The Pythagorean Theorem can be used to calculate b as follows:

$$b^2 + L_2^2 = \left(\frac{d}{2}\right)^2 \qquad (8.16)$$

Rearranging, and replacing Eq. 8.10 into Eq. 8.16 we get:

$$b = \sqrt{dL_1 - L_1^2} \qquad (8.17)$$

Replacing b with its value from Eq.8.17 and L_2 with its value from Eq. 8.10 into Eq. 8.15 leads to:

$$2A_t = \left(\frac{d}{2} - L_1\right)\sqrt{dL_1 - L_1^2} \qquad (8.18)$$

Substituting Eqs. 8.8, 8.14, and 8.18 into Eq. 8.12, we get:

$$A_\alpha = \frac{d^2}{2}\left[\left(\frac{Acos(1-2sin\alpha)}{2}\right) - \left((1-2sin\alpha)(sin\alpha(1-sin\alpha)^{\frac{1}{2}}\right]\right. \qquad (8.19)$$

Therefore, the liquid fraction that should be added to compensate for liquid accumulation, H_{La}, is calculated as follow:

$$H_{La} = \frac{A_\alpha}{A_d} \qquad (8.20)$$

Finally, the adjusted liquid holdup, H_{Lnew}, is obtained as follow:

$$H_{LNew} = H_{LOld} + H_{La} \qquad (8.21)$$

where,

L_1 = the height of the area affected by the change in BUR in ft;

L_2 = droplet radius minus L_1 in ft;

d = droplet diameter in ft;

b = the chord of the area affected by the change in BUR in ft;

α = the BUR angle in deg;

A_α = the area affected by the change in BUR in ft^2;

A_t = the volume of the triangle with the chord as a base and the sides as droplet radius in ft^3;

H_{La} = additional H_L normalized to the flow conduit area;

H_{LNew} = the adjusted new holdup value

H_{LOld} = the holdup calculated using any given correlation i.e. the Gray correlation

8.3 The effect of H_{Lnew} on flow correlations

This section demonstrates how the BUR is used to modify the method implemented to compute H_L. As an example, the Gray correlation is used to illustrate this effect. Gray (1978) used 108 well test data to develop a pressure drop correlation for two-phase flow in vertical wet gas wells. The resulting equation is as follows:

$$\frac{dp}{dL} = \rho_s g + \frac{f\rho_n V_m^2}{2d} \qquad \text{----------} \qquad (8.22)$$

Currently, modifications of the Gray correlation allow its usage in horizontal wells, mainly by changing the manner in which the hydrostatic and friction components are computed. The Gray correlation considers slippage and uses dimensionless numbers when calculating the liquid holdup; this H_L will be subject to modification using the effect of the BUR as explained earlier. The modified H_L will be referred to as H_{Lnew} and will be compared to the original H_L.

$$H_L = 1 - \frac{1-e^{\left\{-2.314\left[N_v\left(1+\frac{205}{N_D}\right)\right]^B\right\}}}{R+1} \qquad \text{----------} \qquad (8.23)$$

As described by the Eq. 8.23, H_L depends on the three dimensionless numbers—N_v, N_D, and B, and the ratio of the superficial velocity of the liquid and gas. The dimensionless numbers require a good estimation of the PVT and flow conduit data and are defined as follows:

$$N_v = \frac{\rho_n^2 V_m^4}{g\sigma_l(\rho_l - \rho_g)} \quad \text{----------} \quad (8.24)$$

$$N_D = \frac{gd^2(\rho_l - \rho_g)}{\sigma_l} \quad \text{----------} \quad (8.25)$$

$$B = 0.0814\left[1 - 0.0554 \ln\left(1 + \frac{730R}{R+1}\right)\right] \quad \text{----------} \quad (8.26)$$

The superficial velocity ratio is defined as follows:

$$R_v = \frac{V_{sl}}{V_{sg}} \quad \text{----------} \quad (8.27)$$

where,

$$V_{sl} = \frac{q_l}{A_d} = \frac{q_o B_o + (q_w - W_{cond} * q_g) B_w}{\pi/4 d^2} \quad \text{----------} \quad (8.28)$$

and,

$$V_{sg} = \frac{q_g}{A_d} = \frac{(q_g - q_o R_s) B_g}{\pi/4 d^2} \quad \text{----------} \quad (8.29)$$

Once the H_L is identified, the well's deviation survey is used to correct for the effect of the BUR.

$$H_{Lnew} = \left[1 - \frac{1 - e^{\left\{-2.314\left[N_v\left(1 + \frac{205}{N_D}\right)\right]^B\right\}}}{R+1}\right] + 0.6367\left[\left(\frac{Acos(1-2sin\alpha)}{2}\right) - \left((1 - 2sin\alpha)(sin\alpha(1 - sin\alpha)^{\frac{1}{2}}\right)\right] \quad \text{----------} \quad (8.30)$$

where V_{sl} is the superficial liquid velocity, V_{sg} is the superficial gas velocity, V_m is the mixture velocity, W_{cond} is the water of condensation, q_o oil production, q_w is water

production, q_g is gas production, q_L is total liquid production, B_o is the oil formation volume factor, B_W is the water formation volume factor, B_g is the gas formation volume factor, R_S is the solution gas/oil ratio, ρ_g is the gas density, ρ_l is the liquid, and σ is the gas / liquid surface tension.

Equation 8.30 is referred to as the adjusted liquid holdup and should be used to calculate H_{Lnew} for any given BUR.

The H_{Lnew} value is used to identify areas throughout the wellbore that are prone to carry higher liquid fractions and cause a transition outside the mist flow region. Barnea (1986; 1987) stated that the flow regime changes to a slug or churn flow pattern when the liquid holdup value is higher than 0.24. The proposed H_L adjustment is not unique to the Gray model and can also be expanded to other pressure traverse models.

8.4 Example using Horizontal Wells 1 and 2

8.4.1 Horizontal Well 1

Table B4 in Appendix B shows the calculated H_L distribution along the wellbore using the Gray correlation and the adjust Gray correlation, H_{Lnew}, coupled with the conventional models and the new model for critical gas rate predictions for Horizontal Well 1.

Using the conventional models, Turner and Coleman, coupled with the H_L from the Gray correlation (Fig. 8.4) suggests that the well is supposed to be flowing in the mist flow region and no liquid accumulation is occurring, as suggested by an H_L of 0.13. The same is shown when using the new model for critical gas rate predictions, coupled with the H_L from Gray (Fig. 8.5). The new model shows better H_L distribution along the

wellbore than the conventional models with a maximum H_L of 0.10. Using the adjusted H_{Lnew}, coupled with either the conventional models or the new model for critical rate predictions shows the emergence of an area around the curved section from 12,681 to 12,808 ft as having liquid holdup values higher than 0.24 (see Figs. 8.6 and 8.7). Therefore, the latter identified area is the location that is prone to liquid accumulation and should be taken into account when planning to run production equipment.

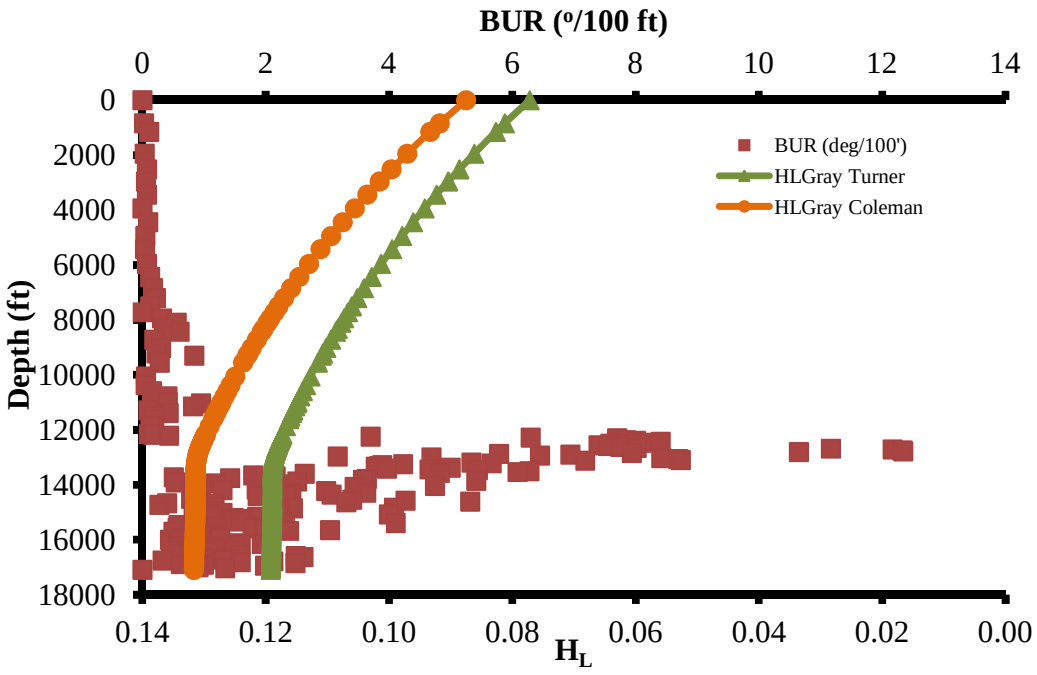

Figure 8.4: Conventional models for critical gas rate prediction coupled with H_L from the Gray correlation, Horizontal Well 1

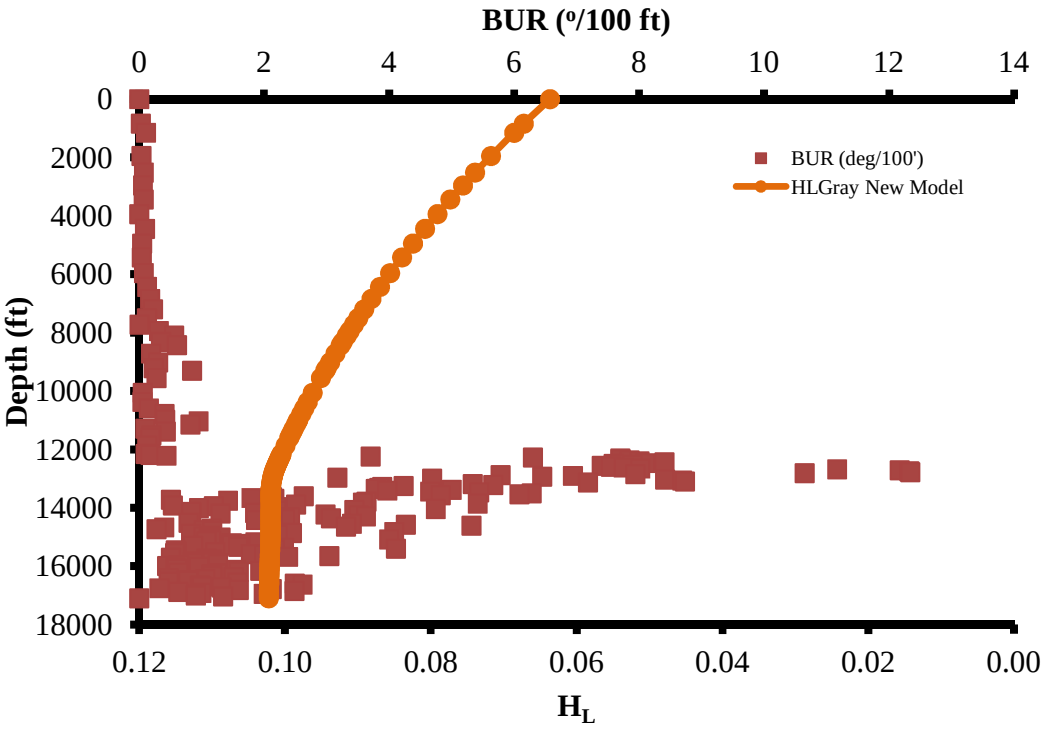

Figure 8.5: New model for critical gas rate prediction coupled with H_L from the Gray correlation, Horizontal Well 1

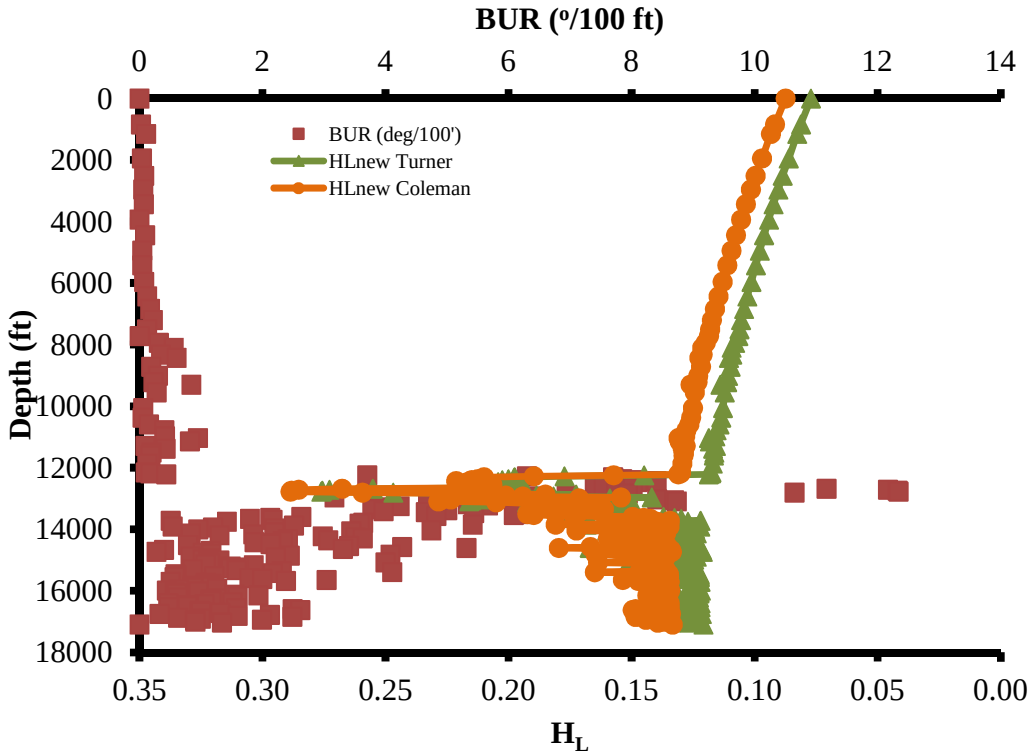

Figure 8.6: Conventional models for critical gas rate prediction coupled with H_{Lnew} from the adjusted Gray correlation, Horizontal Well 1

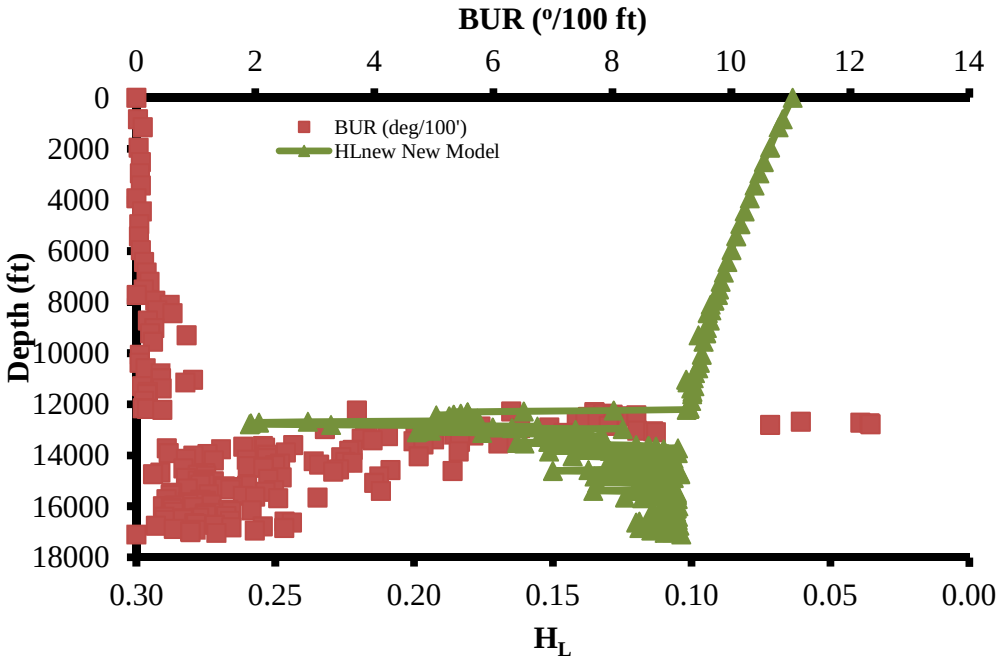

Figure 8.7: New model for critical gas rate prediction coupled with H_{Lnew} from the adjusted Gray correlation, Horizontal Well 1

Once the problem areas in the wellbore are identified, designing the tubing, both sizing and placement, becomes clear and provides a good solution for resolving liquid accumulation in these areas. Figure 8.8 shows the H_L distribution for 2 7/8" tubing coupled with the new model's critical gas rate prediction value calculated for Horizontal Wells 1 and the adjusted H_{Lnew}. The latter combination shows a good distribution of liquid holdup throughout the wellbore, with all values below 0.24 and a maximum value of 0.19. Figure 8.9 shows the overlay of all models and the progressive improvement of the well liquid holdup when moving away from conventional models and the Gray H_L towards the new model and the adjusted Gray H_L. For the same method of critical gas rate prediction, both the Gray and adjusted Gray holdup models overlap in the vertical section of the wellbore; however, in the curved and horizontal sections, the Gray correlation projects a constant value for TD, while H_{Lnew} shows variation as function of

deviation. The latter is what leads to the identification of areas along the wellbore that are more likely to be triggers of liquid loading.

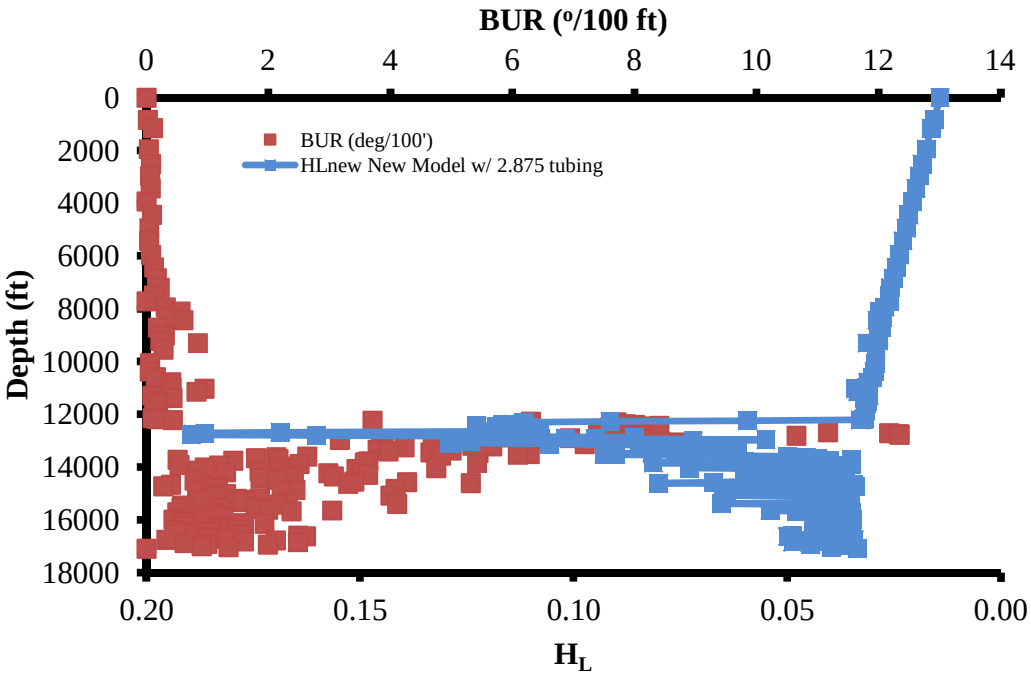

Figure 8.8: Tubing placement and its effects on H_L using the new model critical gas rate prediction coupled with H_{Lnew} the adjusted Gray correlation, Horizontal Well 1

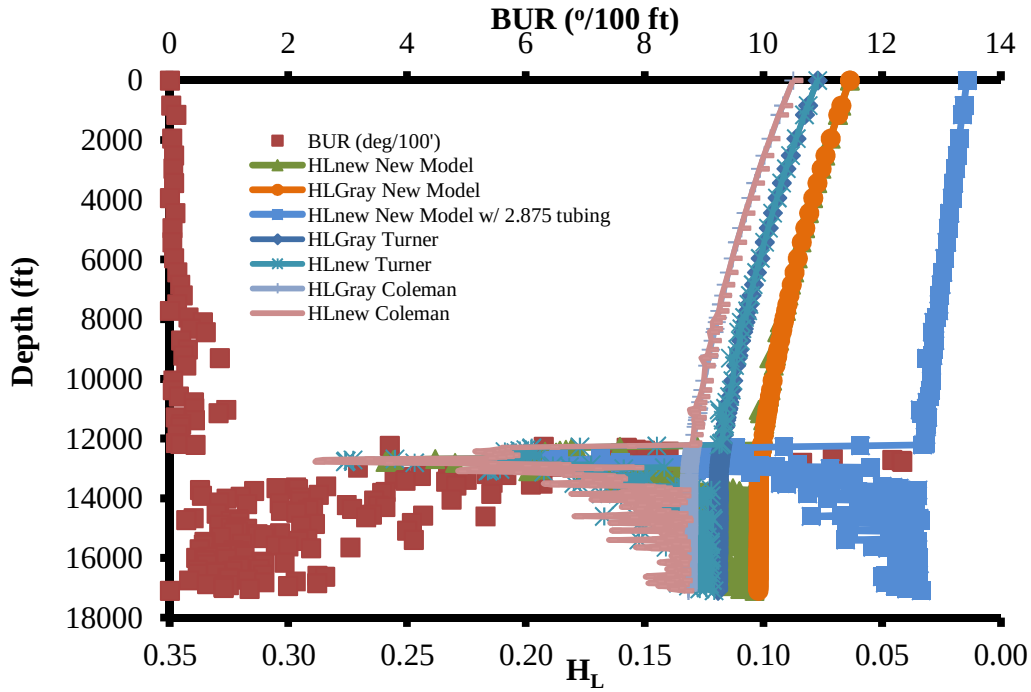

Figure 8.9: Overlay showing differences between H_L and H_{Lnew} using the new model for critical gas rate, Horizontal Well 1

8.4.1 Horizontal Well 2

Similar to Horizontal Well 1, Table B5 in Appendix B shows the calculated H_L distribution along the wellbore using the Gray correlation and the adjusted Gray correlation, H_{Lnew}, coupled with the conventional models and the new model for critical gas rate predictions for Horizontal Well 2. Using the conventional models, Turner and Coleman, coupled with the H_L from the Gray correlation (see Fig. 8.10) suggests that the well is supposed to be flowing in the mist flow region, and no liquid accumulation is occurring (according to a maximum calculated H_L of 0.22). The same is shown when using the new model for critical gas rate predictions coupled with the H_L from Gray (see Fig. 8.11). The new model shows better H_L distribution along the wellbore than the conventional models, with a maximum H_L of 0.18. All models show a drop in H_L starting at the top of the liner because of the change in casing size from 7" to 4.5" OD.

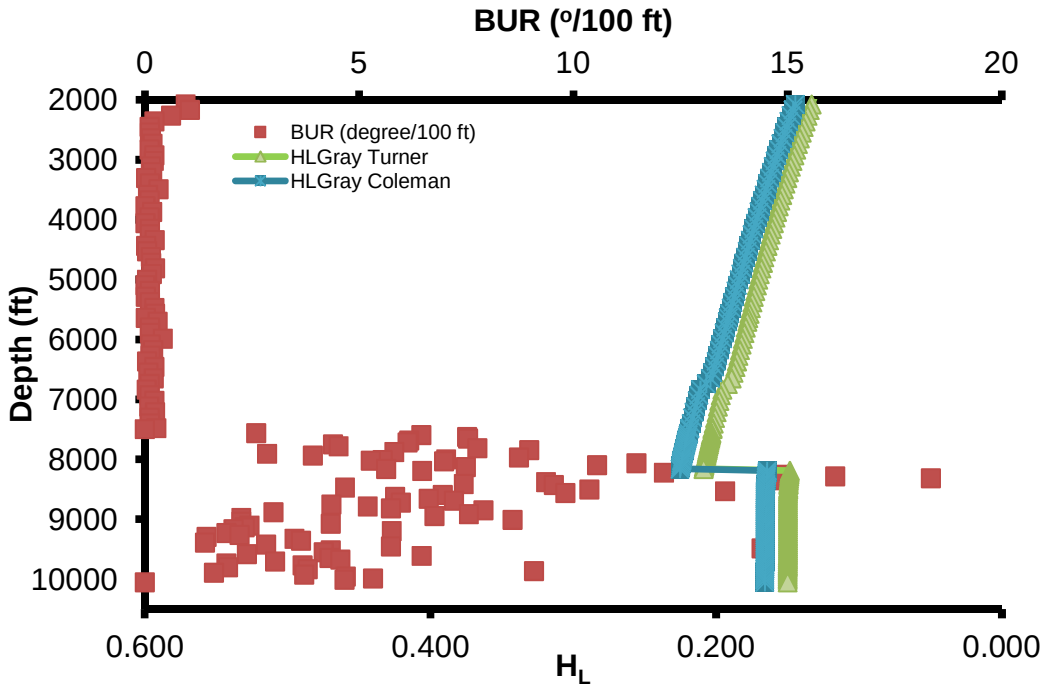

Figure 8.10: Conventional models for critical gas rate prediction coupled with H_L from the Gray correlation, Horizontal Well 2

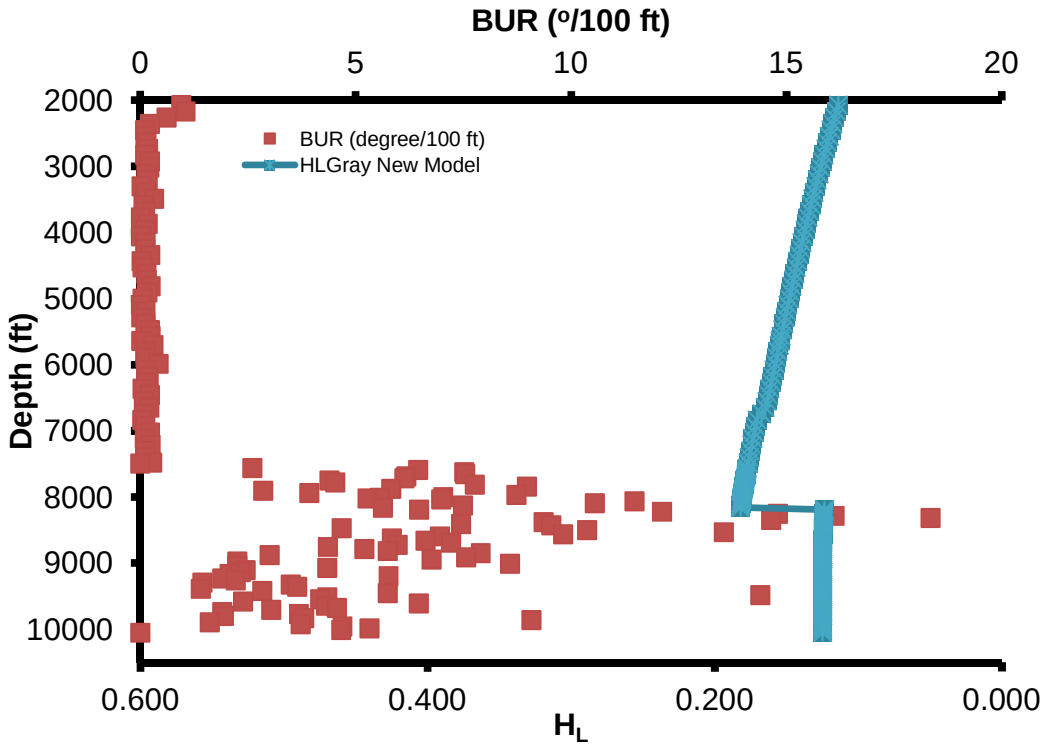

Figure 8.11: New model for critical gas rate prediction coupled with H_L from the Gray correlation, Horizontal Well 2

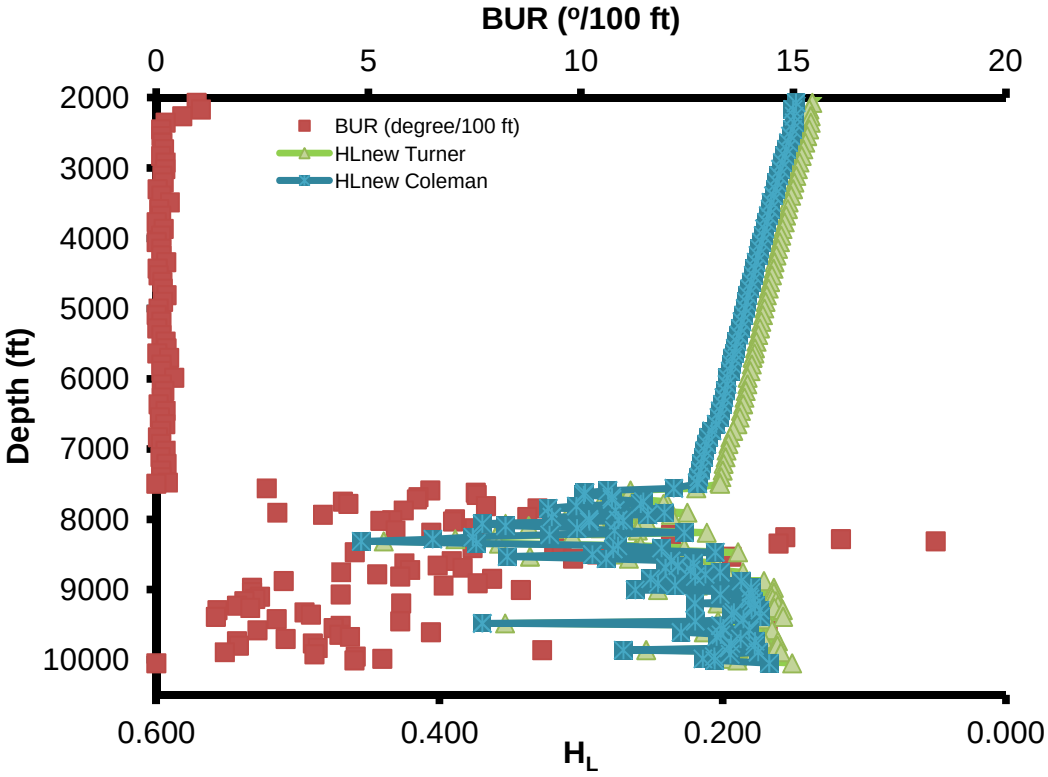

Figure 8.12: Conventional models for critical gas rate prediction coupled with H_{Lnew} from the adjusted Gray correlation, Horizontal Well 2

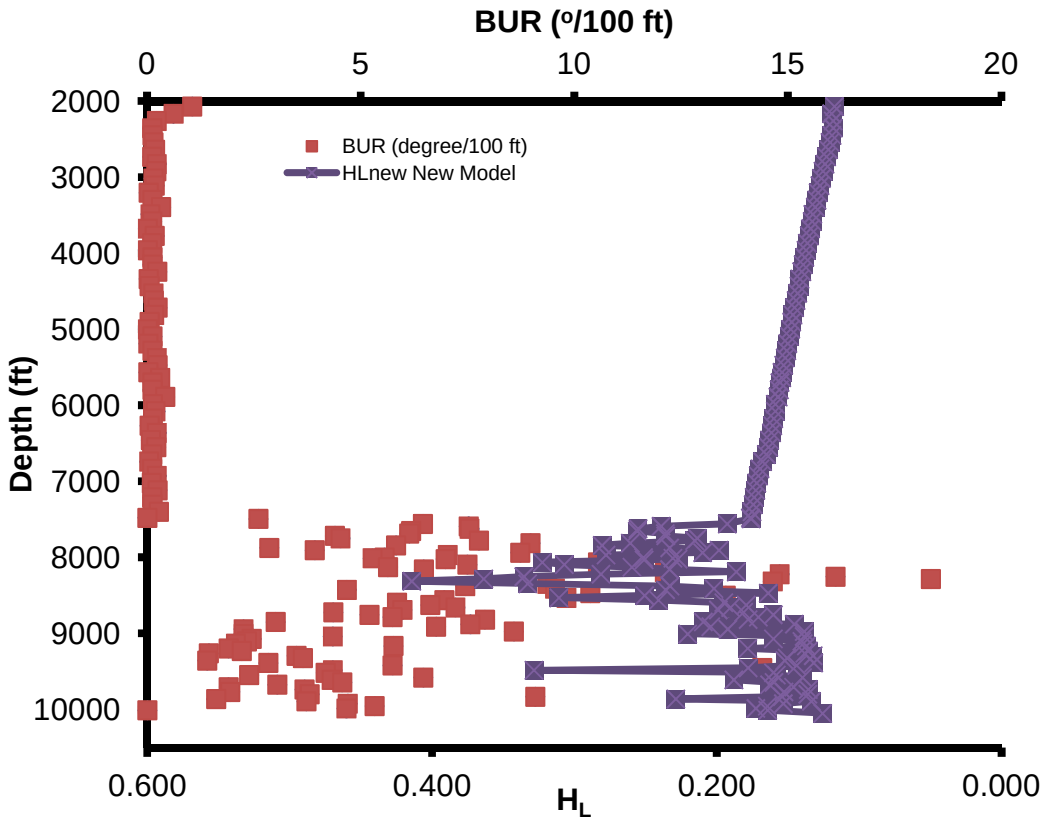

Figure 8.13: New model for critical gas rate prediction coupled with H_{Lnew} from the adjusted Gray correlation, Horizontal Well 2

Using the adjusted H_{Lnew} coupled with either the conventional models or the new model for critical rate predictions shows the emergence of an area around the curved section from 7,590 to 8,689 ft as having liquid holdup values higher than 0.24 (see Figs 8.12 and 8.13). Therefore, the latter identified area is the location that is prone to liquid accumulation and should be taken into account when planning to run production equipment. Once again, the emergence of these zones as prone to liquid loading is completely missed by the Gray method estimation of liquid holdup, especially when coupled with the conventional critical rate models.

Thus, the area identified earlier is the ideal location to place the end of tubing. Results with the 2 7/8" tubing (Fig. 8.14) show that the well now has better H_L distribution along the wellbore. The majority of the wellbore sections have gas velocities above the critical rate and therefore are able to keep the liquid droplets moving upward with H_L less than 0.24. There are only three points showing H_L values higher than 0.24 which is a tremendous improvement over the other models.

This is in agreement with the experimental data which proves that coupling the new model for critical gas rate calculation with H_{Lnew} provides the best chance in keeping the wells following at high enough rates to keep liquid droplets from settling and accumulating in the wellbore therefore, interfering with the wells true production potential.

Figure 8.15 shows the overlay of all models and the progressive improvement of the liquid holdup distribution along the wellbore. Moving away from the conventional critical gas rate and the standard H_L models towards the new critical gas rate and the adjusted H_{Lnew} clearly yields better performance.

The results from the two horizontal wells indicate the importance of using the correct models while preparing to produce a well. If the inappropriate models are used, there will be discrepancies between how the well should be performing and how it is actually performing. Using the new critical gas rate prediction model coupled with the adjusted liquid holdup method will help improve planning and producing horizontal wells therefore, resolving the disconnection between the modeling expectation and reality typically encountered in this type of wells.

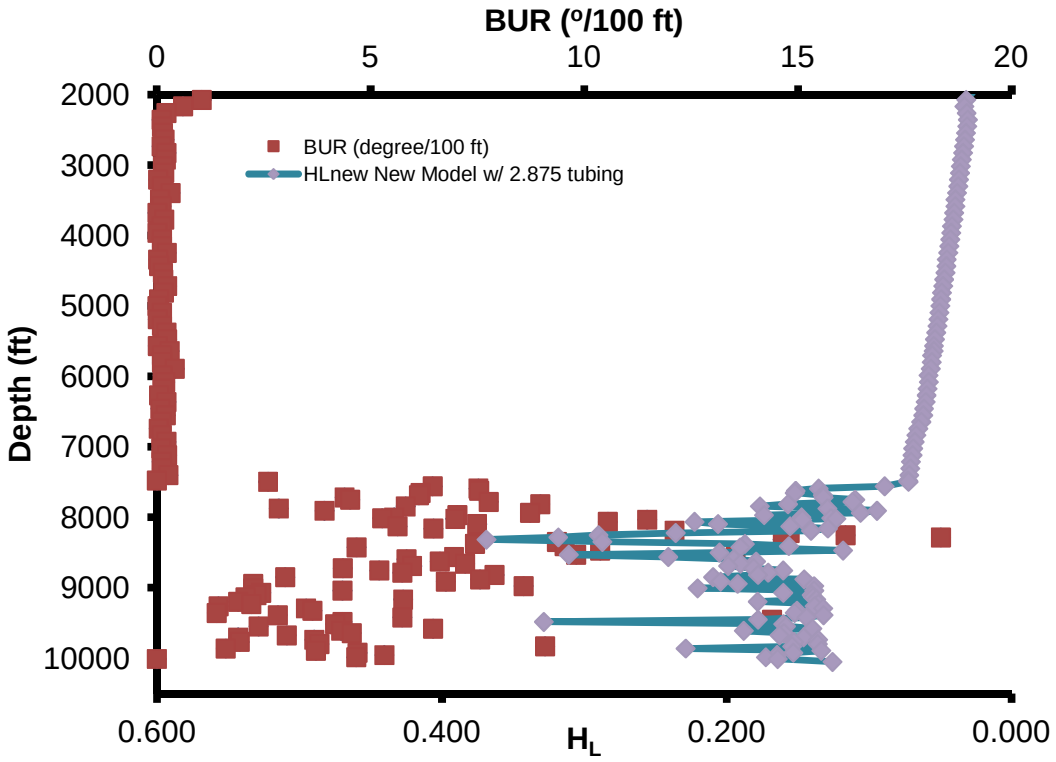

Figure 8.14: Tubing placement and its effects on H_L using the new model for critical gas rate prediction coupled with H_{Lnew} from the adjusted Gray correlation, Horizontal Well 2

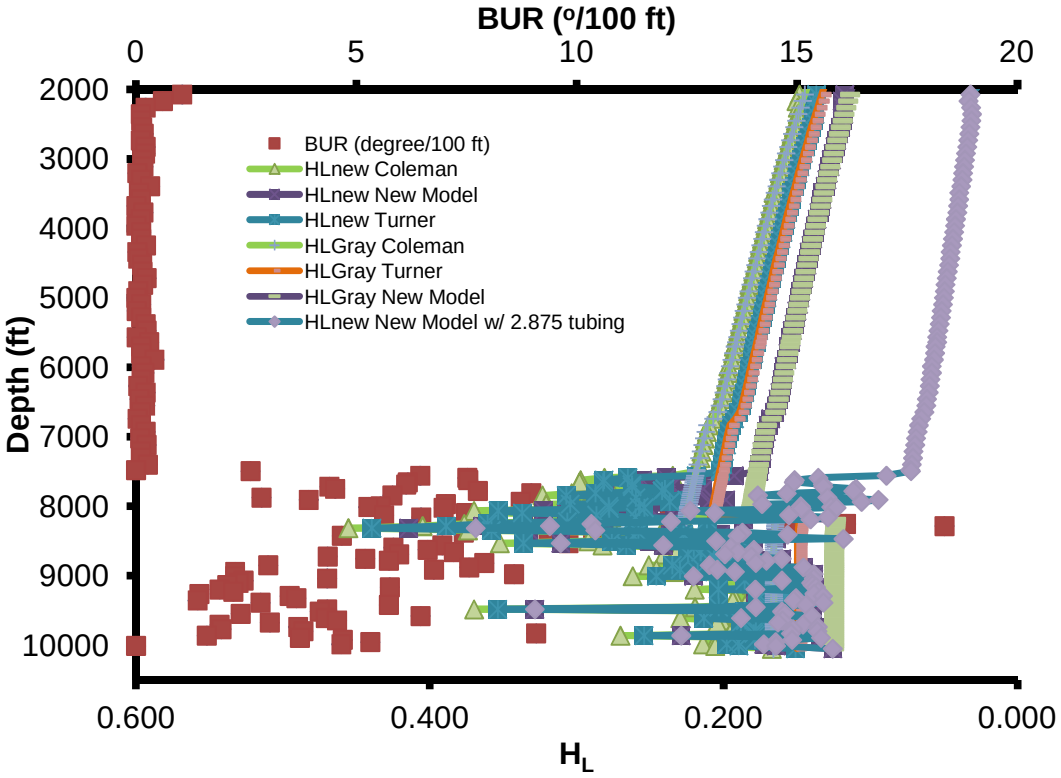

Figure 8.15: Overlay showing differences between H_L and H_{Lnew} using the new model for critical gas rate, Horizontal Well 2

CHAPTER IX

Conclusions and Recommendations

This chapter is composed of two sections. The first section consists of conclusions that are deduced from the theoretical and experimental work to identify the effective gas rate to lift horizontal and deviated wells. The second section proposes future work to improve the understanding of liquid loading in horizontal and deviated wells.

9.1 Conclusions

Critical gas rate in horizontal and deviated wells was studied through theoretical and experimental means. A predictive model was established and proposed as the model to use by the industry to ensure proper planning for horizontal and deviated wells. The following conclusions are made:

1. The new model accounts for the effects of wellbore geometry on liquid loading and predicts the critical rate for horizontal and deviated wells.
2. The new model accuracy of predicting the critical gas rates was tested with data set comprised of 67 wells from literature. Results showed that the new model prediction is within 15.7% from actual which outperforms the horizontal well models, Veeken model and Belfroid model, and the conventional vertical models, Turner model and Coleman model.
3. Experimental work using two horizontal wells supports the finding from the literature comparison and confirms the superiority of the new model. The results showed the new model prediction to be within 5% from actual which,

when compared to the horizontal models, represents an improvement of 24% over Belfroid model and 18% over Veeken model. On the other hand, when compared to the conventional vertical model, the improvement is 23% over Turner model and 35% over Coleman model.

4. The new model yields best results for gas rates less than 10,000 Mscf/d and for BUR's between 4^o and 30^o/100 ft.
5. In vertical wells, the new model collapses to Coleman model.
6. Conventional vertical models should not be used for horizontal and deviated wells.
7. An adjusted liquid holdup, H_{LNew} was proposed to help identify the best location for tubing placement in order to prevent areas prone to liquid accumulation from causing the well to load up.

9.2 Recommendations for future research

Simplification and assumptions have been adopted to solve the liquid loading problem. As a result, there are discrepancies between the predictive critical gas rate models and the actual observed rates. Improvements can be made by building a mechanistic model based on laboratory apparatus that mimic the continuous change in geometry from the horizontal section through the curved section to the vertical section. This will allow obtaining actual in-situ real time sampling and measurement of the rate of accumulation of liquid as function of the geometry change along the wellbore and its effect on the critical gas rate.

Finally, it is recommended that the effect of undulations in the horizontal section on different well layouts be investigated, i.e., toe up, toe down, or flat geometries. It is believed that these undulations act as traps for liquids and can block the perforations laying at the bottom part of the casing from contributing, especially in low pressure toe down wells, thus impairing both reservoir and production efficiency.

NOMENCLATURE

A = conduit cross sectional area, ft^2

A_χ = adjusted liquid holdup areas, ft^2

BHFP = bottom hole flowing pressure, psia

BFPD = barrels of fluid per day

B_g = gas formation volume factor

B_o = oil formation volume factor

B_w = water formation volume factor

BUR = build up rate, ^{o}/100 ft

CP = casing pressure, psia

C_d = drag coefficient

DLS = dogleg severity, ^{o}/100 ft

d_d = droplet diameter, in.

E_k = kinetic energy function defined by Guo el al., lbf-ft/ft^3

f = Fanning friction factor

FTP = flowing tubing pressure, psia

$F_{d,after}$ = drag force on particle after impact

$F_{d,before}$ = drag force on particle prior to impact

$F_{d,mup}$ = difference in drag before and after impact

H_L = liquid hold up

g = acceleration of gravity 32.17 ft/sec^2, or 9.8 m/sec^2

g_c = gravitational conversion factor 32.17 lbm-ft/lbf-sec^2

GOR = gas oil ratio, scf/bbl

N_{Re} = pipe Reynolds number

N_{Rep} = particle Reynolds number

P = pressure at the evaluation point, psia

q_c = critical gas rate, Mscf/d

q_o = oil rate, BOPD

q_w = water rate, BWPD

S = Guoua et al. energy loss factor

T = temperature at the evaluation point, ^{o}R

TR = Turner Ratio

V_b = particle restitution velocity, ft/s

V_c = critical velocity as expressed by Turner's derivation, ft/s

V_{eff} = effective lift velocity, ft/s

V_i = particle Initial velocity, ft/s

V_{mup} = additional velocity above the critical velocity necessary to maintain the critical condition post rebound, ft/s

V_{sg} = superficial gas velocity, ft/s

V_{sl} = superficial liquid velocity, ft/s

R = superficial velocity ratio

We = Webber number

Z = gas compressibility factor

Greek Symbols

α = angle of deviation, degrees

α_z = Zhou et al. (2010) constant for liquid rate calculation

β = effective velocity factor

β_z = Zhou et al. (2010) concentration thereshold

ρ_l = liquid density, lbm/ft^3

ρ_m = mixture density, lbm/ft^3

ρ_s = slip density, lbm/ft^3

ρ_{ns} = non-slip density, lbm/ft^3

ρ_g = gas density, lbm/ft^3

σ = surface tension, dynes/cm

θ_i = incidence angle in degrees

θ_b = the rebound angle in degrees

γ_g = gas specific gravity

μ = viscosity, lbm/ft/sec

ω = inclination angle from the Belfroid model

REFERENCES

1. Awolusi, 0. 2005. Resolving discrepancies in predicting critical rates in low pressure stripper gas wells. MS thesis, Texas Tech University, Lubbock, Texas.
2. Barnea, D. 1986. Transition from annular flow and from dispersed bubble flow—unified models for the whole range of pipe inclinations. International Journal of Multiphase Flow 12 (5), pp. 733-744.
3. Barnea, D. 1987. A unified model for predicting flow-pattern transitions for the whole range of pipe inclinations. International Journal of Multiphase Flow 13 (1): 1-12.
4. Belfroid, S.P.C., Schiferli, W., Alberts, G.J.N., Veeken, C.A.M. and Biezen, E. 2008. Prediction onset and dynamic behaviour of liquid loading gas wells. Paper SPE 115567 presented at the SPE ATCE, Denver, CO, USA, 21-24 September.
5. Brill, J.P., Mukherjee H. 1999. Multiphase flow in wells, Vol. 17. Richardson, Texas: Monograph Series, SPE.
6. Coleman, S.B., Clay, H.B., McCurdy, D.G., and Norris HI, L.H. 1991b. A new look at predicting gas-well load up. J. Pet Tech 43 (3): 329-333. SPE-20280-PA.
7. Coleman, S.B., Clay, H.B., McCurdy, D.G., and Norris HI, H.L. 1991c. Understanding gas-well load-up behavior. J. Pet Tech 43 (3): 334-338. SPE-20281-PA.
8. Coleman, S.B., Clay, H.B., McCurdy, D.G., and Norris HI, H.L. 1991a. Applying gas-well load-up technology. J. Pet Tech 43 (3): 344-349. SPE-20283-PA.
9. Daas, M., Golczynski, T., and Msikenny, H. 2012. Minimum flow rate to unload gas wells: dynamic multiphase modeling to validate existing correlations. Paper SPE 152597 presented at the SPE Offshore Latin American and Caribbean Petroleum

Engineering Conference, Mexico, 16-18 April.

10. Dousi, N., Veeken, C.A.M. Currie, P.K. 2005. Numerical and analytical modeling of the gas-well liquid-loading process. SPE Prod & Operations 21 (4): 475-482. SPE-95282-PA.
11. Engineering Data Book, 12th edition. 2004. Gas processors suppliers association, Tulsa, Ok.
12. Fiedler, S. and Auracher. H.2004. Experimental and theoretical investigation of reflux condensation in an inclined small diameter tube. International Journal of Heat and Mass Transfer 47 (19–20): 4031-4043.
13. Ghuo, B. and Ghalambor, A. 2005. A systematic approach to predicting liquid loading in gas wells. Paper SPE 94081 presented at the SPE Prod. and Ops. Symposium, Oklahoma City, OK, 17-19 April.
14. Gray H.E., 1978. User's Manual for API 114B, SSCSV Sizing Computer Program, Appendix B pp. 38-41.
15. Guohua, L., Shunli, H. 2012. A new model for the accurate prediction of liquid loading in low pressure gas wells. J. Cdn. Pet. Tech 51 (6): 493-498. SPE-158385-PA.
16. Hagedorn, A.R. and Brown, K.E. 1965. Experimental study of pressure gradient occurring during continuous two-phase flow in small diameter vertical conduit. J. Pet Tech 17 (4) 475. SPE-940-PA
17. Jayaratne, O. W., Mason B. J. 1964. The coalescence and bouncing of water drops at an air/water interface. Proceeding of the Royal Society of London. Series A, Mathematical and Physical Sciences, 280 (1383): 545-565.
18. Lea, J. F. and Nickens, H.V. 2003. Gas well deliquification, Massachusetts: Elsevier

Burlington.

19. Li, M., Li, S.L., and Sun, L.T. 2002. New view on continuous-removal liquids from gas wells. SPE Prod & Fac 17 (1): 42-46. SPE-75455-PA.
20. Nosseir, M.A., Darwich, T.A., Sayyouh, M.H., and Sallaly, M.E.2000. A new approach for accurate prediction of loading in gas wells under different flowing conditions. SPE Prod. & Facilities, 15, (4): 241-246. SPE-66540-PA
21. Oudeman, P 1990. Improved prediction of wet-gas-well performance. SPE Prod. Eng pp. 212-216.
22. Sutton, R.P., Cox, S.A., Williams, E.G. Jr., Stoltz, R.P., and Gilbert, J.V. 2003. Gas well performance at subcritical rates. Paper SPE 80887 presented at the SPE Production and Operations Symposium, Oklahoma City, Oklahoma, USA, 23-25 March.
23. Sutton, R.P. 2005. Fundamental PVT calculations for associated and gas/condensate natural-gas systems. Paper SPE 97099 presented at the ATCE, Dallas, TX, USA, 9 -12 October.
24. Sutton, R.P. 2009. An improved model for water-hydrocarbon surface tension at reservoir conditions. Paper SPE 124968 presented at the SPE ATCE, New Orleans, LA, USA, 4-7 October.
25. Sutton, R.P., Cox, S.A., Lea, J.F. and Rowlan, O.L.2009. Guidelines for the proper application of critical velocity calculations. SPE paper 120625 presented at the SPE Prod and Ops Symp., Oklahoma City, OK, 4-8 April.
26. Turner, R.G., Hubbard, M.G., and Dukler, A.E. 1969. Analysis and prediction of minimum flow rate for the continuous removal of liquids from gas wells. J. Pet Tech 21 (11): 1475-1482. SPE-2198-PA

27. Van 't Westende, J.M.C, Kemp H.K., Belt R.J., Portela L.M., Mudde R.F., Oliemans R.V.A. R.2007. On the role of droplets in cocurrent annular and churn-annular pipe flow. International Journal of Multiphase Flow, 33(6), pp 595-615.

28. Veeken, K., Bakker, E. and Verbeek, P. 2003. Evaluating liquid loading-field data and remedial measures. Presented at the Gas Well Deliquification Workshop, Denver, 3-4 March.

29. Veeken, K., Hu, B. and Schiferli, W. 2009. Transient multiphase flow modeling of gas-well liquid loading. Paper SPE 123657 presented at the SPE Offshore Europe Oil & Gas Conference & Exhibition, Aberdeen, UK, 8-11September.

30. Wallis, G.B. 1969. One dimensional two phase flow. McGraw Hill., New York City.

31. Wei, N., Li, Y.C., and Li, Y.Q. 2007. Visual experimental research on gas well liquid loading. Drilling & Production Technology 30 (3): 43-45.

32. Zhou, D. and Yuan, H. 2010. New model for gas well loading prediction. Paper SPE 120580 presented at the SPE Prod and Ops Symp, Oklahoma City, OK, 4-8 April.

APPENDIX A

This work did not rely on static values for calculations. Instead, the recommended correlations to compute the dynamic values for input parameters were adopted. This appendix presents the algorithm used for computation of parameters used by the new critical gas rate model and the adjusted liquid holdup using the Gray (1978) correlation as an example.

NEW MODEL ALGORITHM FOR CRITICAL GAS RATE PREDICTIONS IN HORIZONTAL AND DEVIATED WELLS

Function CRa(p, t, g, N2, Co2, H2S, gw, d, MaxDLS)

```
   Zf = z(p, t, g, N2, Co2, H2S)
   sigmaW = SigmaWater(p, t, g, N2, Co2, H2S, gw)
   rhoWater = rhoW(gw, p, t)
   rhogas = rhog(p, t, g, N2, Co2, H2S)
   If MaxDLS = 0 Then
      veff = 1.593 * (sigmaW * (rhoWater - rhogas) / (rhogas ^ 2)) ^ 0.25
   End If
         M = (0.0406 * MaxDLS ^ 0.7537)
   If M > 0.95 Then M = 0.95
  End If
   K = (1 - M) ^ 0.5 ' K is obtained from Jayaratne and Mason (1964), 1st read value x
at given angle, 2nd 1-X gives (Vi2-Vb2)/Vi2 or 1-(Vb2/Vi2),  '3rd take ^0.5 of 3rd is
```

the current drag velocity, 4th is 3rd^2 is current drag, 5th is (1-4th) is makeup drag, 6th is 5th^0.5 is make up velocity, 7th is Turner*6th is Veffective

```
q = (1 + (1 - K ^ 2) ^ 0.5)
veff = q * 1.593 * (sigmaW * (rhoWater - rhogas) / (rhogas ^ 2)) ^ 0.25
qt = 3.067 * p * Ap(d) * veff / ((t + 460) * Zf)
CRa = qt * 10 ^ 3
```

End Function

ADJUSTED HOLDUP ALGORITHM: USING THE GRAY CORRELATION

Function HLNew(qo, qw, qg, p, t, API, g, gws, Absroughness, d, N2, Co2, H2S, angle, dls)

```
Rs = StandingRs(p, t, API, g)
bo = StandingBo(Rs, t, API, g)
Bgas = Bg(p, t, g, N2, Co2, H2S)
Bw = McCainBw(p, t)
gw = gws / Bw
qoR = qo * bo * cfpb() / spd()  'this is oil rate in ft^3/sec
qlR = (qo * bo + qw * Bw) * cfpb() / spd() 'this is liquid rate in ft^3/sec
qgr = ((qg * 10 ^ 3) - (qo * Rs)) * Bgas / spd() 'this is gas rate in ft^3/sec
ilf = qlR / (qlR + qgr)
vsl = qlR / ((WorksheetFunction.Pi() / 4) * (d / 12) ^ 2)
vsg = qgr / ((WorksheetFunction.Pi() / 4) * (d / 12) ^ 2)
```

```
    vm = vsl + vsg 'calculate mixture velocity vm use eq.3-12
    R = vsl / vsg
    Cl = vsl / vm ' input liquid volume fraction
    igf = vsg / vm ' input gas volume fraction
    fo = qoR / qlR
    fw = 1 - fo
    sigmaO = OilTension(p, t, API) * 0.00220462
    sigmaW = WaterTension(p, t) * 0.00220462
    'sigmaL = (((fo * sigmaO) + (0.617 * fw * sigmaW)) / (fo + 0.617 * fw))  'sigmal is
in lbf/s^2. Hence multiplying sigmaL by 0.00220462 dynes/cm=1lbf/sec^2
    sigmaL = GrayInterfacialTension(wor) * 0.00220462
    If qo = 0 Then
       rhol = rhoW(gw, p, t)
       mul = McCainmuw(p, t)
    Else
       If qw = 0 Then
       rhol = DensityOil(p, t, API, g)
       mul = BeggsRobinsonmuo(p, t, API, g)
    Else
       wor = qw / qo
       rhol = fw * rhoW(gw, p, t) + DensityOil(p, t, API, g) * fo
       mul = fw * McCainmuw(p, t) + BeggsRobinsonmuo(p, t, API, g) * fo
    End If
```

```
    End If
    mugas = viscosityGas(p, t, g, N2, Co2, H2S)
    rhogas = rhog(p, t, g, N2, Co2, H2S)
    rhon = rhol * Cl + rhogas * (1 - Cl) 'Calculate non slip mixture density rhon use eq.
3.23
    muMix = mul * Cl + mugas * (1 - Cl)
    Nv = rhon ^ 2 * vm ^ 4 / (gr() * sigmaL * (rhol - rhogas))
    ND = gr() * (rhol - rhogas) * (d / 12) ^ 2 / sigmaL
    w = 0.0554 * WorksheetFunction.Ln(1 + (730 * R / (R + 1)))
    b = 0.0814 * (1 - w)
    HL = 1 - ((1 - Exp(-2.314 * (Nv * (1 + (205 / ND))) ^ b)) / (R + 1))
    dlsradiant = (dls * WorksheetFunction.Pi / 180)
    Theta = WorksheetFunction.Acos(1 - (2 * Sin(dlsradiant)))
    La = (d / 12) * Sin(dlsradiant)
    Lb = ((d / 12) / 2) - La
    At = (1 / 2) * Lb * (((d / 12) * La) - La ^ 2) ^ 0.5
    Area = ((Theta / 4) * (d / 12) ^ 2) - (2 * At)
    HLa = 1 * Area / ((WorksheetFunction.Pi() / 4) * (d / 12) ^ 2)
    HLn = HL + HLa
    HLNew = HLn
End Function
Function WetArea(d, dls)
    dlsradiant = (dls * WorksheetFunction.Pi / 180)
```

```
    Theta = WorksheetFunction.Acos(1 - (2 * Sin(dlsradiant)))
    La = (d / 12) * Sin(dlsradiant)
    Lb = ((d / 12) / 2) - La
    At = (1 / 2) * Lb * (((d / 12) * La) - La ^ 2) ^ 0.5
    Area = ((Theta / 4) * (d / 12) ^ 2) - (2 * At)
    WetArea = Area
End Function
```

APPENDIX B

Table B1: Comparing different models using Veeken et al. data 20^{o}/100 ft

							Critical Rate (Mscf/d)				
Completion ID (in)	Reservoir ID (in)	Dev (deg)	SG	q_{Turner} ($10^3m^3/d$)	Pressure (psia)	FTHT (F)	q_c	q_{Turner}	$q_{Coleman}$	q_{Model}	q_{Veeken}
4.41	6.28	20	0.59	40	58	61	1306	1412	1136	1844	1636
4.96	4.41	20	0.59	50	58	61	1589	1766	1437	2332	2114
2.81	2.35	24	0.59	19	79.75	61	742	671	542	879	726
2.87	2.36	21	0.59	20	87	61	918	706	590	958	767
2.99	4.42	0	0.59	22	87	61	918	777	641	1040	849
2.99	6.28	23	0.59	22	87	61	918	777	641	1040	849
2.87	2.35	14	0.59	20	79.75	61	847	706	565	917	767
3.96	6.88	27	0.59	39	87	61	1766	1377	1124	1823	1590
4.89	4.42	22	0.59	60	87	61	2154	2119	1714	2781	2622
4.89	4.42	15	0.59	60	87	61	2401	2119	1714	2781	2622
4.89	4.42	20	0.59	60	87	61	2507	2119	1714	2781	2622
4.89	4.42	29	0.59	60	87	61	3072	2119	1714	2781	2622
2.99	6.88	27	0.59	22	87	61	918	777	641	1040	849
1.75	2.44	16	0.59	8	87	61	388	282	219	356	295
4.89	6.88	21	0.59	60	87	61	1942	2119	1714	2781	2622
4.89	4.42	17	0.59	60	87	61	2225	2119	1714	2781	2622
4.89	4.42	30	0.59	60	87	61	2507	2119	1714	2781	2622
4.89	4.42	47	0.59	60	87	61	2613	2119	1714	2781	2622
4.89	6.88	19	0.59	60	87	61	2225	2119	1714	2781	2622
3.96	2.06	42	0.59	42	101.5	61	1871	1483	1215	1971	1729

Completion ID (in)	Reservoir ID (in)	Dev (deg)	SG	q_{Turner} ($10^3 m^3/d$)	Pressure (psia)	FTHT (F)	q_c	q_{Turner}	$q_{Coleman}$	q_{Model}	q_{Veeken}
4.41	6.09	13	0.63	67.4	217.5	144	3531	2380	1932	3135	3018
4.28	6	37	0.63	84.5	348	113	4237	2984	2402	3897	4006
6.09	3.83	18	0.63	125	217.5	163	7768	4414	3595	5834	6763
4.41	3.92	20	0.63	123	667	120	4590	4343	3529	5727	6613
4.41	3.92	20	0.63	165	1189	115	7062	5826	4802	7793	10039
4.28	6	22	0.63	65	217.5	129	3884	2295	1852	3006	2888
6.09	6.09	31	0.63	302	1174.5	138	10946	10664	8773	14236	22475
4.28	3.83	0	0.59	168	1421	122	7062	5932	5024	8153	10303
4.28	3.83	0	0.59	157	1232.5	122	7062	5544	4677	7589	9346
4.28	3.83	0	0.59	112	725	163	6003	3955	3369	5467	5813
4.28	3.83	0	0.59	157	1232.5	122	6356	5544	4677	7589	9346
6.09	4.28	15	0.61	217	667	167	18714	7662	6408	10399	14825
6.09	4.28	15	0.61	190	493	156	13771	6709	5575	9046	12297
6.09	6	39	0.61	233	739.5	154	14477	8227	6868	11144	16331
6.09	6	39	0.61	202	565.5	160	13065	7133	5949	9654	13414
6.09	6	39	0.61	168	391.5	162	10946	5932	4926	7993	10303
6.09	6	39	0.61	166	319	108	12359	5861	4756	7717	10127
4.28	6.09	63	0.61	118	667	109	5297	4167	3424	5556	6244
4.28	6.09	63	0.61	99	478.5	115	4590	3496	2864	4647	4925
4.28	6.09	63	0.61	84	319	91	4943	2966	2400	3894	3976
4.41	3.92	43	0.65	64	174	109	6003	2260	1773	2878	2834
4.41	3.92	35	0.65	80	282.75	120	4767	2825	2239	3633	3736
4.41	3.83	30	0.65	111	522	108	4943	3919	3120	5063	5742
4.41	3.83	30	0.65	92	348	100	4061	3249	2556	4147	4472

Completion ID (in)	Reservoir ID (in)	Dev (deg)	SG	q_{Turner} ($10^3 m^3/d$)	Pressure (psia)	FTHT (F)	q_c	q_{Turner}	$q_{Coleman}$	q_{Model}	q_{Veeken}
4.41	3.83	30	0.65	85	304.5	104	3884	3001	2375	3853	4036
4.41	3.83	30	0.65	80	261	97	3354	2825	2215	3595	3736
4.41	3.83	30	0.65	79	290	138	3531	2789	2216	3597	3677
6.09	441	40	0.63	170	365.4	132	8298	6003	4863	7892	10481
6.18	3.83	18	0.63	121	174	131	7062	4273	3442	5585	6464
6.09	3.83	26	0.63	114	174	153	7768	4025	3255	5282	5955
4.41	3.92	30	0.64	124	638	104	5650	4378	3506	5689	6688
4.41	6	21	0.64	119	652.5	133	5120	4202	3405	5525	6317
4.41	4.28	19	0.63	84	355.25	158	4237	2966	2432	3947	3976
4.28	4.28	26	0.63	82	391.5	163	6709	2895	2390	3879	3855
4.28	4.28	26	0.63	97	522	154	5297	3425	2799	4542	4793
4.28	4.28	26	0.63	81	362.5	151	4590	2860	2336	3790	3796
4.28	6.09	32	0.65	154	1261.5	140	7062	5438	4425	7180	9090
4.41	3.83	29	0.61	76	275.5	145	6003	2684	2209	3584	3502
4.41	3.83	31	0.66	85	275.5	77	2825	3001	2323	3769	4036
4.28	4.28	48	0.59	88	362.5	100	5650	3107	2572	4173	4221
4.67	4.67	62	0.58	115	391.5	72	2966	4061	3340	5419	6027
2.88	2.88	49	0.56	45	435	90	2048	1589	1329	2157	1871
4.28	4.28	64	0.6	104	449.5	68	4449	3672	2983	4840	5259
3.92	3.92	56	0.58	77	336.4	61	2860	2719	2210	3585	3560
4.41	4.41	46	0.6	105	449.5	95	3990	3708	3047	4945	5327
6.18	4.28	30	0.66	370	1609.5	127	19950	13065	10577	17163	27564
6.09	6.18	15	0.65	326	1319.5	127	26023	11511	9351	15174	24392

Table B2: Comparing different models using Veeken et al. data at 12°/100 ft

							Critical Rate (Mscf/d)				
Completion ID (in)	Reservoir ID (in)	Dev (deg)	SG	q_{Turner} ($10^3 m^3/d$)	Pressure (psia)	FTHT (F)	q_c	q_{Turner}	$q_{Coleman}$	q_{Model}	q_{Veeken}
4.41	6.28	20	0.59	40	58	61	1306	1412	1136	1720	1636
4.96	4.41	20	0.59	50	58	61	1589	1766	1437	2176	2114
2.81	2.35	24	0.59	19	79.75	61	742	671	542	820	726
2.87	2.36	21	0.59	20	87	61	918	706	590	893	767
2.99	4.42	0	0.59	22	87	61	918	777	641	970	849
2.99	6.28	23	0.59	22	87	61	918	777	641	970	849
2.87	2.35	14	0.59	20	79.75	61	847	706	565	855	767
3.96	6.88	27	0.59	39	87	61	1766	1377	1124	1701	1590
4.89	4.42	22	0.59	60	87	61	2154	2119	1714	2594	2622
4.89	4.42	15	0.59	60	87	61	2401	2119	1714	2594	2622
4.89	4.42	20	0.59	60	87	61	2507	2119	1714	2594	2622
4.89	4.42	29	0.59	60	87	61	3072	2119	1714	2594	2622
2.99	6.88	27	0.59	22	87	61	918	777	641	970	849
1.75	2.44	16	0.59	8	87	61	388	282	219	332	295
4.89	6.88	21	0.59	60	87	61	1942	2119	1714	2594	2622
4.89	4.42	17	0.59	60	87	61	2225	2119	1714	2594	2622
4.89	4.42	30	0.59	60	87	61	2507	2119	1714	2594	2622
4.89	4.42	47	0.59	60	87	61	2613	2119	1714	2594	2622
4.89	6.88	19	0.59	60	87	61	2225	2119	1714	2594	2622
3.96	2.06	42	0.59	42	101.5	61	1871	1483	1215	1838	1729
4.41	6.09	13	0.63	67.4	217.5	144	3531	2380	1932	2924	3018
4.28	6	37	0.63	84.5	348	113	4237	2984	2402	3635	4006

Completion ID (in)	Reservoir ID (in)	Dev (deg)	SG	q_{Turner} ($10^3 m^3/d$)	Pressure (psia)	FTHT (F)	q_c	q_{Turner}	$q_{Coleman}$	q_{Model}	q_{Veeken}
6.09	3.83	18	0.63	125	217.5	163	7768	4414	3595	5442	6763
4.41	3.92	20	0.63	123	667	120	4590	4343	3529	5342	6613
4.41	3.92	20	0.63	165	1189	115	7062	5826	4802	7269	10039
4.28	6	22	0.63	65	217.5	129	3884	2295	1852	2804	2888
6.09	6.09	31	0.63	302	1174.5	138	10946	10664	8773	13279	22475
4.28	3.83	0	0.59	168	1421	122	7062	5932	5024	7605	10303
4.28	3.83	0	0.59	157	1232.5	122	7062	5544	4677	7079	9346
4.28	3.83	0	0.59	112	725	163	6003	3955	3369	5099	5813
4.28	3.83	0	0.59	157	1232.5	122	6356	5544	4677	7079	9346
6.09	4.28	15	0.61	217	667	167	18714	7662	6408	9700	14825
6.09	4.28	15	0.61	190	493	156	13771	6709	5575	8438	12297
6.09	6	39	0.61	233	739.5	154	14477	8227	6868	10395	16331
6.09	6	39	0.61	202	565.5	160	13065	7133	5949	9005	13414
6.09	6	39	0.61	168	391.5	162	10946	5932	4926	7455	10303
6.09	6	39	0.61	166	319	108	12359	5861	4756	7199	10127
4.28	6.09	63	0.61	118	667	109	5297	4167	3424	5183	6244
4.28	6.09	63	0.61	99	478.5	115	4590	3496	2864	4334	4925
4.28	6.09	63	0.61	84	319	91	4943	2966	2400	3633	3976
4.41	3.92	43	0.65	64	174	109	6003	2260	1773	2684	2834
4.41	3.92	35	0.65	80	282.75	120	4767	2825	2239	3389	3736
4.41	3.83	30	0.65	111	522	108	4943	3919	3120	4723	5742
4.41	3.83	30	0.65	92	348	100	4061	3249	2556	3868	4472
4.41	3.83	30	0.65	85	304.5	104	3884	3001	2375	3594	4036
4.41	3.83	30	0.65	80	261	97	3354	2825	2215	3353	3736
4.41	3.83	30	0.65	79	290	138	3531	2789	2216	3355	3677

Completion ID (in)	Reservoir ID (in)	Dev (deg)	SG	q_{Turner} ($10^3 m^3/d$)	Pressure (psia)	FTHT (F)	q_c	q_{Turner}	$q_{Coleman}$	q_{Model}	q_{Veeken}
6.09	441	40	0.63	170	365.4	132	8298	6003	4863	7361	10481
6.18	3.83	18	0.63	121	174	131	7062	4273	3442	5210	6464
6.09	3.83	26	0.63	114	174	153	7768	4025	3255	4927	5955
4.41	3.92	30	0.64	124	638	104	5650	4378	3506	5306	6688
4.41	6	21	0.64	119	652.5	133	5120	4202	3405	5153	6317
4.41	4.28	19	0.63	84	355.25	158	4237	2966	2432	3682	3976
4.28	4.28	26	0.63	82	391.5	163	6709	2895	2390	3618	3855
4.28	4.28	26	0.63	97	522	154	5297	3425	2799	4236	4793
4.28	4.28	26	0.63	81	362.5	151	4590	2860	2336	3535	3796
4.28	6.09	32	0.65	154	1261.5	140	7062	5438	4425	6697	9090
4.41	3.83	29	0.61	76	275.5	145	6003	2684	2209	3343	3502
4.41	3.83	31	0.66	85	275.5	77	2825	3001	2323	3516	4036
4.28	4.28	48	0.59	88	362.5	100	5650	3107	2572	3892	4221
4.67	4.67	62	0.58	115	391.5	72	2966	4061	3340	5055	6027
2.88	2.88	49	0.56	45	435	90	2048	1589	1329	2012	1871
4.28	4.28	64	0.6	104	449.5	68	4449	3672	2983	4515	5259
3.92	3.92	56	0.58	77	336.4	61	2860	2719	2210	3344	3560
4.41	4.41	46	0.6	105	449.5	95	3990	3708	3047	4613	5327
6.18	4.28	30	0.66	370	1609.5	127	19950	13065	10577	16009	27564
6.09	6.18	15	0.65	326	1319.5	127	26023	11511	9351	14154	24392

Table B3: New model versus Turner model predictions using Turner data

WHP (psia)	Tubing ID (in)	Tubing OD (in)	Casing ID (in)	Cond. Yield	Water. Yield	API	Depth (ft)	Status	q_c (Mscf/d)	q_{Turner} (Mscf/d)	q_{Model} (Mscf/d)	T. Model Prediction	New Model Prediction
725	2.441	2.375	4.95	6	0	63.8	6404	Near LU.	775	779	1841	Loaded Up	Loaded Up
400	1.995			18	1.995	0	6739	Near LU.	417	583	957	Loaded Up	Loaded Up
108	2.041			96	12.4	64.3	6529	Near LU.	568	306	516	Unloaded	Unloaded
540	1.995			10.5	10.5	70.8	6700	Near LU.	712	661	1116	Unloaded	Loaded Up
450	1.995			11.3	0	61	6770	Near LU.	442	419	1016	Unloaded	Loaded Up
3607	1.995			37.4	0	61	11200	Loaded Up	1525	1156	2707	Unloaded	Loaded Up
3434	1.995			37.4	0	61	11200	Unloaded	2926	1160	2668	Unloaded	Unloaded
3773	1.995			36.8	0	58	11340	Questionable	2494	1158	2741	Unloaded	Loaded Up
3660	1.995			36.8	0	58	11340	Unloaded	3726	1142	2718	Unloaded	Unloaded
3340	2.992			130.8	0	56.4	11416	Loaded Up	2611	2412	5949	Unloaded	Loaded Up
3295	2.992			130.8	0	56.4	11416	Questionable	3264	2401	5923	Unloaded	Loaded Up
3280	2.992			130.8	0	56.4	11416	Questionable	4095	2395	5915	Unloaded	Loaded Up
3540	2.441			113.5	0	56.4	11417	Loaded Up	1814	1635	4030	Unloaded	Loaded Up
3330	2.441			113.5	0	56.4	11417	Questionable	2915	1600	3956	Unloaded	Loaded Up
3525	1.995			106.9	0	55	11426	Unloaded	1792	1108	2689	Unloaded	Loaded Up
3472	1.995			106.9	0	55	11426	Questionable	2572	1085	2676	Unloaded	Loaded Up
3338	2.441			117.6	0	55	11355	Unloaded	2261	1623	3959	Unloaded	Loaded Up
3245	2.441			117.6	0	55	11355	Loaded Up	2503	1610	3923	Unloaded	Loaded Up
3092	2.441			117.6	0	55	11355	Questionable	3351	1574	3861	Unloaded	Loaded Up
3556	1.995			104.3	0	55	11390	Unloaded	2069	1091	2696	Unloaded	Loaded Up
3455	1.995			104.3	0	55	11390	Loaded Up	2769	1082	2672	Unloaded	Unloaded

WHP (psia)	Tubing ID (in)	Tubing OD (in)	Casing ID (in)	Cond. Yield	Water. Yield	API	Depth (ft)	Status	q_c (Mscf/d)	q_{Turner} (Mscf/d)	q_{Model} (Mscf/d)	T. Model Prediction	New Model Prediction
3665	2.441			68.3	0	80	8690	Unloaded	2542	1860	4071	Unloaded	Loaded Up
3644	2.441			68.3	0	60	8690	Loaded Up	3182	1654	4064	Unloaded	Loaded Up
3615	2.441			68.3	0	60	8690	Questionable	3890	1648	4055	Unloaded	Loaded Up
3212	2.441			54.8	0	60	8840	Unloaded	2547	1604	3910	Unloaded	Loaded Up
3025	2.441			54.8	0	60	8840	Questionable	3517	1569	3833	Unloaded	Loaded Up
8215	2.441			10.8	0	67.5	11850	Unloaded	3472	1956	4762	Unloaded	Loaded Up
7950	2.441			10.8	0	67.5	11850	Loaded Up	4896	1941	4740	Unloaded	Unloaded
7405	2.441			10.8	0	67.5	11850	Questionable	6946	1930	4692	Unloaded	Unloaded
2335	1.995			17.9	0	65	6995	Unloaded	1116	936	2318	Unloaded	Loaded Up
2226	1.995			17.9	0	65	6995	Unloaded	1959	910	2271	Unloaded	Loaded Up
2182		4.5	6.184	2.5	0	70	5725	Loaded Up	5501	3767	11454	Unloaded	Loaded Up
2175		4.5	6.184	2.5	0	70	5725	Questionable	6405	3757	11438	Unloaded	Loaded Up
2169		4.5	6.184	2.5	0	70	5725	Unloaded	7504	3747	11424	Unloaded	Loaded Up
1590	3.958			13.1	0	65	5515	Loaded Up	3009	3281	7638	Loaded Up	Loaded Up
1550	3.958			13.1	0	65	5515	Questionable	3551	3233	7543	Unloaded	Loaded Up
1520	3.958			13.1	0	65	5515	Unloaded	4150	3196	7470	Unloaded	Loaded Up
1245		2.875	6.184	10.3	0	67	6180	Loaded Up	4441	4920	3564	Loaded Up	Unloaded
1184		2.875	6.184	10.3	0	67	6180	Loaded Up	4843	4793	3473	Unloaded	Unloaded
1117		2.875	6.184	10.3	0	67	6180	Unloaded	5513	4649	3371	Unloaded	Unloaded
1958		2.875	6.184	24.8	0	62.5	6031	Loaded Up	8185	5931	4452	Unloaded	Unloaded
1938		2.875	6.184	24.8	0	62.5	6031	Questionable	9039	5902	4431	Unloaded	Unloaded
1913		2.875	6.184	24.8	0	62.5	6031	Unloaded	9897	5857	4405	Unloaded	Unloaded
2040		2.875	6.184	31.8	0	65	5962	Loaded Up	6702	6082	4537	Unloaded	Unloaded

WHP (psia)	Tubing ID (in)	Tubing OD (in)	Casing ID (in)	Cond. Yield	Water. Yield	API	Depth (ft)	Status	q_c (Mscf/d)	q_{Turner} (Mscf/d)	q_{Model} (Mscf/d)	T. Model Prediction	New Model Prediction
1993		2.875	6.184	31.8	0	65	5962	Questionable	8210	6015	4489	Unloaded	Unloaded
1953		2.875	6.184	31.8	0	65	5962	Unloaded	9289	5957	4447	Unloaded	Unloaded
2284		3.5	6.184	15.1	0	67.5	5905	Loaded Up	7109	5590	7067	Unloaded	Unloaded
2271		3.5	6.184	15.1	0	67.5	5906	Questionable	8406	5559	7050	Unloaded	Unloaded
2256		3.5	6.184	15.1	0	67.5	5906	Unloaded	9747	5535	7030	Unloaded	Unloaded
2352		3.5	6.184	37	0	70	5934	Loaded Up	6361	5641	7156	Unloaded	Loaded Up
2338		3.5	6.184	3.7	0	70	5934	Questionable	8057	5671	7138	Unloaded	Unloaded
2223		3.5	6.184	3.7	0	70	5934	Unloaded	9860	5485	6985	Unloaded	Unloaded
2003		3.3	6.184	3.7	0	70	5934	Unloaded	1767	5212	5928	Loaded Up	Loaded Up
2042		4.5	6.184	26.7	0	65	6850	Loaded Up	4124	3613	11120	Unloaded	Loaded Up
1818		4.5	6.184	26.7	0	65	6850	Questionable	4998	3412	10535	Unloaded	Loaded Up
1600		4.5	6.184	26.7	0	65	6850	Unloaded	6423	3199	9904	Unloaded	Loaded Up
1835	1.995			27.8	0.4	52.7	7346	Unloaded	8672	1239	2080	Unloaded	Unloaded
2421	1.995			27.8	0.4	52.7	7346	Unloaded	6654	1407	2353	Unloaded	Unloaded
2705	1.995			27.8	0.4	52.7	7346	Unloaded	5136	1467	2459	Unloaded	Unloaded
2834	1.995			27.8	0.4	52.7	7346	Unloaded	3917	1502	2502	Unloaded	Unloaded
5056	1.995			7.5	1.4	43.9	8963	Unloaded	3376	1770	2938	Unloaded	Unloaded
4931	1.995			7.5	1.4	43.9	8963	Unloaded	4830	1732	2923	Unloaded	Unloaded
4786	1.995			7.5	1.4	43.9	8963	Unloaded	6221	1705	2905	Unloaded	Unloaded
4575	1.995			7.5	1.4	43.9	8963	Unloaded	7792	1659	2876	Unloaded	Unloaded
1902	1.995			30.9	0	71	5294	Unloaded	1138	851	2115	Unloaded	Loaded Up
1737	1.995			3	0	71	5294	Unloaded	1712	814	2026	Unloaded	Loaded Up
1480	1.995			0.9	0	71	5294	Unloaded	2473	750	1873	Unloaded	Unloaded

WHP (psia)	Tubing ID (in)	Tubing OD (in)	Casing ID (in)	Cond. Yield	Water. Yield	API	Depth (ft)	Status	q_c (Mscf/d)	q_{Turner} (Mscf/d)	q_{Model} (Mscf/d)	T. Model Prediction	New Model Prediction
1246	1.995			0.9	0	71	5294	Unloaded	2965	686	1717	Unloaded	Unloaded
1895	1.995			54.1	0	71.7	5234	Unloaded	1797	875	2112	Unloaded	Loaded Up
1861	1.995			54.1	0	71.7	5234	Unloaded	2502	859	2094	Unloaded	Unloaded
1784	1.996			54.1	0	71.7	5234	Unloaded	3460	832	2054	Unloaded	Unloaded
1680	1.996			54.1	0	71.7	5234	Unloaded	4439	803	1996	Unloaded	Unloaded
2814	1.75			3.3	1	53.5	7639	Unloaded	1596	1216	1920	Unloaded	Loaded Up
2582	1.75			3.3	1	33.5	7639	Unloaded	2423	1176	1858	Unloaded	Unloaded
2104	1.75			3.3	1	53.5	7639	Unloaded	3598	1070	1705	Unloaded	Unloaded
1575	1.75			3.3	1	53.5	7639	Unloaded	4410	918	1486	Unloaded	Unloaded
2783	1.75			3.4	0	52.4	7475	Unloaded	2939	834	1912	Unloaded	Unloaded
2655	1.75			3.4	0	52.4	7475	Unloaded	4140	817	1878	Unloaded	Unloaded
2406	1.75			3.4	0	52.4	7475	Unloaded	5820	770	1806	Unloaded	Unloaded
2205	1.75			3.4	0	52.4	7475	Unloaded	6871	746	1740	Unloaded	Unloaded
2574	1.75			4.1	0.6	52.2	7546	Unloaded	1943	899	1856	Unloaded	Unloaded
2224	1.75			4.1	0.6	52.2	7546	Unloaded	2910	833	1747	Unloaded	Unloaded
1839	1.75			4.1	0.6	52.2	7546	Unloaded	3742	755	1602	Unloaded	Unloaded
1509	1.75			4.1	0.6	52.2	7546	Unloaded	4485	683	1455	Unloaded	Unloaded
2611	1.995			5.5	0	52.6	7753	Unloaded	3436	1082	2425	Unloaded	Unloaded
2527	1.995			5.5	0	52.6	7753	Unloaded	4471	1058	2394	Unloaded	Unloaded
2556	1.995			7.7	0	36.7	8162	Unloaded	1550	1026	2405	Unloaded	Loaded Up
2415	1.995			7.7	0	56.7	8162	Unloaded	1804	996	2351	Unloaded	Loaded Up
2149	1.995			7.7	0	56.7	8162	Unloaded	2385	941	2236	Unloaded	Unloaded
1765	1.995			7.7	0	56.7	8162	Unloaded	2949	856	2042	Unloaded	Unloaded

WHP (psia)	Tubing ID (in)	Tubing OD (in)	Casing ID (in)	Cond. Yield	Water. Yield	API	Depth (ft)	Status	q_c (Mscf/d)	q_{Turner} (Mscf/d)	q_{Model} (Mscf/d)	T. Model Prediction	New Model Prediction
2862		2.375	4.974	5	0	52.2	7810	Unloaded	3024	5098	3558	Loaded Up	Loaded Up
2823		2.375	4.974	5	0	52.2	7810	Loaded Up	3863	5045	3540	Loaded Up	Unloaded
760	2.441			46.1	45.1	54.9	7531	Loaded Up	1247	1148	1992	Unloaded	Loaded Up
704	2.441			31.6	40.8	54.9	7531	Loaded Up	1313	1099	1915	Unloaded	Loaded Up
822	2.441			26.7	26.3	54.9	7531	Loaded Up	1356	1197	2075	Unloaded	Loaded Up
1102	2.441			26.1	23.8	54.9	7531	Loaded Up	1365	1419	2413	Loaded Up	Loaded Up
552	2.441			25.1	22.3	54.9	7531	Near LU.	1607	958	1690	Unloaded	Loaded Up
315	7.386			10	0	30	3278	Loaded Up	5740	5093	11612	Unloaded	Loaded Up
422	7.386			10	0	50	3278	Loaded Up	3890	5923	13481	Loaded Up	Loaded Up
459	7.386			10	0	50	3278	Loaded Up	2780	6186	14073	Loaded Up	Loaded Up
484	7.386			10	0	50	3278	Loaded Up	1538	6359	14461	Loaded Up	Loaded Up
500		2.375	4.974	14	0	50	5080	Loaded Up	400	2184	1520	Loaded Up	Loaded Up
500		2.375	4.052	0	5	0	7200	Loaded Up	800	1726	1520	Loaded Up	Loaded Up
660		2.375	6.276	0	3.5	0	6776	Loaded Up	4300	6367	1754	Loaded Up	Unloaded
280		2.375	4.974	0	28	0	3077	Loaded Up	500	2083	1131	Loaded Up	Loaded Up
210		2.375	6.276	0	24	0	2250	Loaded Up	470	3248	977	Loaded Up	Loaded Up

Table B4: Horizontal Well 1 deviation survey showing H_L variation with BUR

Depth (ft)	TVD (ft)	Angle (degrees)	BUR (^{o}/100 ft)	H_{LGray} Coleman	H_{LGray} Turner	H_{Lnew} Coleman	H_{Lnew} Turner	H_{LGray} New Model	H_{Lnew} New Model	H_{Lnew} New Model w/ 2.875 Tubing
0	0	0.00	0.0	0.09	0.08	0.09	0.08	0.06	0.06	0.01
840	840	0.20	0.0	0.09	0.08	0.09	0.08	0.07	0.07	0.02
1151	1151	0.20	0.1	0.09	0.08	0.09	0.08	0.07	0.07	0.02
1947	1947	0.20	0.0	0.10	0.09	0.10	0.09	0.07	0.07	0.02
2514	2514	0.30	0.1	0.10	0.09	0.10	0.09	0.07	0.07	0.02
11865	11864	1.75	0.1	0.13	0.12	0.13	0.12	0.10	0.10	0.03
12149	12148	1.86	0.1	0.13	0.12	0.13	0.12	0.10	0.10	0.03
12180	12179	1.85	0.2	0.13	0.12	0.13	0.12	0.10	0.10	0.03
12212	12211	1.72	0.4	0.13	0.12	0.13	0.12	0.10	0.10	0.03
12243	12242	2.39	3.7	0.13	0.12	0.16	0.15	0.10	0.13	0.06
12275	12274	4.24	6.3	0.13	0.12	0.19	0.18	0.10	0.16	0.09
12306	12305	6.59	7.7	0.13	0.12	0.21	0.20	0.10	0.18	0.11
12338	12337	9.05	7.7	0.13	0.12	0.21	0.20	0.10	0.18	0.11
12369	12367	11.47	7.8	0.13	0.12	0.21	0.20	0.10	0.18	0.12
12401	12398	13.99	8.0	0.13	0.12	0.22	0.20	0.10	0.19	0.12
12432	12428	16.53	8.4	0.13	0.12	0.22	0.21	0.10	0.19	0.12
12464	12459	19.03	8.1	0.13	0.12	0.22	0.21	0.10	0.19	0.12
12496	12489	21.30	7.6	0.13	0.12	0.21	0.20	0.10	0.18	0.11
12528	12518	23.68	7.9	0.13	0.12	0.22	0.20	0.10	0.19	0.12
12555	12543	25.62	7.4	0.13	0.12	0.21	0.20	0.10	0.18	0.11
12587	12571	27.97	7.5	0.13	0.12	0.21	0.20	0.10	0.18	0.11

Depth (ft)	TVD (ft)	Angle (degrees)	BUR (^{o}/100 ft)	H_{LGray} Coleman	H_{LGray} Turner	H_{Lnew} Coleman	H_{Lnew} Turner	H_{LGray} New Model	H_{Lnew} New Model	H_{Lnew} New Model w/ 2.875 Tubing
12618	12598	30.36	7.7	0.13	0.12	0.21	0.20	0.10	0.18	0.11
12650	12626	32.87	8.0	0.13	0.12	0.22	0.21	0.10	0.19	0.12
12681	12651	36.32	11.2	0.13	0.12	0.27	0.26	0.10	0.24	0.17
12713	12676	40.20	12.2	0.13	0.12	0.29	0.28	0.10	0.26	0.19
12745	12700	44.14	12.3	0.13	0.12	0.29	0.28	0.10	0.26	0.19
12776	12722	47.96	12.3	0.13	0.12	0.29	0.28	0.10	0.26	0.19
12808	12742	51.36	10.6	0.13	0.12	0.26	0.25	0.10	0.23	0.16
12839	12761	53.82	7.9	0.13	0.12	0.22	0.20	0.10	0.19	0.12
12871	12780	55.67	5.8	0.13	0.12	0.19	0.17	0.10	0.16	0.09
12902	12797	57.82	6.9	0.13	0.12	0.20	0.19	0.10	0.17	0.10
12934	12813	59.87	6.4	0.13	0.12	0.19	0.18	0.10	0.17	0.10
12966	12829	60.88	3.2	0.13	0.12	0.15	0.14	0.10	0.12	0.06
12997	12844	62.32	4.7	0.13	0.12	0.17	0.16	0.10	0.14	0.07
13029	12858	65.00	8.4	0.13	0.12	0.22	0.21	0.10	0.20	0.13
13060	12870	67.62	8.7	0.13	0.12	0.23	0.22	0.10	0.20	0.13
13092	12882	70.40	8.7	0.13	0.12	0.23	0.22	0.10	0.20	0.13
13123	12892	72.46	7.2	0.13	0.12	0.21	0.19	0.10	0.18	0.11
13186	12909	75.81	5.3	0.13	0.12	0.18	0.17	0.10	0.15	0.08
13218	12916	77.61	5.7	0.13	0.12	0.18	0.17	0.10	0.15	0.08
13249	12923	78.88	4.2	0.13	0.12	0.17	0.15	0.10	0.14	0.07
13281	12928	80.12	3.9	0.13	0.12	0.16	0.15	0.10	0.13	0.06
13312	12933	81.31	3.8	0.13	0.12	0.16	0.15	0.10	0.13	0.06

Depth (ft)	TVD (ft)	Angle (degrees)	BUR (^{o}/100 ft)	H_{LGray} Coleman	H_{LGray} Turner	H_{Lnew} Coleman	H_{Lnew} Turner	H_{LGray} New Model	H_{Lnew} New Model	H_{Lnew} New Model w/ 2.875 Tubing
13344	12938	82.52	3.8	0.13	0.12	0.16	0.15	0.10	0.13	0.06
13375	12941	84.07	5.0	0.13	0.12	0.18	0.16	0.10	0.15	0.08
13407	12944	85.19	4.0	0.13	0.12	0.16	0.15	0.10	0.13	0.06
13439	12947	86.61	4.7	0.13	0.12	0.17	0.16	0.10	0.14	0.07
13470	12948	88.28	5.4	0.13	0.12	0.18	0.17	0.10	0.15	0.08
13501	12949	90.22	6.3	0.13	0.12	0.19	0.18	0.10	0.16	0.09
13533	12948	92.16	6.1	0.13	0.12	0.19	0.18	0.10	0.16	0.09
13565	12946	93.70	4.8	0.13	0.12	0.17	0.16	0.10	0.14	0.07
16971	12934	88.80	0.9	0.13	0.12	0.14	0.12	0.10	0.11	0.04
17003	12935	89.01	0.9	0.13	0.12	0.14	0.12	0.10	0.11	0.04
17034	12935	89.38	1.3	0.13	0.12	0.14	0.13	0.10	0.11	0.04
17096	12936	89.38	0.0	0.13	0.12	0.13	0.12	0.10	0.10	0.03

Table B5: Horizontal Well 2 deviation survey showing H_L variation with BUR

Depth (ft)	TVD (ft)	Angle (degrees)	BUR (^{o}/100 ft)	H_{LGray} Coleman	H_{LGray} Turner	H_{Lnew} Coleman	H_{Lnew} Turner	H_{LGray} New Model	H_{Lnew} New Model	H_{Lnew} New Model w/ 2.875 Tubing
0	0	0	0	0.109	0.099	0.109	0.099	0.082	0.082	0.014
1758	1758	2.17	0	0.140	0.128	0.140	0.128	0.109	0.109	0.026
1882	1882	2.2	0.19	0.142	0.130	0.142	0.131	0.111	0.112	0.027
1976	1975	2.2	0.03	0.143	0.132	0.143	0.132	0.113	0.113	0.028
2071	2070	1.3	0.95	0.145	0.133	0.148	0.137	0.114	0.118	0.032
7304	7303	0.6	0.11	0.217	0.201	0.216	0.200	0.175	0.174	0.071
7399	7398	0.7	0.12	0.218	0.202	0.217	0.201	0.176	0.175	0.072
7477	7476	0.5	0.27	0.218	0.203	0.218	0.202	0.177	0.176	0.073
7493	7492	0.4	0	0.219	0.203	0.218	0.202	0.177	0.176	0.073
7559	7558	1.8	2.6	0.219	0.203	0.235	0.219	0.177	0.193	0.089
7590	7589	3.8	6.45	0.220	0.204	0.281	0.265	0.178	0.239	0.136
7622	7621	6.2	7.52	0.220	0.204	0.297	0.281	0.178	0.255	0.152
7653	7652	8.5	7.54	0.220	0.204	0.298	0.282	0.178	0.256	0.152
7685	7683	10.2	6.17	0.221	0.205	0.278	0.262	0.178	0.236	0.133
7716	7714	12	6.13	0.221	0.205	0.278	0.262	0.179	0.236	0.132
7748	7745	13.4	4.39	0.221	0.205	0.256	0.240	0.179	0.214	0.110
7779	7775	14.8	4.52	0.222	0.206	0.258	0.242	0.179	0.216	0.112
7811	7806	17.2	7.76	0.222	0.206	0.303	0.287	0.179	0.261	0.157
7842	7835	19.9	8.97	0.222	0.206	0.323	0.307	0.180	0.281	0.177
7873	7864	21.7	5.82	0.223	0.206	0.276	0.260	0.180	0.233	0.129
7905	7894	22.6	2.85	0.223	0.207	0.241	0.225	0.180	0.199	0.095

Depth (ft)	TVD (ft)	Angle (degrees)	BUR (^{o}/100 ft)	H_{LGray} Coleman	H_{LGray} Turner	H_{Lnew} Coleman	H_{Lnew} Turner	H_{LGray} New Model	H_{Lnew} New Model	H_{Lnew} New Model w/ 2.875 Tubing
7936	7922	23.8	3.92	0.223	0.207	0.253	0.237	0.181	0.210	0.106
7968	7951	26.5	8.73	0.224	0.207	0.321	0.304	0.181	0.278	0.174
8000	7980	28.7	7.03	0.224	0.208	0.295	0.278	0.181	0.252	0.148
8010	7988	29.2	5.55	0.224	0.208	0.274	0.258	0.181	0.231	0.127
8020	7997	29.6	5.27	0.224	0.208	0.270	0.254	0.181	0.227	0.123
8032	8008	30.4	6.98	0.224	0.208	0.294	0.278	0.181	0.251	0.147
8063	8034	33.7	11.47	0.225	0.208	0.370	0.353	0.181	0.327	0.223
8094	8059	36.8	10.55	0.225	0.208	0.353	0.337	0.182	0.310	0.206
8126	8084	39.1	7.49	0.225	0.209	0.303	0.287	0.182	0.260	0.156
8158	8109	40.9	5.63	0.225	0.209	0.277	0.260	0.182	0.233	0.129
8189	8132	42.9	6.47	0.164	0.148	0.227	0.211	0.124	0.186	0.141
8220	8154	46.6	12.11	0.165	0.149	0.322	0.306	0.124	0.281	0.236
8252	8175	51.2	14.8	0.165	0.149	0.377	0.361	0.124	0.336	0.290
8283	8193	55.9	16.11	0.165	0.149	0.405	0.389	0.124	0.364	0.318
8314	8210	61.1	18.34	0.165	0.149	0.455	0.439	0.124	0.414	0.369
8346	8224	65.5	14.64	0.165	0.149	0.374	0.358	0.124	0.333	0.287
8377	8236	68.4	9.36	0.165	0.149	0.274	0.258	0.124	0.233	0.187
8408	8247	70.7	7.44	0.165	0.149	0.243	0.227	0.124	0.202	0.157
8424	8252	72.2	9.54	0.165	0.150	0.277	0.261	0.124	0.236	0.191
8469	8265	74.3	4.67	0.166	0.150	0.205	0.189	0.125	0.164	0.118
8500	8273	77.5	10.37	0.166	0.150	0.292	0.276	0.125	0.251	0.205
8530	8278	81	13.54	0.166	0.150	0.352	0.336	0.125	0.311	0.311
8561	8283	82.9	9.81	0.166	0.150	0.282	0.266	0.125	0.241	0.241

Depth (ft)	TVD (ft)	Angle (degrees)	BUR (^{o}/100 ft)	H_{LGray} Coleman	H_{LGray} Turner	H_{Lnew} Coleman	H_{Lnew} Turner	H_{LGray} New Model	H_{Lnew} New Model	H_{Lnew} New Model w/ 2.875 Tubing
8593	8286	83.9	6.95	0.166	0.150	0.237	0.220	0.125	0.195	0.195
8625	8289	85.7	5.84	0.166	0.150	0.221	0.205	0.125	0.179	0.179
8657	8291	87.7	6.62	0.166	0.150	0.232	0.216	0.125	0.190	0.190
8689	8292	89.9	7.21	0.166	0.150	0.240	0.224	0.125	0.199	0.199
8721	8291	91.3	5.97	0.166	0.150	0.223	0.207	0.125	0.181	0.181
9985	8304	88	5.32	0.166	0.150	0.214	0.198	0.125	0.173	0.173
10009	8305	87.8	4.66	0.166	0.150	0.206	0.190	0.125	0.164	0.164
10050	8306	87.8	0	0.166	0.150	0.167	0.151	0.125	0.126	0.126